

# **Surface Modification Technique for Acoustic Chemical Sensor Arrays based on CMUTs**

## **Dissertation**

zur Erlangung des akademischen Grades  
doctor rerum naturalium (Dr. rer. nat.)

vorgelegt der

Naturwissenschaftlichen Fakultät I  
Biowissenschaften

der Martin-Luther-Universität Halle-Wittenberg

von

Frau Yingchun Li

geboren am 05. Dezember 1982 in Xinjiang, China

Gutachter

1. Prof. Dr. rer. nat. habil. Dr. h. c. Reinhard Neubert
2. Prof. Dr. habil. Dipl.-Phys. Maximilian Fleischer
3. Priv.-Doz. Dr. rer. nat. Ralf Lucklum

Halle (Saale) im November 2010

---

# Acknowledgement

---

The work was done at the institute for micro and sensor system (**IMOS**), Otto-von-Guericke- University Magdeburg. This is a vital experience that made me grown up a lot from the scientific point of view, surrounded by a very professional environment.

First of all I would like to thank all the people who have involved directly or indirectly during the preparation of this thesis. All what you have done for me formed valuable contributions that are fundamental for the achievement of this work.

It is a great pleasure for me to express my deepest sense of gratitude and indebtedness to my advisor, Priv.-Doz. Dr. **Ralf Lucklum**, for his scholastic guidance, constant support and encouragement throughout my study and work at IMOS. Besides his very busy schedule he always provided helpful discussion and constructive suggestions for my research work as well as writing my PhD thesis. I will never forget his friendly manner which made my work smooth and progressive.

I would like to express my sincere gratitude to Prof. Dr. **Peter Hauptmann** for drawing my attention to the field of sensor, offering me great opportunity to work in his group and giving me support in every aspect during my stay in Germany.

Particular gratitude goes to my doctoral advisor, Prof. Dr. **Reinhard Neubert** from institute for pharmacy in Martin-Luther-University Halle-Wittenberg, for all his kindness and helpfulness to make my graduation possible and accept to be a reviewer of this work.

I would like to thank **Siemens AG** and particularly Prof. Dr. **Maximilian Fleischer** for the financial support, generous provision of CMUT substrates for my research work, as well as the kind and hospitable reception during my visit in Siemens. I am very much thankful to him for reviewing my thesis.

I want to thank **Stephan Adler**, who helped me continuously in overcoming experimental problems and operation of several instruments. Special thank is addressed to Dr. **Thomas Hempel** (Institute of experimental physics, University of Magdeburg), who generously offered his time for enormous numbers of SEM measurements. **Andreas Brose** is also highly acknowledged for modifying sensors with aerosol jetting technique.

I am deeply grateful to Dr. **Benedikt Schlatt-Masuth**, Dr. **Ulrike Hempel**, **Christian Kutzner**, **Marcel Thränhardt**, **Jörg Fochtmann** and **Anja Kästner**, for assisting me in the lab and making friendly, scientific and creative atmosphere. Especially I would like to

thank Dr. **Manzhu Ke**, who shared precious experience and exchanged inspiring academic ideas with me. Moreover, our secretaries, **Annett Wertan** and **Petra Hellwig**, deserve thanks for being very nice and friendly and I have improved my German language a lot by talking with them.

I would like to thank all of my friends and all past and present colleagues for making my life happy and convenient in Germany.

Finally I express my thankfulness to my family to be always by my side in all my choices and giving me their patience, understanding and encouragement during the whole four-year journey abroad.

Magdeburg, November 2010

---

# Abstract

---

This thesis reports:

- i) Syntheses of nanoparticles
- ii) 2-step modification of LFE and CMUT sensors including a bottom nanoparticle layer and a top sensitive agent layer deposited in selected regions
- iii) Physical (spectroscopic) and chemical characterization of the sensor coatings
- iv) Application of the modified sensors for detecting organic vapors
- v) Evaluation of the vapour uptake ability and selectivity of the sensing coatings
- vi) Analysis of mechanism about sensing process
- vii) Preparation of in situ sensing film based on molecularly imprinted polymerization

Complex films made up of nanoparticles (NPs) and various sensitive materials have been fabricated by double-coating process onto two types of sensors: piezoelectric quartz crystal resonators and capacitive micromachined ultrasonic transducers (CMUTs). NP films have been deposited firstly as support for immobilizing the subsequent layer. Different sensing agents have been dispensed onto the selected areas of the NP film in the second step. The bottom uniformly-arranged NP layer defines the acoustic properties of the whole device, provides an easy loading platform and vapor response, while the second dispensed layer contributes to varied sensitivity, whereby providing selectivity. Such composite coating procedure is able to realize localized deposition of different sensitive materials which allows for fabrication of sensor array on one substrate, especially taking advantage of the inherent sensor array configuration of CMUTs.

Comparison has been made after each coating step by SEM and impedance analysis technique. These measurements have revealed that both steps in the deposition process are highly reproducible and the resulting films are uniform and stable. Due to the rigidity of NPs and the uniformity of the NP films, NP coating could be used without significant attenuation of the acoustic wave and decrease in quality factor of the sensors. The fairly ordered arrangement of NPs guarantees a sufficient homogeneity of the second sensitive films.

The materials deposited in the second step include polymers and supramolecules, existing in solid or viscous liquid status at room temperature. They have modified the sensors in desired locations with satisfied control in area and amount.

The chemically modified sensors have been successfully developed into organic vapor detector. Due to the diversity in the responsive ability of different sensing materials, the sensors have demonstrated certain levels of selectivity in contact with several analytes, as well as good stability and fast uptake and release time. The underlying mechanism has been discussed by analyzing the Hansen solubility parameters of vapor and sensing matrix. It is evident that the interactions between the analytes and the sensing materials are dependent

on the chemical structures of the substances and the physical properties such as glass transition temperature of the sorbents, saturated vapor pressure of the gases and so on.

Long time exposure of CMUTs to vapors has been performed in order to evaluate the sensor signals regarding equilibrium of sorption. An ostensible sensing response lasting for several hours may not be out of vapor uptake, but arise from inner pressure change of measurement settings. Repeated purging of sensors with vapors showed reproducible sensing response, although the phenomenon named pre-condition has been found to exist for some sensors.

With such a sensor array it is now possible to identify gas mixtures and odorants from different sources, e.g. applying the CMUT sensor as a vapor mixture tester in vehicle engines and for breath gas. It is also believed that the abundant candidates serving as sensitive part will open a wide application scale for the selective and sensitive determination or testing of huge amount of analytes in many fields.

---

# Zusammenfassung

---

Diese Arbeit thematisiert:

- i) die Synthese von Nanopartikeln
- ii) die Modifizierung von LFE- und CMUT-Sensoren in 2 Schritten, welche die Abscheidung einer unteren Nanopartikelschicht und in ausgesuchten Bereichen einer darüber liegenden sensitiven Schicht umfassen
- iii) die physikalische (spektroskopische) und chemische Charakterisierung der Sensorbeschichtung
- iv) die Verwendung der modifizierten Sensoren zur Detektion organischer Gasen
- v) die Auswertung des Absorptionsvermögens und der Selektivität der sensitiven Schichten
- vi) die Analyse der Mechanismen des Messverfahrens
- vii) die Herstellung von in situ sensitiven Filmen, welche auf molekulare Abdruckpolymerisation basieren

Komplexe Filme, bestehend aus Nanopartikel (NP) und verschiedenen sensitiven Materialien, wurden mittels Doppelbeschichtung auf zwei Arten von Sensoren aufgetragen, den piezoelektrischen Quarzkristall-Resonatoren und den kapazitiven mikromechanischen Ultraschallwandlern (englisch CMUTs). Hierfür wurde zuerst die NP-Schicht aufgebracht, welche unter anderem zu der Immobilisierung der zweiten Schicht beiträgt, die in einem zweiten Schritt, als sensorisch wirksamer Stoff auf ausgewählte Bereiche der NP-Schicht aufgebracht wurde. Die untere, homogen angeordnete NP-Schicht definiert dabei die akustischen Eigenschaften des gesamten Sensorsystems, schafft eine einfache Grundlage für weitere Schichten und ist verantwortlich für die Gasantwort, während die zweite Schicht zur Variierung der Sensitivität beiträgt und daher über die Selektivität entscheidet. Dieses zusammengesetzte Beschichtungsverfahren ermöglichte die örtlich begrenzte Ablagerung verschiedener Materialien für die Herstellung von Sensor-Arrays auf einem Substrat, insbesondere durch die Nutzung der inhärenten Sensor-Array-Konfiguration der CMUTs. Nach jedem Beschichtungsschritt wurde ein Vergleich zwischen SEM und Impedanzanalyse-Technik durchgeführt. Diese Messungen ergaben, dass beide Schritte der Abscheidung gut reproduzierbar sind und die daraus resultierenden Filme sowohl homogen, als auch beständig sind. Aufgrund der Steifigkeit der Nanopartikel und der Gleichmäßigkeit der NP-Filme, konnten die Sensoren mit NP-Beschichtung ohne signifikante Verringerung

der Güte und ohne nennenswerte Dämpfung der akustischen Welle verwendet werde. Die annehmbar geordnete NP-Schicht garantiert eine ausreichende Homogenität der zweiten, sensorisch aktiven Schicht.

Zu den Materialien, welche im zweiten Schritt abgelagert wurden zählten Polymere und Supramoleküle, die unter Raumtemperatur als Feststoff oder viskose Flüssigkeit vorliegen. Beide Substanzklassen modifizierten den Sensor mit adäquater Genauigkeit des Bereiches und der Menge. Die chemisch modifizierten Sensoren wurden erfolgreich zu organische Gassensoren entwickelt. Aufgrund der vielfältigen Antwortmöglichkeiten der sensitiven Materialien wurde eine bestimmte Ebene an Selektivität für mehrere Analyten erreicht, wobei gleichzeitig eine gute Stabilität und eine schnelle Reaktionszeit erlangt wurden.

Der zugrunde liegende Mechanismus wurde anhand der Analyse der Hansen Löslichkeitsparameter von Dampf und des Beschichtungsmaterials diskutiert. Es ist offensichtlich, dass die Wechselwirkungen zwischen dem Analyten und der sensitiven Materialien von der chemischen Struktur der Stoffe und den physikalischen Eigenschaften abhängig sind, dazu gehören die Glasübergangstemperatur der Sorbentien, der gesättigte Dampfdruck der Gase und andere.

Zur Bewertung der Sensorsignale hinsichtlich des Gleichgewichtes der Sorption wurden Langzeitmessungen mit CMUTs in Gasen durchgeführt. Eine mehrstündige Sensorantwort wurde dabei möglicherweise nicht durch die Gasaufnahme verursacht, sondern können sich aus der Änderung des Innendruckes während der Messung ergeben haben. Dabei zeigte wiederholtes Spülen der Sensoren mit Gasen reproduzierbare Sensorantworten, obwohl bei einigen Sensoren das so genannte Pre-condition Phänomen zu beobachten war.

Mit einem solchen Sensor-Array ist es nun möglich, Gasgemische und Geruchsstoffe aus unterschiedlichen Quellen zu charakterisieren, z.B. für die Kontrolle von Gasgemischen in Fahrzeugmotoren oder von Atemgas mittels CMUT-Sensoren. Es wird davon ausgegangen, dass die vielen Kandidaten, die eine sensitive Rolle einnehmen, eine breite Anwendungsskala zur selektiven und sensitiven Bestimmung oder Prüfung enorm vieler Analyten und Bereiche eröffnen.

---

## Symbols

---

$A$	active area
$C_0$	electrical capacitance across the electrodes
$C_g$	vapor concentration in the gas phase
$C_p$	capacitance from parasitic effects
$C_s$	vapor concentration in the sorbent phase
$C_v$	vapor concentration
$C_x$	capacitance of capacitor
$f_0$	start frequency
$f_r$	resonant frequency
$G$	conductance
$G_{\max}$	maximum value of conductance
$h$	thickness of coating
$K$	partition coefficient
$L_x$	inductance of inductor
$m$	mass
$M_v$	molar mass of vapor
$\varnothing$	diameter
$P_0$	saturated vapor pressure
$R$	universal gas constant
$R_1$	resistance
$R_p$	resistance from parasitic effects
$R_x$	resistance of resistor
$T$	temperature
$T_g$	glass transition temperature
$V$	molar volume
$v_q$	acoustic wave velocity of quartz
$\gamma$	surface tension
$\Delta C$	change of concentration
$\Delta f_r$	resonant frequency shift
$\Delta f_r^{\text{NP}}$	frequency shift due to NP coating
$\Delta f_s$	frequency shift due to coating
$\Delta f_v$	frequency shift due to vapor sorption
$\Delta f_w^{1/2}$	full width at half height of conductance spectrum
$\Delta m$	change of mass
$\Delta T$	change of temperature
$\Delta \varepsilon$	change of permittivity
$\varepsilon_r$	relative permittivity

---

$\theta$	wetting angle
$\mu_q$	shear modulus of quartz
$\rho_q$	density of quartz
$\rho_s$	density of coating

---

# Table of Contents

---

<i>Acknowledgement</i> .....	<i>i</i>
<i>Abstract</i> .....	<i>iii</i>
<i>Zusammenfassung</i> .....	<i>v</i>
<i>Symbols</i> .....	<i>vii</i>
<i>Table of Contents</i> .....	<i>ix</i>
<b>1 Introduction</b> .....	<b>1</b>
<b>2 Fundamentals</b> .....	<b>4</b>
2.1 Chemical sensors.....	4
2.1.1 Common working principle of acoustic wave sensor.....	5
2.1.2 Sensor response mechanism and assessment of sensitivity.....	6
2.1.3 Sensing materials.....	7
2.1.4 Deposition strategies for sensing materials and localized deposition.....	8
2.2 LFE sensor.....	10
2.3 CMUT.....	10
2.3.1 Operating principles.....	11
2.3.2 Development and applications.....	11
<b>3 Preparation of in situ Sensing Film Based on MIP Technology.....</b>	<b>13</b>
3.1 Introduction.....	13
3.2 Experimental.....	14
3.2.1 Reagents and instruments .....	14
3.2.2 Polymerization process.....	15
3.3 Results and discussion.....	16
3.3.1 Photo-initiator.....	16
3.3.2 Porogen and solvent.....	16
3.3.3 Features of MIP films following different recipes.....	17
<b>4 Preparation and Modification of NPs and Sensors.....</b>	<b>19</b>
4.1 Reagents and instrumentation.....	19
4.2 Synthesis and features of NPs.....	20
4.2.1 Preparation and functionalization of NPs.....	20
4.2.2 Features of NPs.....	21
4.3 Utilization of LFE sensor and silicon wafer for preliminary work.....	21
4.4 Preparation of LFE sensors.....	22
4.5 Surface modification of LFE, CMUTs and silicon wafer.....	23
4.5.1 Surface cleaning of the substrates.....	23
4.5.2 Pre-modification.....	24
4.5.3 NP layer preparation.....	27

4.5.4	<i>Localized Deposition of second layers.....</i>	<i>28</i>
4.5.5	<i>Deposition of ceramide AP with LB film trough.....</i>	<i>30</i>
<b>5</b>	<b><i>Physical Characterization of Films.....</i></b>	<b><i>32</i></b>
5.1	<i>Instruments.....</i>	<i>32</i>
5.2	<i>Morphology of NP coating from different deposition approaches.....</i>	<i>32</i>
5.2.1	<i>LB-like deposition.....</i>	<i>32</i>
5.2.2	<i>Localized deposition of NPs through photolithography and self-deposition..</i>	<i>33</i>
5.2.3	<i>Spin coating.....</i>	<i>34</i>
5.3	<i>Pre-modification effect.....</i>	<i>36</i>
5.4	<i>Morphology of complex layers from different deposition approaches.....</i>	<i>38</i>
5.4.1	<i>Drop coating on NP layer.....</i>	<i>38</i>
5.4.2	<i>Aerosol jetting on NP layer.....</i>	<i>39</i>
<b>6</b>	<b><i>Chemical Characterization by Impedance Analysis.....</i></b>	<b><i>42</i></b>
6.1	<i>Measurement setting.....</i>	<i>42</i>
6.2	<i>Coating influence on sensor behavior.....</i>	<i>43</i>
6.2.1	<i>The behavior of LFEs.....</i>	<i>43</i>
6.2.2	<i>The behavior of CMUTs.....</i>	<i>45</i>
6.2.3	<i>The behavior of NP-coated CMUTs with ceramide AP membrane.....</i>	<i>47</i>
<b>7</b>	<b><i>VOC Measurement.....</i></b>	<b><i>49</i></b>
7.1	<i>Measurement setting.....</i>	<i>49</i>
7.2	<i>Gas application system.....</i>	<i>50</i>
7.3	<i>Mass sensing verification.....</i>	<i>50</i>
7.4	<i>Performance of LFE gas sensor.....</i>	<i>51</i>
7.4.1	<i>Modification effect.....</i>	<i>51</i>
7.4.2	<i>Real-time response.....</i>	<i>52</i>
7.4.3	<i>Sensitivity and selectivity to various VOCs.....</i>	<i>53</i>
7.4.4	<i>Stability.....</i>	<i>54</i>
7.5	<i>Performance of CMUT gas sensor.....</i>	<i>54</i>
7.5.1	<i>Response and recovery time.....</i>	<i>57</i>
7.5.2	<i>Sorption isotherm analysis.....</i>	<i>58</i>
7.5.3	<i>Sensitivity.....</i>	<i>60</i>
7.5.4	<i>Reproducibility and aging effects.....</i>	<i>62</i>
7.5.5	<i>Response mechanism analysis.....</i>	<i>62</i>
7.5.6	<i>Equilibrium analysis on vapour sorption.....</i>	<i>68</i>
7.5.7	<i>Study of pre-condition.....</i>	<i>69</i>
7.5.8	<i>Tentative kinetics study on vapour sorption.....</i>	<i>73</i>
7.5.9	<i>Anomalous response analysis.....</i>	<i>75</i>
7.6	<i>Conclusion.....</i>	<i>76</i>
<b>8</b>	<b><i>Conclusion.....</i></b>	<b><i>78</i></b>
	<b><i>References.....</i></b>	<b><i>81</i></b>

---

# Chapter 1

## Introduction

---

Demand is increasing for monitoring various chemical compounds in environmental, medical, industrial and numerous other fields. Chemical sensors serve as tools for such detection by transducing chemical signals into appropriate electrical signals. They can be fabricated as small, robust, and inexpensive devices and used as bio/chemical probes for investigating and controlling bio/chemically significant processes in both gaseous and liquid phases.

Typical sensor consists of two major components: one is electrical part to convert physical, chemical or biological response into a signal that can be measured, and the other is bio/chemical part, usually manifesting itself as an additional layer on the surface of sensor and selectively responding to ingredients in surrounding by altering its properties.

One specific class of sensors based on piezoelectricity has been predominantly used for chemical analysis, process monitoring, ultrasonic imaging etc.. Natural or man-made piezoelectric materials such as quartz crystal has been broadly studied and applied in various types of acoustic wave sensors. By comparison, the widespread recognition and vigorous development of capacitive sensors just began in the 1990s, although the idea of electrostatic transducers is as old as the early piezoelectric transducers. Even so, the current capacitive ultrasound transducers have been believed to compete with piezoelectric transducers in many respects, largely thanks to the sophisticated micro electronic mechanical system (MEMS) technology. The capacitive micromachined ultrasonic transducer (CMUT) is an outstanding representative on the basis of MEMS technology and has behaved as a promising implement for medical imaging. The innate multi-channel, multi-membrane structure of CMUT allows for many promising applications in the sensor field.

With regard to the bio/chemical part of sensor system, sensing layers which are uniform, continuously defect-free, and stable are crucial for the chemical microsensor development, plus the sensitivity and selectivity of the prepared films. In this sense, however, most sensing film fabricating methods are problematic in producing nanometer thick layers and have minimum control in film properties.

The tremendous significance of molecular recognition in various applications gives rise to the incentive to develop materials interacting with other molecules with high specificity. Nevertheless, the development of new materials, one-at-a-time for particular cases, could be costly and time consuming.

Alternatively, realization of high selectivity can be achieved by building up sensor array system, where a set of sensors combined together to provide information for discriminating

multicomponents. As to this aim, localized deposition of sensing agents with varied functions is required, especially for sophisticated microsensors like CMUT, which has an array-on-a-chip structure. It is for this reason that we set out to develop a versatile approach for designing a sensor prototype that allows a diversity of materials to readily modify multisensors and offer particular sensitivity while afford predictable chemical signals and physical characteristics.

When it comes to CMUT, such conception can be expressed as modifying respective channels with chemically sensitive materials of different recognition ability.

In bio/chemical sensor industry, manufactured sensors must be calibrated prior to use in order to ensure the comparability and repeatability between sensors. However, calibration usually behaves as a time and money-consuming work and is viewed as a common bottleneck in sensor fabrication. Thus it is frequently a major challenge of setting up a reproducible coating scheme to minimize or even preclude calibration in mass production.

In this work, a 2-step modification strategy has been developed for sensor modification with deposition of nanoparticles on the bottom plus other sensitive layers on the top. Such double-layer system is aiming to overcome the need of complicated calibration and regarded as the most distinct feature for the obtained CMUT sensor. Besides, localized deposition has been readily achieved in the second coating step by using aerosol jetting technique. Sensors prepared by this procedure have exhibited their vapor detection ability with satisfied reversibility and recognition capacity.

Selection of target volatile organic compounds (VOCs) originates from two considerations. Firstly, renewable fuel utilization has gained more and more attention due to the increasingly serious global energy crisis and environmental pollution. Bioalcohols have been serving as one major form of biofuels being sold and distributed around the world. Besides, a special type of so-called “flexible-fuel vehicle” (FFV) has been developed, which operates on variable mixture of gasoline with alcohols [1, 2]. Therefore, the detection of alcoholic compounds has become a hot topic, especially by sensor devices which are usually small-dimensional, and thus suitable to fit into automobile vehicles [3-5].

Secondly, sample selection lies on the basis of breath analysis. Some of organic constituents in exhaled breath have been viewed as biomarkers [6-8], for they can indicate an individual’s health status, pre-clinical metabolic abnormality and presence of pathogenic sources. Take acetone for example, which is associated with dextrose metabolism and lipolysis, as well as severe diabetics [9, 10]. Breath sensor development shows great potential in clinical diagnosis as a non-invasive approach [11, 12], characterizing low cost, small size and user friendliness.

The subgroups of VOCs which have been paid special attention in this research are: alcohols (e.g. 1-propanol, ethanol and methanol), small aromatic compounds (e.g. toluene and *p*-xylene), and ketones (e.g. acetone). Other representative reagents belonging to

several subsets of solvent have also been tested, including alkanes (e.g. *n*-hexane, *n*-octane), chlorinated hydrocarbons (e.g. chloroform), and water.

The main tasks in this thesis are structured according to the following sequence.

The work starts with the fundamental section (Chapter 2), including an introduction of CMUT, a general depict of chemical sensor and a summary of the mostly common technologies for fabricating sensors. The lateral filed excited (LFE) sensor is also introduced for it has been employed as an effective preliminary tester for CMUT.

Attempt to prepare highly sensitive films through the concept of molecularly imprinted polymer (MIP) is announced in Chapter 3.

The followed chapter (Chapter 4) describes the scheme of preparing chemical sensor based on LFE quartz crystals and CMUT. As LFE sensor also work as a new-developed transducer and has its own peculiarity and requirement with respect to coating materials, relevant explanation is made to illustrate this issue. Preparation, functionalization and deposition approaches of NPs are elaborated firstly and utilization of sensitive materials is stated in the latter part. Modification of an NP-coated CMUT with a bioactive lipid, ceramide AP, is also presented in this chapter, as an example of the potential of CMUTs for pharmaceutical applications.

The physical and chemical characterization of the obtained sensors is reflected in Chapters 5 and 6. The morphology of coatings and the influence of attempted operation are described. In Chapter 7, the practical application of the modified sensors as gas detectors has been thoroughly studied and the mechanisms of sensing process are analyzed so as to found an elementary guideline in sieving sensitive materials for specific organic solvent species. The performance parameters, including selectivity, sensitivity, response/recovery time, reproducibility and working lifetime are reported. In this chapter, some preliminary studies on sensing process is also reported, which includes long time and repeating gas measurement to find out real reasons behind experimental phenomena and provide pertinent suggestions on practical operation.

Conclusions to the work and future prospects of the 2-layer CMUT sensors are summarized in Chapter 8.

---

## Chapter 2

# Fundamentals

---

Sensors have been playing an important role in a great many fields, encompassing industry, medicine, military, civil use and so on. Its importance will be increasingly evidenced with development of our society and sensor system itself.

### 2.1 Chemical sensors

General definition of sensors has been acknowledged as: A sensor is a device that receives a stimulus and responds with an electrical signal. The stimulus is often a nonelectrical value like quantity, property, condition etc., and the output signal of sensor may be in the form of voltage, current, or charge. These may be further described in terms of amplitude, frequency, phase or digital code (Figure 2-1). In particular, chemical sensors are devices that characterize a chemical state by transforming chemical information (e.g. a single concentration or total composition) into an analytically useful signal. One of the ways to classify various chemical sensors can be based on their transducing principles, such as electronic, electrochemical, mass sensitive, magnetic, optical transducers and so on. Acoustic wave sensors on the ground of mass sensitivity in gas phase are elaborated in the following sections.

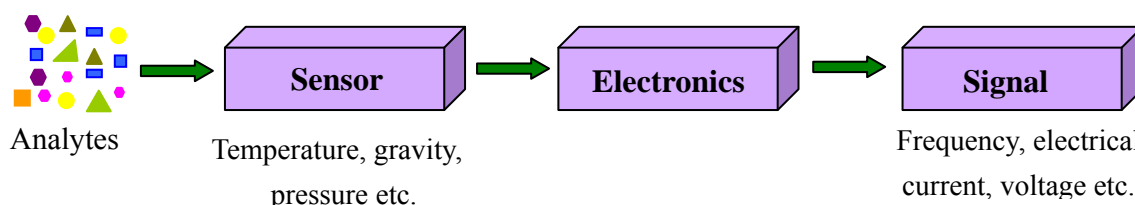


Figure 2-1: Schematic demonstration of sensor.

Generally, chemical acoustic wave sensors are fabricated by modification of the transducer surface with a coating which can physically or chemically interact with analytes. The coated materials must be nonvolatile to remain on the sensor, mostly in the form of a thin film, ideally allowing rapid analyte diffusion throughout the film. Key issue with respect to modifying individual sensors is the extent to which the applied component enhances the sensitivity and selectivity of the sensor, while affording reversibility, reproducibility and long-time stability.

Despite of the abundant availability of various sensing matrixes, most of them are non- or semi-selective to sorbed mass, although they generally promote the sorption of analytes at the surface. In this regard, sensor arrays offer advantages including sensitivity to a wider

range of analytes, improved selectivity, simultaneous multicomponent analysis and the capability for analyte recognition rather than mere detection. In sensor array applications, it is particularly important that sensor materials provide reversible and reproducible performance, so that response patterns are consistent over time. Arrays can be empirically constructed using sets of commercially-available or self-synthesized substances, like polymer, supramolecule etc., and in many applications these arrays are very effective [13-16].

Sensors should not only be designed to selectively detect trace analytes, but should also be small, portable, and inexpensive. Sensor systems that can be adapted easily to various detection demands are also advantageous. Microelectronic chemical sensor or sensor array meet the size requirement and they can be very sensitive as well.

### 2.1.1 Common working principle of acoustic wave sensor

Acoustic wave sensor can be categorized as bulk acoustic wave (BAW), surface acoustic wave (SAW), flexural plate wave (FPW), shear horizontal acoustic plate-mode (SH-APM) sensors [17, 18]. They have the operating principle in common that metal electrodes on piezoelectric substrate convert electrical energy into mechanical energy in the form of acoustic wave. For sensor applications, such device is usually placed in an oscillating circuit, where it functions as a resonant element. In mass-sensitive sensing, resonant frequency is tracked and it shifts according to the mass change on transducer surface originating from, for example, sorption of analyte molecules at the sensor interface.

Quantitative relations between mass deposition on sensor surface and the resulting change in fundamental oscillation frequency of the resonator have been built up for different sensor types. Only two of them are introduced here, for the transducers involved in this research are quartz crystal microbalance (QCM) and capacitive micromachined ultrasonic transducer (CMUT), belonging to BAW and FPW sensors, respectively.

The correlation between frequency shift and mass change of BAW sensor has been precisely described using the well-known Sauerbrey equation [19], shown in Equation (2.1).

$$\Delta f_r = -\frac{2f_0^2}{A\sqrt{\rho_q\mu_q}} \Delta m \quad (2.1)$$

where  $\Delta f_r$  and  $\Delta m$  are changes of resonant frequency and mass,  $f_0$  is the fundamental oscillation frequency,  $\rho_q$  and  $\mu_q$  are the density and shear modulus of quartz, and  $A$  is the active area.

The other one for FPW sensor [20] is illustrated in Equation (2.2).

$$\Delta f_r = \frac{f_0}{2\rho hA} \Delta m \quad (2.2)$$

where  $\rho$  and  $h$  are the density and thickness of the substrate.

### 2.1.2 Sensor response mechanism and assessment of sensitivity

It is usually a challenge to find optimal interactions between analyte and sensing agent, in order to keep sensitivity and meanwhile avoid irreversible sorption. A variety of non-covalent interactions, compared with covalent ones, are dominant types which widely exist in nature and have been extensively applied in chemical sensing. For instance, the capability of vapors to gain van der Waals force to transfer from the monomeric state in the gas phase to the condensed phase of the sensing films, serves as the primary driving power for sorption. Other non-covalent interactions include dispersion interactions, dipole-induced dipole interactions, dipole-dipole interactions, and hydrogen bonding.

Films with preformed cavities or channels provide other promising sensing concepts. There are substances with such conformational cavities, for instance, cyclophanes (poly cyclic aromatic hydrocarbons), cyclodextrines, calixarenes, fullerene molecules and so on. Filling the cavities often cost little or even no energy [21, 22], thus sorption of analyte onto these molecular components can proceed in an easy manner and favorable interactions between them allow for potential selectivity on the basis of size, shape and group branches. These receptors often own good molecular flexibility, facilitating an optimized adaptation to a large variety of guest molecules.

After exposure of sensor to certain analytes, a final equilibrating sorption is built in the sensing interface. The resulting equilibrium can be quantified by the partition coefficient,  $K$ , which describes the distribution of vapor from the gas phase into a sorbent phase (coating of the sensor) and thus indicates the effect of the interaction on sensing capacity between vapor and sensing material.  $K$  is defined as the ratio of the vapor concentration in the gas phase ( $C_g$ ) to that in the sorbent phase ( $C_s$ ) at sensing equilibrium status.

$$K = C_s / C_g \quad (2.3)$$

The value of  $K$  can be determined by acoustic wave devices, as it is related to the frequency change when vapor is sorbed into the coating, which is given in Equation (2.4).

$$K = \frac{1}{n} \frac{\Delta f_v \rho_s}{\Delta f_s C_g} \quad (2.4)$$

where  $\Delta f_v$  is the frequency shift as a result of vapor sorption and corresponding mass change,  $\Delta f_s$  is the frequency shift due to the deposition of sorbent onto sensor,  $\rho_s$  is the density of the sorbent.

In many applications, analyte sorption on or in the coating is considered as pure mass accumulation, and expressed as a shift of resonant frequency of the oscillator; the sensor is assumed to work as a microbalance and the multiplier  $n$  in Equation (2.4) is equal to 1 for pure mass responses. Although this assumption is surely acceptable for several applications, non-gravimetric effect should be taken into account for coatings that do not fulfill the

requirement of keeping acoustically thin [23-27]. Vapor sorption on or in films could swell the materials and thus change their viscoelastic properties. In this case, the frequency shift is amplified by analyte-induced modulus changes and  $n$  will be equal to that amplifying factor [28]. Calculation of gathered mass or related parameters such as partition coefficient with a linear gravimetric approximation is hardly possible. To simplify the study, we firstly assumed that  $\Delta f_v$  arises entirely from gravimetric regime and viscoelasticity contributes to no effect, i.e.  $n = 1$  [29]. The calculation of  $K$  value is given by Equation (2.5).

$$K = 82.057 \times T \times \frac{\Delta f_v \rho_s}{\Delta f_s C_v M_v} \quad (2.5)$$

where  $T$  is thermodynamic temperature in Kelvins (K),  $C_v$  is the vapor concentration (mL/mL),  $M_v$  is molecular weight of the vapor.  $K$  is strongly temperature-dependent, because sorption normally decreases with increasing temperature. The more strongly the vapor is sorbed, the more  $K$  decreases with increasing temperature. In our study, the operation temperature was mostly around 25°C so that  $T$  was 298 K. The atmosphere pressure was approximated as 1 standard atmospheric pressure (101325 Pa). The analyte vapor in the carrier gas stream was assumed behaving like an ideal gas.

### 2.1.3 Sensing materials

A great variety of sorbent phases have been investigated and incorporated as sensitive layers on the surfaces of chemical sensors to gain sensitivity and selectivity for chemicals in gas or liquid phase. In all cases the requirements of the sensor are the same: the sensitive material must bind the desired analyte in preference to all competing species and the sensor can respond to the analyte in a measureable form.

Among them, functional polymers are under the most vigorous study because of their film-forming properties, good chemical and thermal stability toward many environmental conditions, and versatility of functional groups and backbone structures. Especially polymers of low glass transition temperature ( $T_g$ ) are more attractive owing to the high diffusion rates of small molecules in them [30, 31].

Supramolecules like dendrimer and cavitand have also been brought into the spotlight due to their far higher capacity to collect and concentrate analytes per certain unit [32-34]. In sensing applications, supramolecules are selected according to their size, shape and charge complementarity with the analyte of interest and “host-guest” complexes can form relying on the forces or interactions between them. Most of the interactions are non-covalent ones, like electrostatics, hydrogen bonding, and van der Waals forces.

Gas chromatographic stationary phases such as organosiloxane polymers (polysiloxanes) are useful as well [35]. Polysiloxanes consist of an inorganic silicon-oxygen backbone with organic side groups attached to the silicon atoms. By varying the organic groups, polysiloxane can be adopted with a wide variety of properties and compositions.

Biomaterials have attracted special attention due to their unparalleled selectivity [36]. However, such species like antibodies and enzymes often suffer inherent limitations including costliness, poor stability and short life span.

Besides using those commercial or natural sorptive agents, there remain compelling reasons to synthesize and adapt material formulations with desired properties [37-40]. It is possible to tune physical properties such as  $T_g$ , thickness, film morphology, porosity, and chemical properties like polarity, solubility to analyte samples, chemical and steric structure to enhance performance on various sensing platforms.

Molecular imprinting is an emerging methodology for the preparation of polymeric materials containing recognition sites of predetermined specificity. The molecularly imprinted polymers (MIPs) synthesized in the presence of analyte molecules (template), are frequently referred to as artificial antibodies [39, 40]. Studies have shown that MIPs exhibit a surprisingly high degree of stereo- and region-specific selectivity, making the commercial use of such tailor-made separation materials a realistic possibility in several areas, such as chiral separation of bioactive molecules and as antibody mimics [41, 42]. Although very promising in occupying MIPs for modification of QCM, this technique failed to generate sufficiently thin films suitable for CMUT sensors. Generally speaking, the high cross-linking degree of MIPs results in features such as high  $T_g$  and low permeability. More details and related work on MIPs have been elucidated in Chapter 3.

#### **2.1.4 Deposition strategies for sensing materials and localized deposition**

Fabricating ultrathin polymer films with defined structures and properties such as film thickness, uniformity, stability, and reproducibility is a perpetual pursuit in sensor industry. Simple coating approaches include solvent casting (e.g. drop, spraying, and spin coating) and dip-coating [43, 44]. In general, direct coating only render weak physical bindings in sensor-coating interface. For stronger adhesion, it is preferable to apply chemical modification to immobilize sensing matrix. More elaborate techniques have been developed such as Langmuir-Blodgett film (LB film) preparation [45, 46], physical or chemical vapor deposition [47, 48], and in situ polymerization through electrochemical-, photo-, or thermal-initiation [47, 49, 50]. However, controlled growth of stable polymer films at nanoscale level remains a challenge in the above mentioned techniques, which prompts adaptation of conventional coating techniques and quests for new methods and suitable materials. Some modern technologies, like ink-jetting, dip-pen etc. have been employed to modify sensors as well. The major problem accompanied is that the films appear to be thicker at the periphery and thinner in the center of the deposit due to drying effect [51].

As mentioned above, it is very difficult to find a selective coating for a given analyte. Preparing sensor array system serves to be an eligible way to achieve multiple recognition ability. As microsensor designs become smaller or more complex, accurate location and alignment is indispensable to distribute sensing matrix on sensor top in non-contact manner.

Additionally, cross contamination should be avoided when different materials are positioned on the same chip with sensor array structure. Photolithographic technology represents an attractive approach in defining polymers in desired domains. However, the majority of conventional polymeric photoresists are not usable as sensing agent because they have been prepared with properties different from those intended for chemical sensing. Therefore, they usually lack active sensing function.

Some widely applied deposition strategies have been listed in Table 2-1 with several factors to evaluate their attributes.

Nr.	Deposition strategy	Uniformity	Localized deposition	Effort	Deposition steps
1	Spin coating	+	-	+	1
2	Air brush	-	-	+	1
3	LB-film, SAM	+	-	-	1
4	1-3 combined with lithography	+	+	-	1-N
5	Drop coating, ink-jetting, aerosol-jetting	-	+	+	1

Table 2-1: Commonly employed deposition strategies for sensor production.

Sign “+” refers to a positive attitude towards corresponding factor while sign “-” stands for a negative meaning.

Spin coating generally involves dissolving or dispersing the material to be deposited in a solvent, dispensing the solution or suspension onto a flat substrate, and spinning the substrate until the solvent wholly evaporates, leaving behind a thin coating of the solute. On account of the good control in film thickness and homogeneity that the technique affords, spin coating has gained considerable attention and yielded broad application. However, similar to air brush and LB-film or SAM techniques, spin coating is hardly possible to generate localized deposition; instead, microscopic patterning technique is needed. Nr. 4 in Table 2-1 represents an collaboration of one of the first three ways together with lithography. Such process is usually laborious and subjected to poor compatibility with regard to sensing materials, as stated earlier. Dropping or jetting approaches are outstanding in preparing geometrically precise films, especially by making use of some modern instruments. It is also an easy-operating and flexible method and appealing as long as the uniformity problem could be overcome or reduced.

Since most functional polymers applied have poor selectivity for different analytes, the exploitation of highly discriminating sensor remains the main challenge. Looking for or synthesizing receptor materials are one part of the story, while constructing feasible sensor arrays serves as an alternative or complimentary way to satisfy the selectivity requirement.

## 2.2 LEF sensor

The quartz crystal microbalance (QCM) is a simple, cost effective and high-resolution sensing tool which has covered a wide range of applications [52-54]. The quartz crystal resonators used are usually driven piezoelectrically by an electrical field directed along the thickness axis, so called as thickness field excitation (TFE). Much less common is the excitation by a field in the plane of the plate, named as lateral field excitation (LFE). Different from the conventional TFE resonators equipped with two electrodes on both crystal surfaces, in LFE system, the electrodes are located on one side of crystal while the opposite surface is left bare, acting as sensing surface (Figure 2-2). One reason for including LFE sensor in the work is the fact that sensing surface is bare crystal instead of having metal electrode, which resembles the silicon surface with respect of morphology, making any modification work done on LFE sensor surface easier to be extended to CMUT. Other advantage of using LFE sensors is that they are relatively simple-to-operate devices and produce frequency signals with far lower noise and much higher quality factor in comparison to CMUTs. Despite their inherent sensitivity limits arising from low resonant frequency (5 MHz), they proved, however, to be suitable pretesting sensor devices in quickly screening candidate coating materials and more importantly, providing information in characterizing feature of coating films.

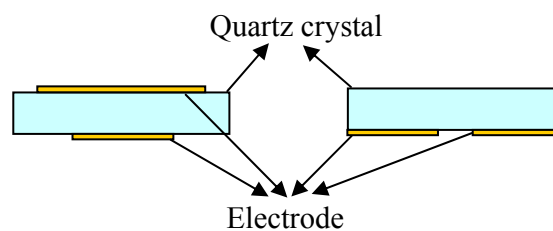


Figure 2-2: AT cut quartz disk driven by thickness field excitation (left) and lateral field excitation (right).

## 2.3 CMUT

A new type of ultrasonic sensor, which is named as capacitive micromachined ultrasound transducer (CMUT), has recently come forth as an alternative to the conventional piezoelectric sensors, owing to its distinctive characteristics such as wide immersion bandwidth, ease of fabricating large arrays, ability to be integrated with supporting electronic circuits, expected reduction of production costs and so forth [55-58]. A CMUT cell is simply a capacitor, composed of a metallized membrane (top electrode), suspended above a heavily doped silicon substrate (bottom electrode), as shown in Figure 2-3. In between is the dielectric medium (either vacuum or air gap). An insulating layer is included to prevent the two electrodes from shorting in case of contact. A single transducer element

usually consists of many capacitor cells electrically connected in parallel.

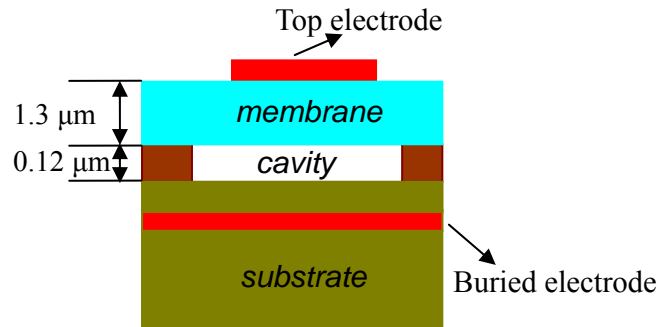


Figure 2-3: Cross view of a single CMUT cell structure.

### 2.3.1 Operating principles

Although both the name and the appearance of CMUT categorize it into capacitive sensor, it works on the foundation of acoustic wave vibration, in particular, flexural plate wave (FPW). The relationship between the frequency shift and the mass loading onto the membrane has been described in Chapter 2.1.1., and a simplified expression is

$$\frac{\Delta f_r}{f_0} \approx -\frac{\Delta m}{2m} \quad (2.6)$$

which is similar to most mass sensitive resonant sensors.

Equation (2.6) indicates that high sensitivity of a sensor requires a high resonant frequency of the membrane,  $f_0$ , and a low mass of the resonant structure,  $m$ . For low limit of detection (LOD), low noise, i.e. high quality factor, is also required.

The operating principle of CMUT is the well-known electrostatic transduction mechanism. The membrane is deflected by DC bias and actuated in AC bursts to generate ultrasonic waves. Efficient electromechanical coupling is achieved as a result of the strong electric field in the gap. External medium can influence the oscillation of the membrane in the form of changes in capacitance and frequency. Our work tracked the frequency alteration of membrane vibration, caused by mass loading change onto the membrane.

### 2.3.2 Development and applications

Since CMUTs were firstly introduced by Khuri-Yakub and coworkers [59, 60], they have experienced rapid development concerning fabrication, characterization, modeling of the transducing process etc. [58, 61-63]. Results over the last decade demonstrate that traditionally fabricated CMUTs modified with respect to such design factors as device size, membrane radius, configuration, thickness, shape, gap height, insulating layer, and operating mode, have gained achievement to optimize working performance, in terms of

bandwidth, frequency range, dynamic range, maximum output pressure and receive sensitivity.

Although the operating idea of generating acoustic waves by the electrostatic attraction force is very old, but the highly advanced MEMS technology allows the realization of miniaturized transducers consisting of a large number of membranes with precisely controlled geometrical and mechanical properties. 1D and 2D CMUT arrays with different number of elements have been successfully designed, fabricated and applied to get 2D or 3D images [57, 64, 65].

CMUTs are originally developed for conventional medical and underwater ultrasonic imaging and developed as chemical sensors recently [66-68]. Robust structure allows their application in harsh circumstances.

The intrinsic attributes of CMUTs in integrating many cells on one chip and better acoustic matching lead to an improved efficiency and reliability. Particularly, such multi-membrane, multi-element arrangement provides the possibility of manufacturing sensor arrays for detecting chemical mixture. The gaps between the electrodes can be made in submicron range and the size of the membranes is on the order of tens of microns and the thickness is around 1-2 microns. These achievements allow for establishing powerful electric fields and thus enhance the transduction efficiency and make CMUTs competitive with piezoelectric transducers in terms of mass sensitivity.

As the multisensor conformation of CMUT has been integrated in high similarity, which is a premise to keep quality factor in using CMUT as sensor array. The critical issue is to prepare uniform coatings with comparable mass loading on individual sensor element to avoid any decrease of quality factor.

The demands in developing well-controlled sensor array made up of ultrathin sensing films, as well as minimizing the need of calibration, motivate us to take advantage of different coating strategies comprehensively. Therefore, a 2-step deposition procedure has been put forward, where a bottom layer is formed on the whole sensor surface in the first step, and then various sensing materials are dispensed onto the bottom layer in a way of localized deposition.

An ideal choice of the bottom material is nanoparticles (NPs) which are able to form an uniform surface, serving as a platform for easy loading of the second coating and contributing to enhancement of sensitivity. Large number of substances can be involved as candidates of the second layers. They can be deposited onto selected areas of the NP layer to offer discriminative sensitivity in contact with diverse analytes. The requirement of the bottom NP layer is to be close packed with regular conformation. Such surface will prevent “coffee ring” structure of the second coating, thereby allowing for a similar mass loading onto each element (membrane). The size of NP is much less compared with a single vibrating membrane of CMUT (diameter around 20  $\mu\text{m}$ ), thus no negative influence on the acoustic wave vibration will be produced due to NP deposition.

## **Chapter 3**

# **Preparation of in situ Sensing Film Based on MIP Technology**

---

Exploration and development of sensing materials owning high discriminating ability has been being important but challenging tasks. The recognition phenomena in molecules' range have been extensively studied for various applications [69-71]. Chemical sensors based on artificially builtup host-guest interactions have attracted increasing attention and the term, molecularly imprinted polymers (MIPs), has been proposed along with the emergence of various synthetic MIPs [72, 73]. We expected to use the MIP technology to modify CMUTs into a sensor array system, where varied MIP films were in situ polymerized onto different sensor elements through photo-lithography.

In detail, the procedure included preparation of monomer solutions, coating of substrate with the solution, polymerization of the monomers under UV light with designed photo-mask, washing (development) of the substrate to get rid of the unpolymerized solution. Finally, MIPs imprinted with different template molecules formed onto the desired locations in accordance with the exposed placement to UV light.

Differently-constituted polymerization solutions have been tested to achieve the required consequence.

### **3.1 Introduction**

Molecular imprinting is a process where functional and cross-linking monomers are copolymerized in the presence of a target analyte, which acts as an imprinted molecular template. The functional monomers initially form a complex with the molecules through certain specific or non-specific interactions or bonds. Then polymerization is initiated and the complex conformation can be fixed in position by the highly cross-linked polymeric structure. The interactions between the monomers and templates are either non-covalent, such as hydrogen bonding, electrostatic forces, van der Waals forces, and hydrophobic interactions, or reversible covalent bonds. Subsequent extraction of the template produces binding sites that are sterically and chemically complementary to the analyte. In that way, a molecular memory is introduced into the polymer, which is now capable of selectively rebinding the analyte with a very high specificity (Figure 3-1).

Although potentially very attractive as recognition elements in chemical sensors, the widespread application of MIP-based sensors has not yet been realized, partly because of the difficulty in producing MIPs in the thin-film format that is required for coupling them to transducers. Practical issues co-occurred with preparing thin MIP film and the corresponding solutions are discussed in the following paragraph.

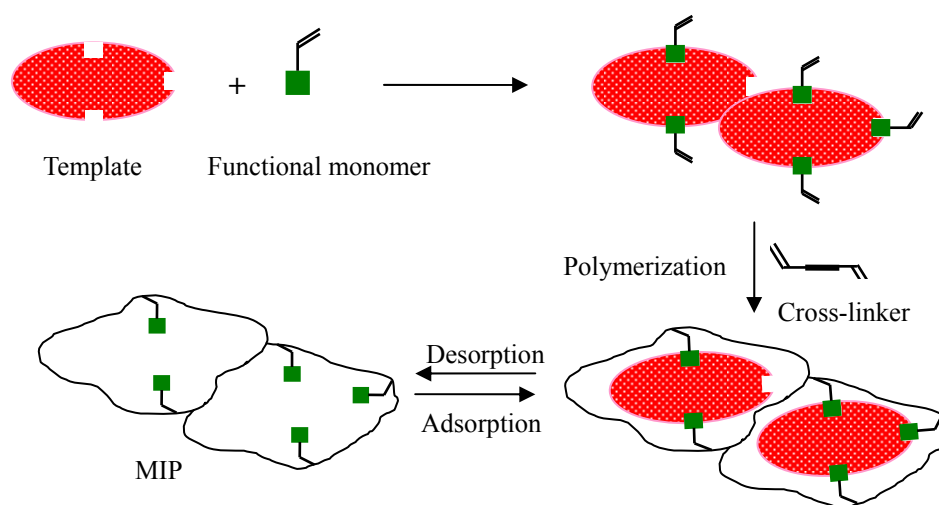


Figure 3-1: Principle of molecular imprinting.

The first barrier is the inhibitory effect on polymerization from oxygen, which can be overcome by employing a sealed reaction cell and purging pure nitrogen in to expel oxygen. Wettability, shrinking and adhesion of polymerizing solution and film on sensor surface often cause problems. Surface modification and specific cleansing of substrate are possible to tackle them. In respect of film thickness and reproducibility of the procedure, spin-coating can be a solution which has had a good fame in producing thin and controllable films in microelectronic industry. Photo-polymerization is preferred to thermal-initiation owing to its easy-handling and shorter reaction time, as well as the potential to fabricate sensor array by photolithography technique.

Most of the templates involved in MIPs are molecules with relatively large and rigid structure. As the sensors in this research aim to serve as gas detectors, the templates here are VOCs. One can assume that the imprinting sites could also be built up for these small molecules during polymerization if monomers are dissolved in the target solvents [74-76]. In addition, Haupt *et al.* reported using poly(vinyl acetate) (PVAc) and diglyme in their recipes, with the former serving as a sacrificial linear polymer and the later as solvent with low volatile rate [77, 78], to enhance the porosity and capacity of MIP films.

## 3.2 Experimental

### 3.2.1 Reagents and instruments

The reagents applied were: monomer: acrylic acid (MAA); cross linker: acrylate (EGDMA or TRIM); initiator: DMPA or AIBN; porogen: dodecanol, biphenyl or PVAc; low volatile solvent: diglyme; template: 1-propanol or toluene. MAA, EGDMA, TRIM, DMPA, AIBN, dedecanol, biphenyl, PVAc, diglyme were purchased from Aldrich or Fluka (Sigma-Aldrich Chemie GmbH, Germany). 1-propanol and toluene are from Carl Roth GmbH (Germany).

All the monomers and cross linkers were vacuum distilled to get rid of inhibitors. A commercial light-curing bonding resin, Heliobond, provided by Ivoclar Vivadent AG (Liechtenstein), was also tested. Major components in Heliobond are two kinds of methacrylate monomers (Bis-GMA and TEGDMA), photo-initiator (CQ) and photo-accelerator (tertiary amine). The full and short names of the above reagents have been listed in Table 3-1.

Abbreviation	Full Name
Bis-GMA	Bisphenol A glycerolate dimethacrylate
TEGDMA	Triethylene glycol dimethacrylate
CQ	Camphorquinone
PVAc	Poly(vinyl acetate)
MAA	Methacrylic acid
TRIM	Trimethylolpropane trimethacrylate
EGDMA	Ethylene glycol dimethacrylate
AIBN	Azo-bis-isobutyronitrile
DMPA	2,2-dimethoxy-2-phenyl-acetophenone

Table 3-1: Abbreviation and full name list for the reagents employed.

A home-built reaction cell was used for some of polymerization processes. A UV lamp (HRL<sup>®</sup>, Osram) was set in a container with a gas suction system to extract ozone produced by UV irradiation. Piezoelectric microgravimetric measurements were carried out with an HP 4395 A network analyzer (Japan) and AT-cut, plano-plano QCM of 10 MHz resonant frequency. The QCM sensors were either 14 mm diameter with Au contacts or 10 mm diameter with Ag films as electrodes. They were purchased from Lap-Tech (Canada) and AL-Elektronik Distribution GmbH (Germany) respectively. Both mechanically polished and unpolished crystals were applied. The sensitivity of prepared MIP films was tested with the gas measurement system which is described in Chapter 7.2.

### 3.2.2 Polymerization process

Here we only list out the optimized recipes in the use of the above reagents.

Recipe 1: EGDMA or TRIM + MAA + Template (7:2:7, in mole ratio) + DMPA (1 %, v/v);

Recipe 2: Heliobond + EGDMA or TRIM + Template + Dodecanol;

Recipe 3: DVB + Styrene + Template (210:90:100, in volume ratio) + DMPA (1 %, v/v).

In practice, all the ingredients in recipes were added together and purged with nitrogen for 5 minutes. Ultrasonication might be needed to make the solution homogeneous and get rid of gas bubbles. Spin coating was applied to cast the mixture onto substrates (silicon wafer or

QCM sensor). The substrates were then exposed under UV light (125 W) for 3 to 30 minutes. After polymerization, the substrates were rinsed with plenty of acetone and 2-propanol and dried with nitrogen flow. The thickness of the film was estimated with frequency shift. Some of the MIP films were further detected in terms of the gas sensitivity.

### 3.3 Results and discussion

#### 3.3.1 Photo-initiator

Initiator is a key component in UV cured system. It creates free radicals to initiate crosslinking of the groups with unsaturated bonding. The photoinitiators employed here are AIBN and DMPA, sourcing from two categories: azo-initiator and phenone initiator. DMPA has been reported to show highly efficiency in catalyzing photo-polymerisation of chemical prepolymers [78], e.g. unsaturated polyesters or acrylates, in combination with mono/multi-functional monomers. In this study, it was found that DMPA was able to finish the photo-polymerisation in less than 5 min, while using AIBN prolonged the time up to half an hour. Thus all the optimum recipes utilized DMPA as photo-initiator (except for Recipe 2, since Heliobond has its own initiator inside.)

#### 3.3.2 Porogen and solvent

In order to form binding sites with the analytes, a polymer has to carry certain level of porosity, which can be achieved by adding sacrificial porogens. Furthermore, diglyme was tried in the recipes in order to improve porosity of the prepared polymer [77, 78]. However, it turned out that the pre-polymerization mixture could not form continuous films in the presence of diglyme, rather than tiny convex spots onto substrates (Figure 3-2). PVAc and biphenyl failed to give good film morphology so dodecanol was utilized.

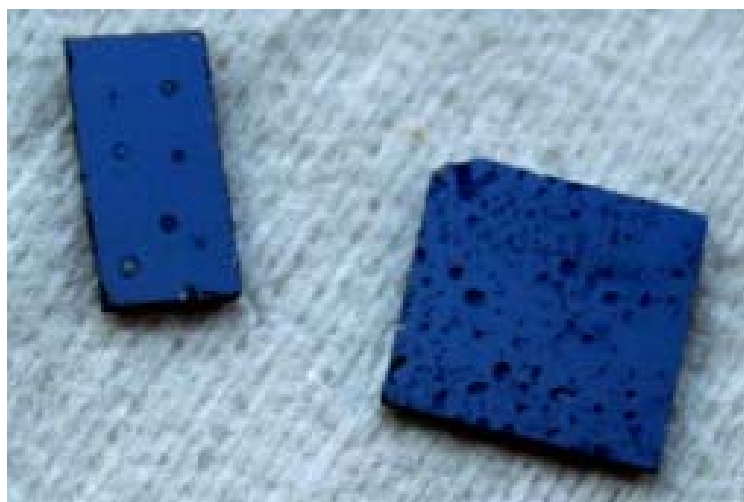


Figure 3-2: Photo of non-continuous MIP films.

### 3.3.3 Features of MIP films coming from different recipes

For Recipe 1, thin MIP films were obtained on QCMs with non-polished crystals, but on polished crystals or silicon wafers, it was difficult to keep the pre-polymerization mixture thinly spreading on the substrates. The solution inclined to shrink towards the center, resulting in thick films and even non-fully covered substrates, as that shown in Figure 3-3. Thickness like that ( $\sim 5 \mu\text{m}$ ) is unsuitable to be applied onto CMUTs since too much mass loading will create serious damping problem on vibration of the membranes, bringing about severely decreased  $Q$ -factors and deteriorating the resolution of the transducer. Moreover, the films indicated very poor response capabilities.

Concerning Recipe 2, by diluting Heliobond, a thin polymer film can be produced easily but no response ability was shown by the polymer. No functional monomer was included in the recipe and thus lacking of recognition sites may be the main reason for this.

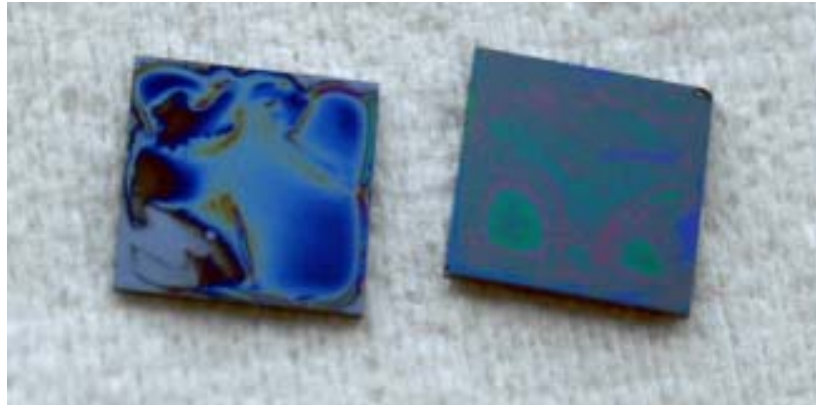


Figure 3-3: Photo of thick MIP films.

As to Recipe 3, thin films were fabricated and by using photomasks, polymer patterns could be formed on silicon wafer (Figure 3-4).

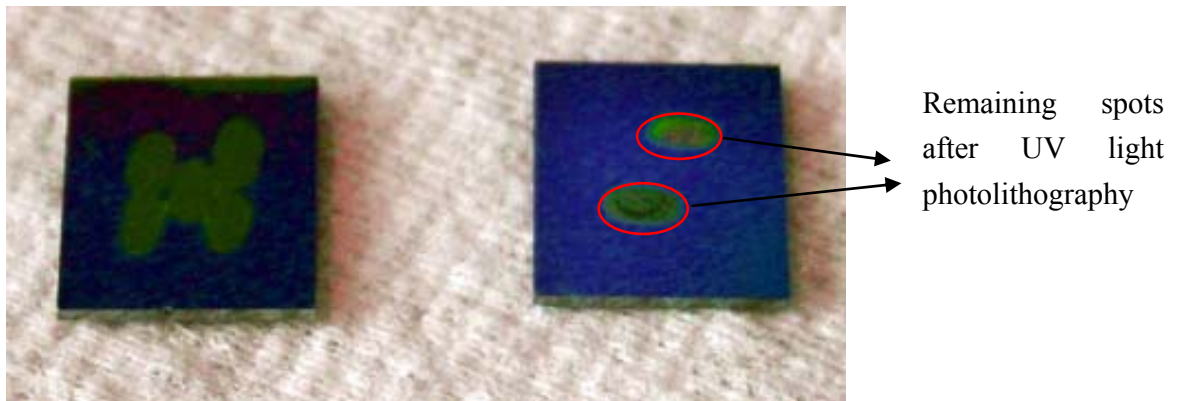


Figure 3-4: Photo of localized MIP films through UV photolithography.

The problems occurred were related to recognition ability and long-term stability. It seemed that the highly cross-linked polymer film was able to operate in strongly solvating liquids, but showed low swelling extent, which was actually the basis of responding to VOCs and generating signals. Besides, templating effect was not demonstrated either.

The functional groups of monomers, which are supposed to interact with template specifically, should remain in the MIP matrix after polymerization and be accessible and active when contact with template molecules again. However, since the templates in this research are all volatile solvents, they may have gone out of the matrix during polymerization procedure so that the expected interacting sites may not be generated or may be “closed”.

Summarizing the experimental results, one can conclude that, continuous and fairly thin films can be formed onto silicon substrates through careful optimization of agents participating in the polymerization. Secondly, localized deposition by use of UV photolithography is also achievable. However, synthesis of ultrathin layers is still problematic. Another issue is related to the sensing ability of the obtained films. Highly cross-linked copolymer failed to show corresponding sensitivity to their templates mainly due to the lack of specific recognition sites in the formed polymer structures.

In order to get satisfied films to modify CMUTs properly, both the instruments for initiating polymerization and the ingredients involved in the process need more research work.

## Chapter 4

# Preparation and Modification of NPs and Sensors

---

### 4.1 Reagents and instrumentation

Five substances were used as sensing agents. Their full name and abbreviations are listed in Table 4-2.  $\beta$ -CD and CA were provided by ASV GmbH (Bitterfeld, Germany); PEI was purchased from Fluka Chemie AG (Switzerland); OV 225 and PDMS were from Supelco Inc. and Aldrich Chem. Co. (USA), respectively. In the case of other reagents, styrene, divinylbenzene (DVB), potassium peroxodisulfate were obtained from Sigma (Sigma-Aldrich, Germany). Concentrated sulphuric acid (98 %) and hydrogen peroxide (35 %) were purchased from Carl Roth GmbH (Germany). All chemicals were of reagent grade or higher. Styrene and DVB were distilled before use and the rest of the reagents were used as received.

In addition, one type of bioactive lipid, ceramide AP was also applied to coat CMUT surface and the method utilized is Langmuir-Blodgett (LB) film deposition. Ceramide AP was kindly provided by the institute of pharmacy (Martin Luther University Halle-Wittenberg, Germany).

Mechanically polished AT-cut plano-plano 10 MHz quartz blanks and plano-convex 5 MHz quartz blanks with a diopter of 1.5 were purchased from Lap-Tech (Canada). Both crystal disks have a diameter of 14 mm.

The CMUT wafers (CT PS8, Siemens AG, Germany) have a resonance frequency in air around 20 MHz and have already cut into 10×3.5 mm pieces (Figure 4-1 a)). The chip was bound onto a 14×10 mm printed circuit board (PCB) made of epoxy resin, with aluminum wires used for connection of the elements (Figure 4-1 b)). Each chip consists of about 45 elements and the size of one element is 2.6×0.2 mm (Figure 4-1 c)). 82×7 cells make up one element and they are electrically connected in parallel. Each cell has a hexagonal surface with internally tangent diameter around 20  $\mu$ m (Figure 4-1 d)). The membrane of each cell is made of bulk silicon with thickness of 1.3  $\mu$ m and the air gap underneath is 0.12  $\mu$ m. A DC voltage (Statron, Germany) was utilized to provide a bias electric field for deforming membrane.

An aerosol jetter (M3D<sup>®</sup> Aerosol Jet<sup>™</sup> Deposition System, from Optomec, Inc., USA) was employed for high-resolution deposition of sensing materials, as well as localized modification. LB film assembling was undertaken using a Minitrough (KSV Instruments LTD, Finland).

The structure and size of crystalline copolymeric NPs were measured by SEM (S-4800, Hitachi, Japan), operating at an accelerating voltage of 15.0 kV.

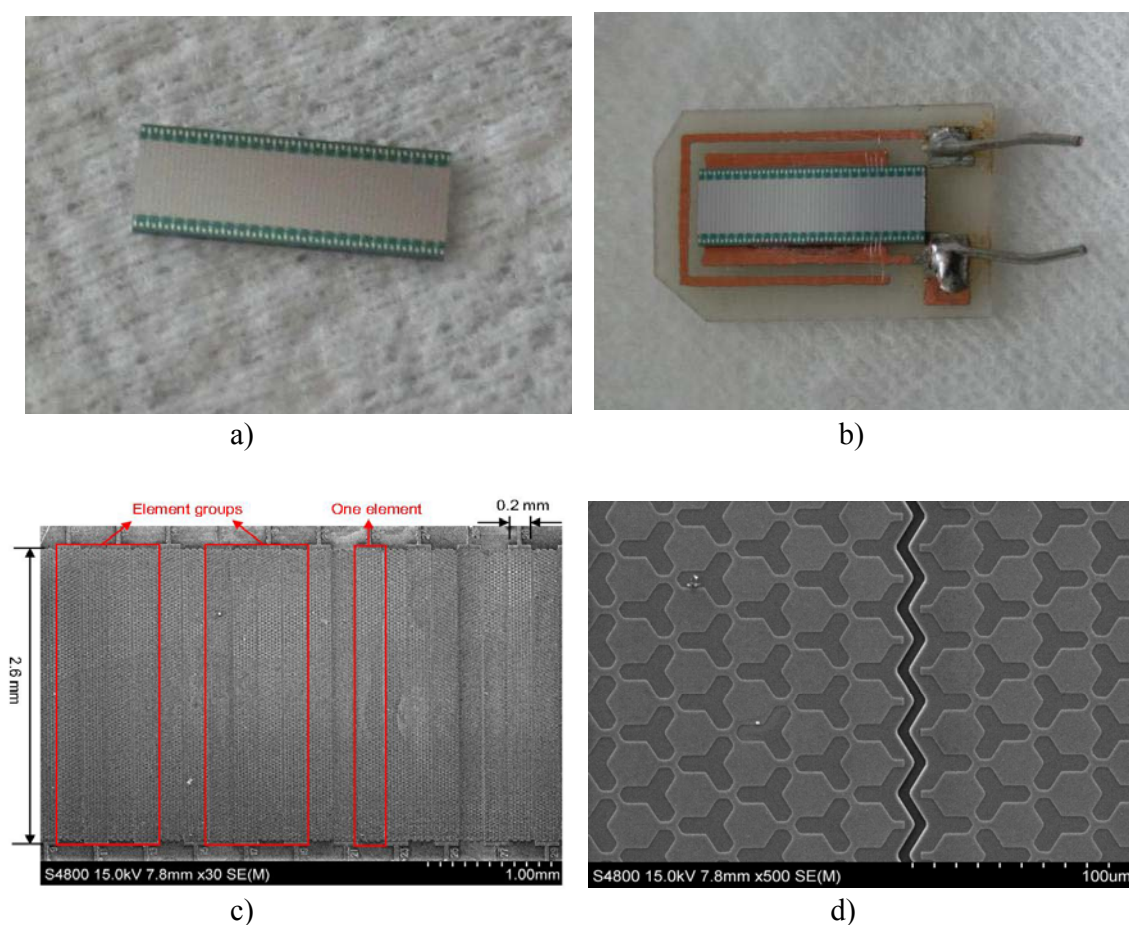


Figure 4-1: Appearance of CMUT sensor arrays.

## 4.2 Synthesis and features of NPs

### 4.2.1 Preparation and functionalization of NPs

Polystyrene-*co*-DVB (PS-*co*-DVB) spheres were synthesized by emulsifier-free emulsification polymerization. 4.54 mL purified styrene and 0.45 mL DVB were added into 236 mL of water with 32 mg potassium peroxydisulfate. The solution was poured into a 500 mL three-necked flask and polymerization was carried out at 70, 80 or 90 °C for at least 3 hours under a nitrogen atmosphere, stirring at a speed of 350 rpm. The obtained PS-*co*-DVB nanobeads with different mono-distribution of diameters (temperature-dependent) were washed with a mixture of methanol and deionized water and finally dried under vacuum and stored at 4 °C. The functionalization of the synthesized nanoparticles (NPs) was done by adding acrylic acid (AA) to graft acrylic groups onto NP surface. In detail, 5 mL deionized water, 1 g NPs and 200 μL acrylic acid were mixed together at 80 °C for 20 min, then potassium peroxydisulfate ( $K_2S_2O_8$ ) solution (32 mg  $K_2S_2O_8$  in 5 mL deionized water) were added. The reaction carried on for 2 h. The functionalized NPs

were filtered and washed with methanol-water mixture for several times and dried under vacuum and stored at 4 °C. Dry particles (NPs or AA-NPs) were redispersed in cyclohexanone at desired concentrations and the suspension was filtrated through a 5 µm syringe filter (Millipore Co., USA) prior to use. The obtained NPs were characterized by SEM to get the information about size, uniformity and size distribution.

#### 4.2.2 Features of NPs

The self-prepared copolymeric NPs were adopted as a loading support in the 2-step modification of sensors for the following reasons.

(i) The constituents of the copolymer, i.e. styrene and DVB, have low permittivity, which is one prerequisite to ensure non-transformation in the electrical field direction of LFE sensor [79]. Besides, the two compounds decide that the copolymer has high glass transition temperature ( $T_g$ ). Therefore, they are not as liable to loss of acoustic energy as the more commonly used polymeric coatings with low  $T_g$ . This merit enables utilization of relatively thick coatings to increase the absolute amount of vapor sorbed in the coating and, consequently, enhance sensitivity as well as lower level of detection.

(ii) The sensor could benefit from the small-sized particles due to the larger surface area they offer and the inherent porous structure, to facilitate sensitivity and accessibility of interaction sites.

(iii) Compared with some other materials (e.g. silica bead, graphite, titanium dioxide, gold spheres etc.) which have already employed by other groups for modification of transducers [80-84], the PS-co-DVB polymers have a relatively low density (less than 1.0 g/cm<sup>3</sup>), averting too much mass burden on sensor surface.

(iv) The polymer beads can be prepared with favorable flexibility and controllability in size and surface characteristic by standard polymerization and functionalization method.

(v) Many biological macromolecules (like protein) can be easily and stably sorbed by polymers, which could extend the application of the NP bottom coating to a wide field. These attributes, coupled with the intrinsic robustness of copolymer materials, make the particulate NP coatings suitable for applications even in harsh environment.

#### 4.3 Utilization of LFE sensor and silicon wafer for preliminary work

Due to the limited amount of CMUTs, silicon wafers and LFE sensors were used for the preliminary research, taking advantage of their similarity in surface property (with hydroxyl groups linked onto silicon atoms), opulent availability and relative simplicity in handle. Particularly, the optimization work to prepare uniformly distributed NP films on whole wafer was majorly done on silicon chips, during which, optical microscope and SEM were deployed for characterizing the obtained NP films. Afterwards, LFE sensors were coated with NP films under the optimized condition. Accurate information including frequency,

resistance and quality factor ( $Q$ -factor), was obtained by impedance analysis, which allowed for evaluating the reproducibility of the coating procedure and the influence of NP film on sensor performance. LFE sensor also served as VOC detector to assess the sensitivity of two of the five sensing materials ( $\beta$ -CD and CA).

Similar to TFE sensor, LFE sensor could produce frequency signal with satisfied rejection to noise and interference and low rate of signal drift. However, it has innate sensitivity limits owing to the relatively low resonant frequency. Another disadvantage concomitant is its restriction in relative permittivity ( $\epsilon_r$ ) of coating materials, which should be smaller than that of the quartz crystal ( $\epsilon_r = 4.0$ ), otherwise transformation in the electrical field direction of LFE sensor will happen [79]. Therefore, they were not further used to screen other candidates.

Sauerbrey equation was used to describe the relationship between resonant frequency shift and mass loading onto LFE sensor surface (Equation (2.1)). The added mass can be a result of external coating or vapor sorption. The partition coefficient ( $K$ ) for varied analyte/receptor pairs was calculated with Equation (2.5).

#### 4.4 Preparation of LFE sensors

This process consists of determination of crystallographic axes and deposition of electrodes, as described in [85]. Briefly, the correct alignment of electric field direction relative to the crystallographic axes of the crystal piece is identified by means of the excited acoustic wave modes, namely mode  $a$  (thickness extensional) and mode  $c$  (slow thickness shear). Their mechanical resonance frequencies rely on acoustic mode velocities ( $v_{q(a)} \approx 7000$  m/s and  $v_{q(c)} \approx 3320$  m/s). The fundamental mode frequencies were estimated as  $f_{(a)} \approx 21$  MHz,  $f_{(c)} \approx 10$  MHz for 10 MHz crystals, and  $f_{(a)} \approx 10.5$  MHz,  $f_{(c)} \approx 5$  MHz for 5 MHz ones.

In practice, bare quartz crystals were placed on a printed circuit board (PCB) with the desired electrode structure on top (Figure 4-2, left). The two semi-circled electrodes on the PCB were connected to RF and GND potential of the impedance analyzer. The electrode diameter was 7 mm each and they were separated by a gap of 1.0 mm. The blank quartz was rotated on the board until the  $a$ -mode was completely suppressed at  $f_{(a)}$  while the  $c$ -mode was at its maximum at  $f_{(c)}$  in the measured impedance spectrum [86].

Shadow mask was used to deposit the desired electrodes onto the quartz crystals (Figure 4-2, middle). Gold was deposited onto the quartz with an initial chromium layer serving as adhesion-promoter. The deposition of the metal layers was performed by using magnetron sputtering technique. The optimized thickness of gold layer is about 100 nm. The prepared sensor has a diameter of each semi-circled electrode being 10 mm and a gap of 0.5 mm in-between (Figure 4-2, right). Note the disparity in electrode gap on the test board (1.0 mm) and the crystals (0.5 mm). As presented in [85], in a limited range, there is no influence of the gap dimension on the response spectrum.

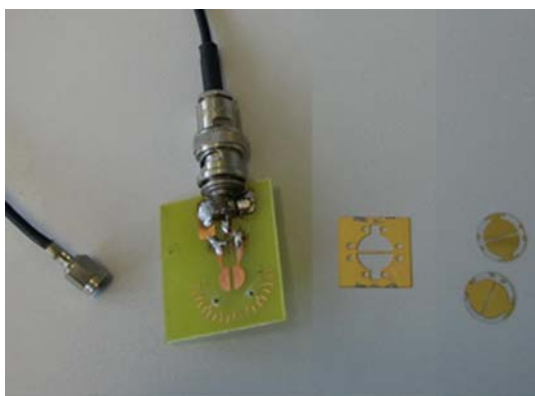


Figure 4-2: LFE sensor equipments.

Left: testing PCB; middle: shadow mask for patterning electrodes; right: prepared LFE sensors.

## 4.5 Surface modification of LFE, CMUTs and silicon wafer

According to the definition of chemical sensors, they have an interface in direct contact with samples in medium. It is very common to immobilize appropriate groups onto sensor surfaces prior to use and ideally the modified sensor can be used repeatedly for an indefinite length of time without regeneration or recondition.

Either for the intention of avoiding loss of functional groups or out of predefinition of desired coating pattern, sensor may be pre-modified by other compounds. Note that we reduce here three types of functionalization concept for sensor fabrication on the basis of different purposes. One is pre-modification, i.e. incorporation of functional groups onto sensor surface to enhance binding firmness of the succedent coating; the second is preparation of NP films on sensor surface; the last one refers to the deposition of sensing agents which interact with analytes.

### 4.5.1 Surface cleaning of the substrates

The first step in surface modification is generally cleaning. Removing the undesired adsorptives is sometimes key for the following coating operation.

Piranha solution has been frequently used in the microelectronics industry. Here it was employed not only for cleaning but also to make substrate hydrophilic by hydroxylating the surface, thus increasing the number of silanol groups on the surface [87]. Piranha solution was prepared by mixing 98 % concentrated sulphuric acid and 35 % hydrogen peroxide at the ratio of 3:1 in volume. (Caution: Piranha solution is highly explosive and should be handled with great care.)

In practice, naturally oxidized silicon substrates were immersed in piranha solution at 80 °C for 30 min, followed by fully rinsing of water and dried with nitrogen flow. Quartz crystals were cleaned in the same manner. For gold-sputtered crystals, thorough cleaning was

carried out by dipping sensors in piranha solution for less than 10 seconds. Silicon nitride-coated silicon wafers were also applied in the research, for the purpose of resembling the possible surface composition of CMUT and they were simply washed by sonication in acetone for 5 min.

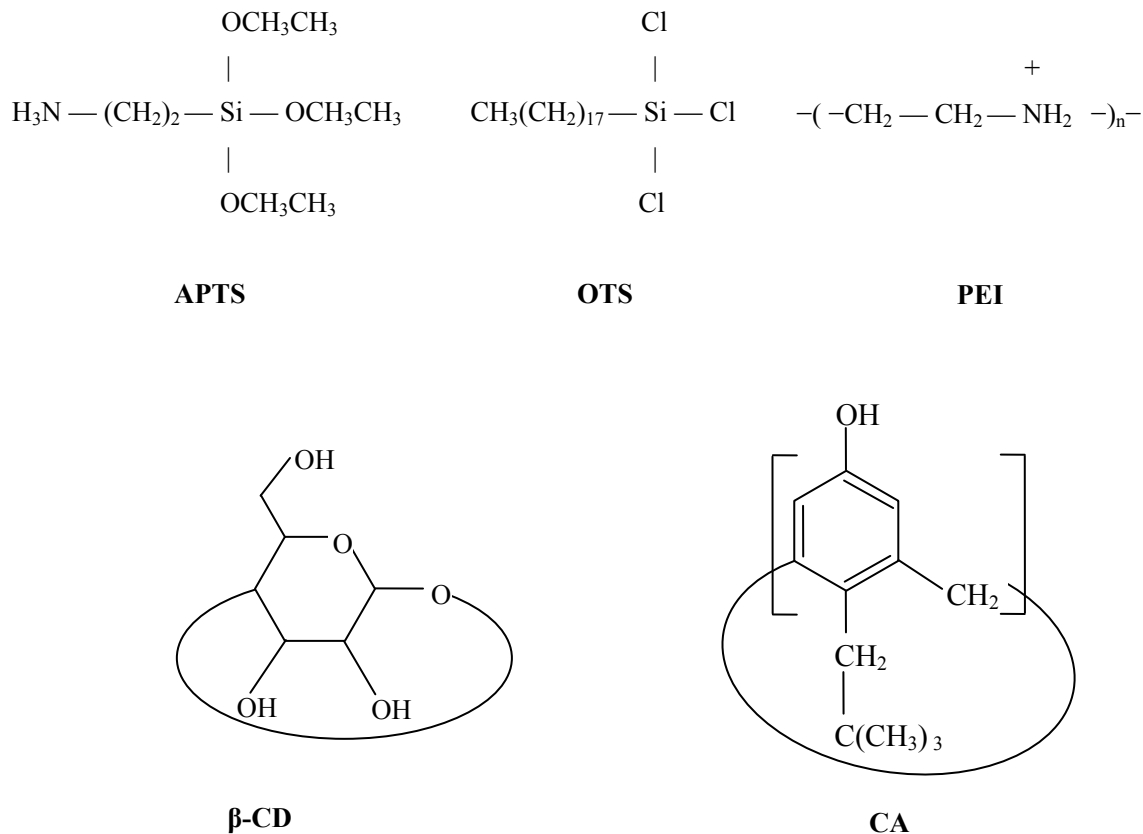
CMUTs were gently cleaned with acetone, methanol and 2-propanol, and then dried under nitrogen stream prior to use. For deep cleaning of CMUTs, we strongly recommend gas plasma (argon plasma for instance) to enhance desorption of loosely bound contaminants.

#### 4.5.2 Pre-modification

The coupling agents applied here are:

- 1) two silane agents for localized deposition of NPs combined with photolithography: octadecyl trichlorosilane (OTS) and aminopropyl triethoxysilane (APTS);
- 2) polyelectrolyte–polyethylene imine (PEI), mainly for improving the attachment between the wafer and the NP coating.

Figure 4-3 demonstrates their chemical structures. As mentioned above, the modification comprises: a) Wafer lithographically modified for localized NP deposition; b) Wafer grafted with PEI for AA-NPs deposition.



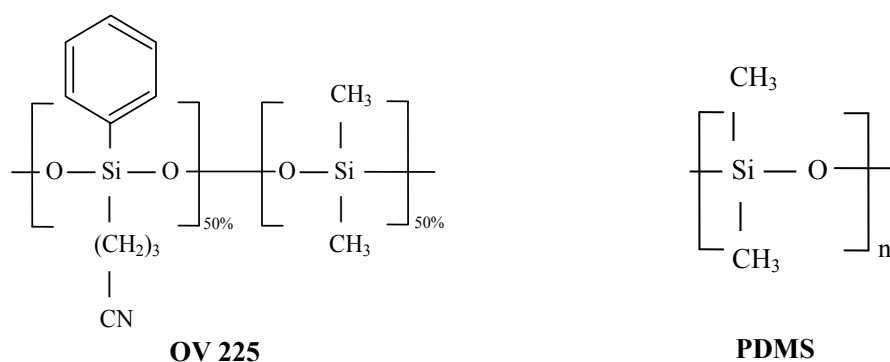


Figure 4-3: Chemical structures of the coupling and sensing agents.

### a) Lithographical modification with silanes

In many cases, self-assembled monolayers can be bound on substrate in an easy way, and after adsorption step, the unadsorbed molecules can be removed by washing. One conventional way for organic modification of inorganic surface (e.g. silica) is to utilize silane coupling agents to react with the hydroxyl groups which intrinsically exist on silica surface. Many kinds of coupling agents are now commercially available. The ones having amino groups can react with acrylic groups. In our study, functionalization of NPs with acrylic acid aimed for grafting acrylic groups on NP surface and allowing for reactions with silane agent bearing amino groups.

Figure 4-4 illustrates the experimental scheme to fabricate NP pattern on silicon surface. The pretreatment with piranha solution made the silicon surface rich in hydroxyl groups (silanols), which were expected to link the silane molecules. OTS self-assembled monolayers (SAMs) were formed on the surface by immersing the substrates in OTS solution (20 mmol/L in toluene) for 30 min, followed by successive rinsing in toluene to remove the unassembled residuals and blowing to dry with nitrogen. UV irradiation with a photomask for 30 min was intended to create two kinds of regions grafting different groups. The UV-irradiated regions became hydrophobic due to Si-OH group regeneration, while the non-irradiated area remained unchanged, i.e. it is grafted with hydrophobic octadecyl groups, which gave rise to patterned OTS-SAM. The subsequent immersion in APTS solution (20 mmol/L in toluene) for another 30 min led to APTS coupling onto silanol groups, and hence resulted in formation of octadecyl/amino groups pattern. Water contact angle measurement exhibited OTS-SAM having a water contact angle of 80° and APTS of 30°, which confirmed the successful formation of two different silane pattern (Table 4-1). Octadecyl groups from OTS-SAM were supposed to hinder the deposition of NPs, and amino groups from APTS-SAM were expected to bind AA-modified NPs. In this way, NPs were able to choose their preferred regions (APTS-SAM covered) to locate themselves.

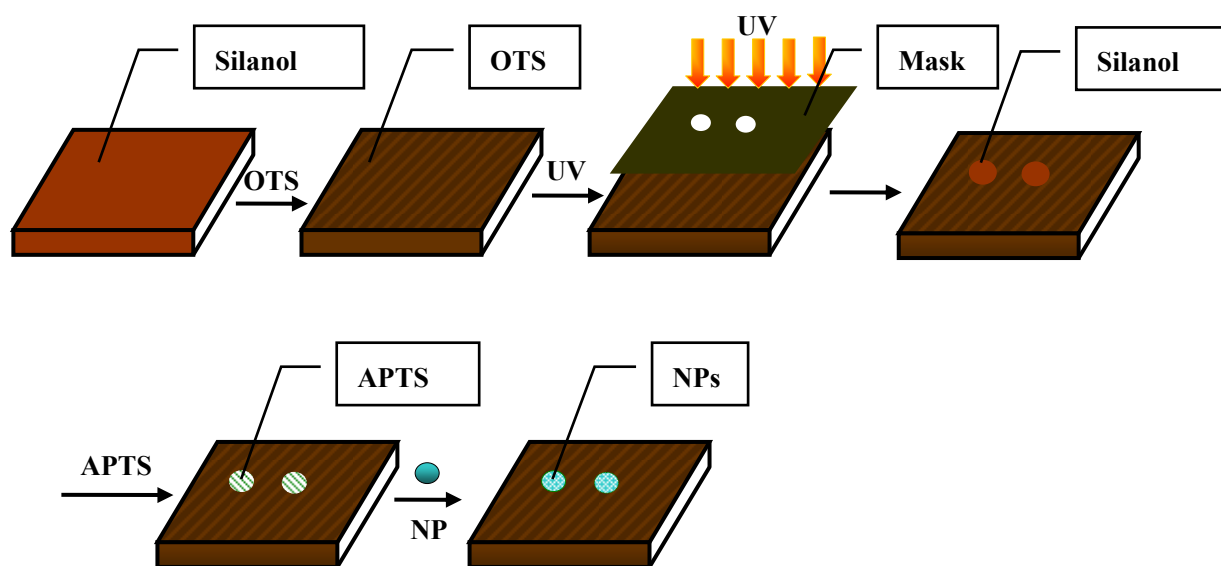


Figure 4-4: Experimental procedure for fabricating NP pattern on silicon surface.

Surface condition	Si/-OH	Si/APTS	Si/OTS	Si/PEI
Contact Angle ( $\theta$ )	15°	25°	80°	15°

Table 4-1: Water contact angles of variously modified silicon substrates.

Si/-OH: Silicon substrate with silanol groups;

Si/APTS, Si/OTS, Si/PEI: Silicon substrates modified with APTS, OTS and PEI, respectively.

### b) Modification with PEI

Layer-by-layer (LBL) assembly is a simple, versatile, and significantly inexpensive approach by which nanocomponents of different groups, particularly of oppositely charged layers, can be combined to coat both macroscopically flat and non-planar (e.g., colloidal core-shell particles) surfaces [88-92]. In general, the LBL process is achieved by alternatively exposing a substrate to positively and negatively charged polymer or particle solutions. The driving force for film formation is multi-point electrostatic interactions between polyions. Since the freshly piranha-treated silicon wafer bears negative charges, a polycation, polyethylene imine (PEI) was employed with the aim of improving the attachment of the AA-modified NPs (negatively charged due to acrylic groups on the surface) on silicon wafer (Figure 4-5).

Concretely, PEI polyion layers with positive ions were formed on silicon by immersing the substrates in PEI solution (3 %, w/v in water with 50 mmol/L NaCl) for 30 min.

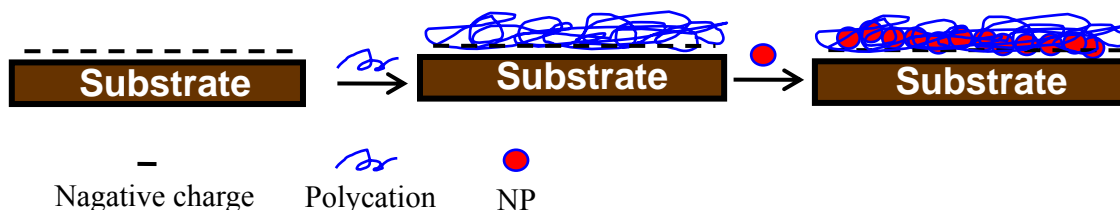


Figure 4-5: Scheme of LBL film and NP film deposition.

#### 4.5.3 NP layer preparation

As stated before, the expectation that NP layer could burden the majority of mass loading from the coating, and reduce the variance of different sensor elements on the same wafer to avoid calibration, is uppermost. For this purpose, the NP layer must be homogeneous in large region. Reproducibility and easy operation are also favorable requirement for the deposition technique. Here LB-like deposition, self precipitation and spin coating have been tested to achieve these demands. Three categories of silicon wafers (lithographically modified with silanes, PEI-modified and bare ones) have been involved.

##### a) LB-like deposition

The first procedure for depositing NPs is so-called LB-like coating approach, named after the well-known Langmuir-Blodgett film preparing technique [45, 46]. Firstly, an NP monolayer formed by adding one drop of NP suspension in cyclohexanone at concentration of 10 mg/mL on top of water in a delimited area. After some time of self arrangement of the particles on water surface to get a stable monolayer, substrates were dipped into the water, tilted to certain angles and then dragged out with the self-assembled NP layer seated on the top. After evaporation of cyclohexanone and water, the NP film was transferred to the surface of the substrates. For the localized deposition of NPs on silane-modified silicon wafers (Figure 4-4), the substrates were further washed with chloroform to remove NPs on undesired regions.

##### b) Self precipitation of NPs

Self precipitation was carried out by simply immersing silicon wafers in NP suspensions (10 mg/mL in water) for 24 h and then purging them with 2-propanol. After that, all the substrates were covered by certain amount of NPs and among which, the lithographically treated ones were assumed to hold localized deposition of NPs according to the silane-SAM pattern.

### c) Spin coating

As described in Chapter 2.1.4, spin casting allows for coatings of controllable thickness and mass loading, which can be easily formed by evaporation of solvents. Herein, this method was applied to get NP films. Different amounts of NP suspension in cyclohexanone were dispensed on substrates and spread at varying velocities in a house-built spin-coater, until dry NP layers were obtained.

The spin coating procedure was optimized in terms of spin setting (operation sequence, spin time, spin speed), concentration of NP suspension solution and other factors (circumstance control, treatment of substrate).

Rough screening was performed in order to determine proper concentration and spin speed range first. NP concentrations of 10, 25, 50, 60, 80, 100 mg/mL were tested at different spin rates (800, 1000, 1300, 1700, 2000, 2500, 2700, 3000, 3300, 3500, 4000 rpm). Then optimal spin procedure was studied, including one step, two or more steps in tandem at varied speeds. The NPs involved in the research are of two different diameters ( $125 \pm 5$  nm and  $330 \pm 5$  nm), with or without AA functional groups on the surface.

#### 4.5.4 Localized deposition of second layers

There are five sensing materials involved in the research, ranging from supramolecules to polymers, all of which have been widely serving as sensitive agents in various fields [93-99]. The structures of the sensing materials applied are shown in Figure 4-3 and the solutions prepared in corresponding solvents and concentrations are tabulated in Table 4-2. The abbreviated names were used throughout the thesis for all the materials.  $\beta$ -CD was employed during optimization of the deposition process. The rest four materials (CA, PEI, OV 225, PDMS), either of liquid or solid state, proceeded to modify sensors under the optimized condition. The boiling points (BP) of the adopted solvents are also listed out, which are considered as a crucial feature in determining the jetting consequence. The state of all the materials refers to that in room temperature and pressure.

Material	Abbreviation	State	Solvent	Solvents' BP (°C)	Concentration (mg/mL)
Methyl- $\beta$ -Cyclodextrin	$\beta$ -CD	Solid	Ethanol	78.4	3 or 6
4-tert-Amyl-Calix[8]arene	CA	Solid	Chloroform	61.2	0.5
Polyethyleneimine	PEI	Liquid	Water	100	1.5
Cyanopropylphenyl Dimethylpolysiloxane	OV 225	Liquid	Ethyl acetate	77.1	3
Polydimethylsiloxane	PDMS	Liquid	Ethyl acetate	77.1	3

Table 4-2: Sensitive materials for modification of sensors.

**a) Drop coating**

Firstly, simple drop-coating was utilized for deposition of the sensitive layers. Typically, one microliter of solution was dispensed onto selected element groups on CMUT wafers or LFE sensors by using a microliter pipette.

**b) Aerosol jetting**

The aerosol jetter also belongs to drop dispensing instrument. As shown in Figure 4-6, it consists of an atomizing reservoir, a gas inlet for carrier gas (nitrogen) coming in and a gas outlet for discharging the aerosol. The reservoir with coating solution or suspension is situated inside water tank equipped with an ultrasonic device. A fine mist (aerosol) of coating solution is produced owing to the ultrasonic vibration. The carrier gas flow entrains the generated mist at controlled rate. The deposition head forms an annular, coaxial flow between the aerosol stream and a sheath gas stream (nitrogen). The co-axial flow exits the print head through a nozzle directed to the substrate. The vertical separation between the nozzle and the sample is typically 3 - 5 mm. The print head is capable of focusing an aerosol stream to as small as a tenth of the size of the nozzle orifice. A two-axis (X and Y) micropositioning system with variable Z-height is outfitted, having an accuracy of  $\pm 6 \mu\text{m}$ . A microscope camera provides visual control to adjust the process parameters for reliable droplet ejection and to avoid satellite drops. At relative humidity of 20 - 50 % in air, the printed droplets evaporate from the substrate within a few seconds.

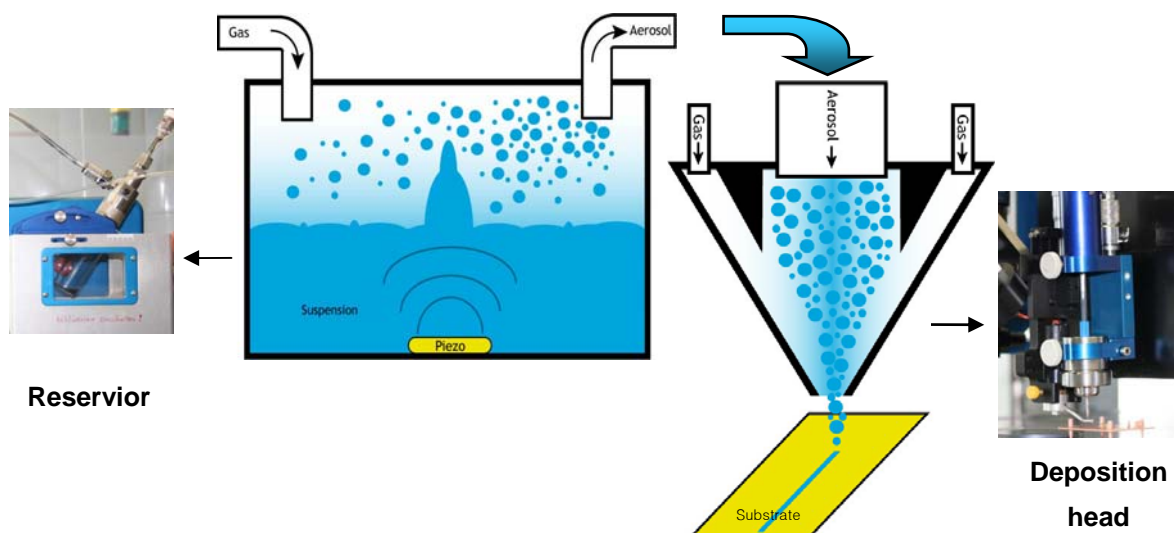


Figure 4-6: Working scheme of aerosol jetter and photos of the reservoir and the deposition head.

In general, the volume of jetted materials onto substrate is determined by the flow rate of carrier gas and sheath gas, the amount of aerosols generated inside the reservoir, the size of the nozzle, and the mobilization speed of the substrate during deposition. Amongst them, the quantity of the yielded aerosols is dependent on the position of the atomizing reservoir in the water tank (peculiarly the depth under water) and the vibration frequency of the ultrasonic oscillator.

Particularly, the whole passage of the jetter was emptied and thoroughly rinsed with deionized water and 2-propanol to ensure there was no impurity left in the reservoir, the passing tube and the nozzle. Then they were further cleaned by ultrasonication in water for 10 min and dried with nitrogen gas. 1 mL solution with sensing materials dissolved in appropriate solvents were added into the reservoir to generate aerosol ready for coating. According to the expected coating configuration and the parameters related to the sensor used, the aerosol jet system was programmed to coat and pattern sensors in accurate dimension.

LFE sensors did not undergo aerosol jetting. As for CMUTs, the aerosol jetting has been implemented in unit of element groups. Figure 4-1 c) illustrates that four elements constitute one element group with two-element interval in between.

During deposition of both NPs and sensing agents, the CMUT membranes were either biased by optimal DC voltage or without such connection, with the aim of enhancing the final coating performance. Since no significant difference was found, all the CMUT sensors were coated without extra bias voltage.

#### 4.5.5 Deposition of ceramide AP with LB film trough

Ceramides comprise nine subclasses and play a crucial role in maintaining the barrier function of the skin [100]. The structure and properties of a quaternary membrane based on ceramides have been investigated in order to optimize drug penetration and permeation [101-103]. The bioactive lipid, ceramide AP (Figure 4-7), was employed as coating agent so as to extend the application range of CMUTs in pharmaceutical and biological fields.

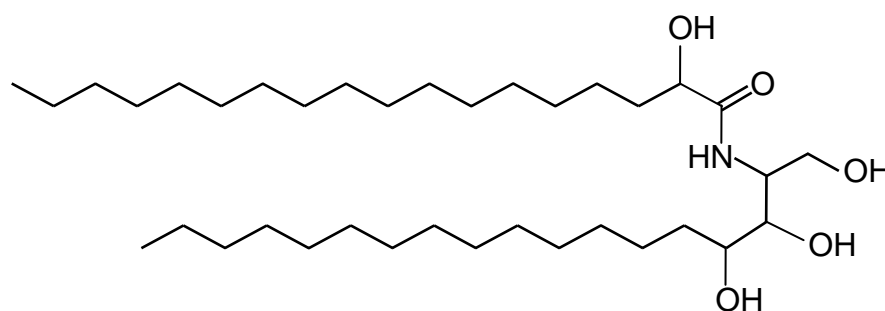


Figure 4-7: Structure of ceramide AP employed for CMUT modification.

Solution of ceramide AP was made using chloroform and methanol mixture (3:1, v:v) at a concentration of 1.0 mg/mL. Then the ceramides were spread onto a deionized water surface at the temperature of 35 °C. The assembly pressure was 17 mN/m. The first layer deposited onto CMUT was the hydrophobic chains of ceramide molecules. 31 layers were transferred onto the substrate in total with the outermost one having hydrophilic heads to outside environment.

In this chapter, the whole procedure of the 2-step modification is described, starting from synthesis of nanoparticles (NPs) and preparation of LFE sensors. Then in the first step, three deposition strategies (LB-like deposition, self precipitation and spin coating) were attempted to form NP film onto three types of substrates (silicon wafer, LFE sensor and CMUT). Furthermore, five sensing agents were adapted to produce thin layers on desired areas of the substrates, either with or without the bottom NP films. Manual drop coating and aerosol jetting were employed in this step. Besides, ceramide AP assembling on NP-coated CMUT substrate was accomplished with assistance of a LB film trough. Multi-self assembling layers formed in this way, though the ceramide membrane covered the whole CMUT wafer instead of localized modification. Introduction of biological materials allows for the modified sensor to play a role in more potential applications.

The films deposited in both steps were investigated and evaluated by SEM and impedance analysis which are presented in chapter 5 and chapter 6. Optimal conditions and results are also drawn out.

---

## Chapter 5

# Physical Characterization of Films

---

### 5.1 Instruments

The surface morphology of the deposited materials after the first and second preparation coating steps were inspected by direct observation, optical microscopy or SEM. Optical microscopy was carried on a Zeiss-Opton microscope (Carl Zeiss, Germany). SEM measurements were conducted using the same instrument (S-4800, Hitachi, Japan) as that in Chapter 4.

### 5.2 Morphology of NP coating from different deposition approaches

The substrates for observing the coating morphology were pure silicon wafers, silicon nitride-coated silicon wafers and CMUTs. We failed to get SEM picture when crystal served as coating substrate due to its low conductivity.

#### 5.2.1 LB-like deposition

As described in Chapter 4.5.3 a), this deposition process was done by hand. The random fashion of this operation often made the films non-uniform over broad area of the wafer surface. Figure 5-1 and 5-2 show the configuration of NP layers on silicon and CMUT wafers from LB-like deposition. In limited range, rather uniformly distributed NP layer has been formed (Figure 5-1). But on large field of view, fractures exist, which damage the continuity of the NP layer seriously (Figure 5-2).

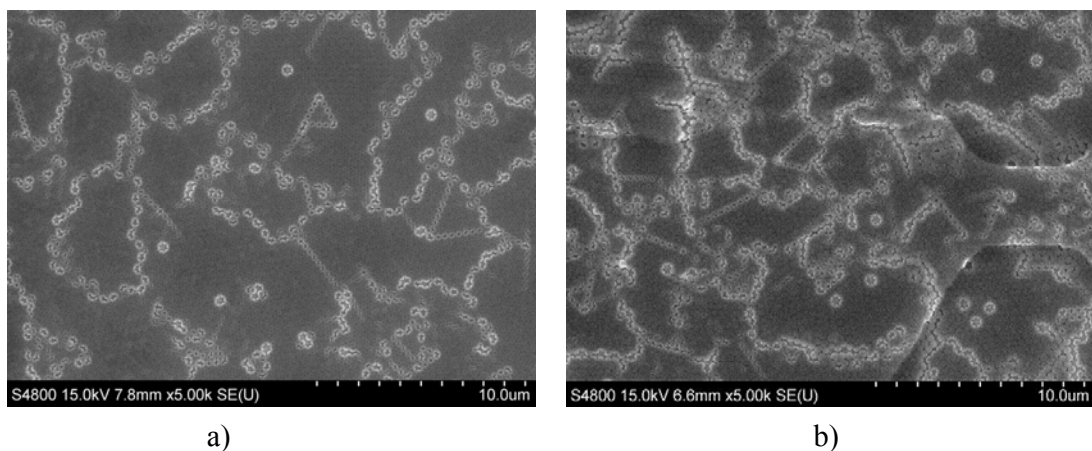


Figure 5-1: SEM images of NP covered substrates through LB-like deposition.  
a) Silicon wafer; b) CMUT.

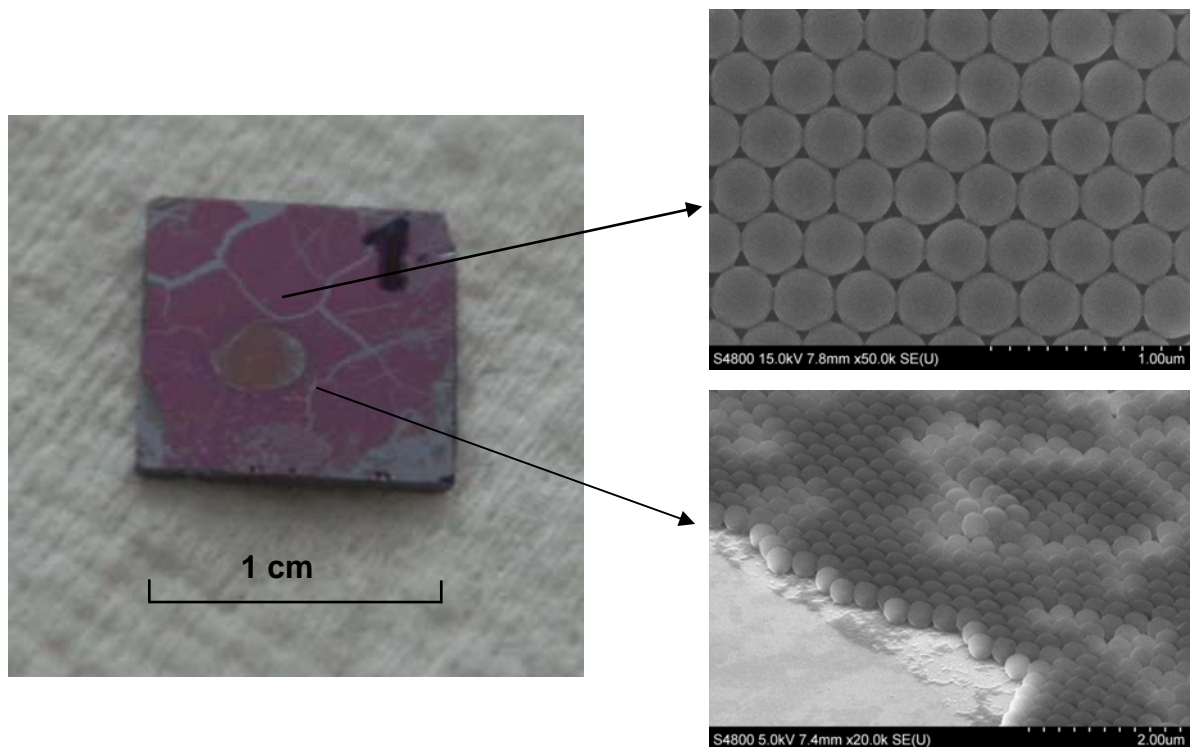


Figure 5-2: Photos of an NP-covered silicon wafer through LB-like deposition.

### 5.2.2 Localized deposition of NPs through photolithography and self-precipitation

Corresponding to the operation depicted in Chapter 4.5.2 a), wafers were modified with two silane agents which bear different functional heads, together with photolithography to design patterns on substrates. The photos in Figure 5-3 exhibit the results of self-precipitation of NPs after silane-SAM pattern. The round, brighter regions are covered with NPs of higher density in comparison with the surrounding area. The phenomena match the practical modification expectation and prove the selective deposition of NPs on their preferred locations. Closer observation with SEM, however, reveals the non-uniformity of the NP layers, where both NP piles and voids coexist. Such fact, in addition to a lot more consumption of NPs in store, led to no further development with this strategy.

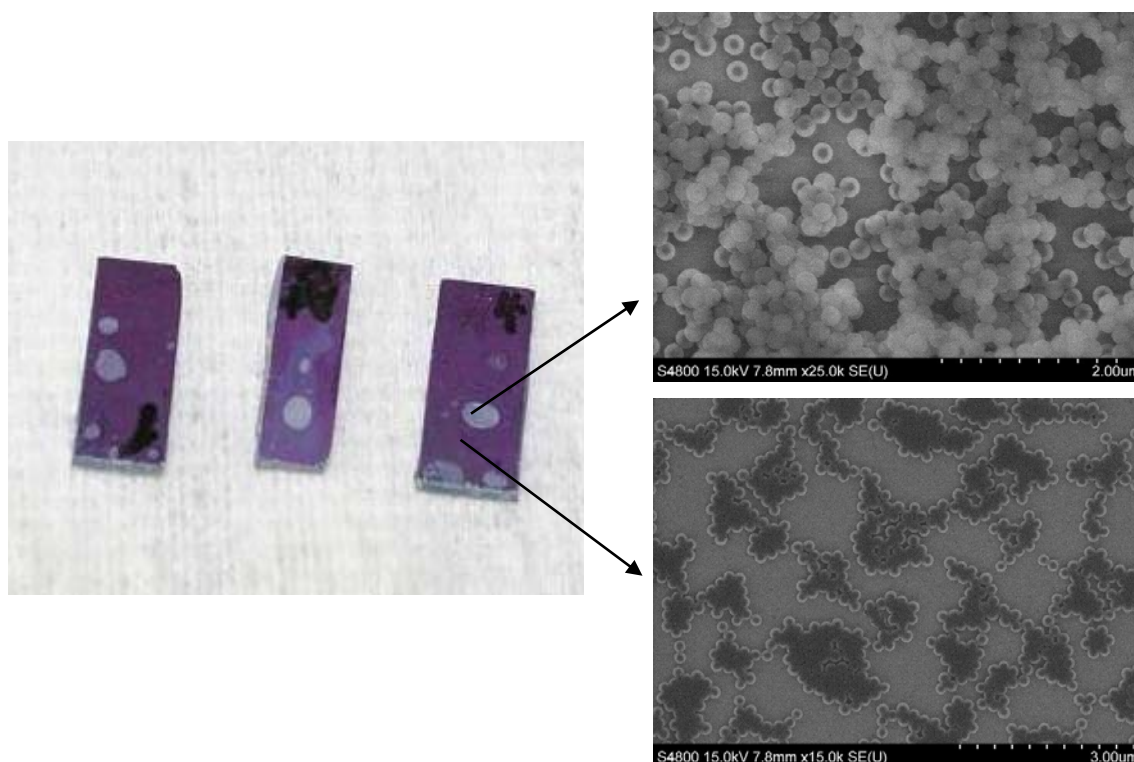


Figure 5-3: Localized deposition of NPs based on Silane-SAM pattern.

### 5.2.3 Spin coating

The spin coating conditions are shown in Table 5-1. It has been found that the results from spin coating are very much dependent on the NP suspension concentration and spin rate but not on the spin time, for the evaporation speed of cyclohexanone (suspension medium for NPs) is quite fast. Concerning spin operation, firstly loading excessive NP suspension followed by immediate rotation is recommended.

Lower concentration and higher speed usually create a non-fully covered surface while the opposite conditions give an NP-multilayer surface. The two lowest concentrations in Table 5-1 (i.e. 10 and 25 mg/mL) were screened out for they always generated non-fully covered surface at even lowest spin rates (Figure 5-4 a)). By contrast, NP suspensions at 80 and 100 mg/mL were too thick, resulting in NP overlapping phenomena (Figure 5-4 b)). Suspensions at 50 or 60 mg/mL showed better coating morphology when the spin speed was within 2000 and 2500 rpm. After that, two-step spin procedure was tested: a short-time spinning at lower rate, followed by higher rate until substrates were completely dry. The initial lower spinning was supposed to disperse the suspension evenly onto the whole substrate and let the NPs slowly spin and locate themselves in suitable position. The subsequent faster rotation was expected to spin away the upper suspension without disturbing the bottom NP layer. The optimal condition we obtained was: spinning at 1100 rpm for 5 seconds in the first step, followed by 3800 rpm till all the solvent evaporated, and the concentration of NP suspension was in the range of 50 - 60 mg/mL. Figure 5-5 exhibits

an optical photo of NP layer acquired under the optimized spin condition.

Concentration (mg/mL)	Spin speed (rpm)								
	800	1000	1300	1700	2000	2500	3000	3300	3500
10	× <sup>1</sup>	× <sup>1</sup>	–	–	–	–	–	–	–
25	× <sup>1</sup>	× <sup>1</sup>	× <sup>1</sup>	–	–	–	–	–	–
50	–	× <sup>2</sup>	× <sup>2</sup>	× <sup>2</sup>	√	√	× <sup>3</sup>	× <sup>3</sup>	× <sup>3</sup>
60	–	–	× <sup>2</sup>	× <sup>2</sup>	√	√	× <sup>3</sup>	× <sup>3</sup>	× <sup>3</sup>
80	–	–	× <sup>2</sup>	× <sup>2</sup>	× <sup>4</sup>				
100	–	–	–	–	× <sup>4</sup>				

Table 5-1: The outcome for NP coating by spin casting under different conditions.

×: the condition was tested but gave poor consequence.

×<sup>1</sup>: the concentration of the suspension was too low.

×<sup>2</sup>: the spin speed was too low.

×<sup>3</sup>: the spin speed was too high.

×<sup>4</sup>: the concentration of the suspension was too high.

–: the condition was not tested.

√: the condition worked well.

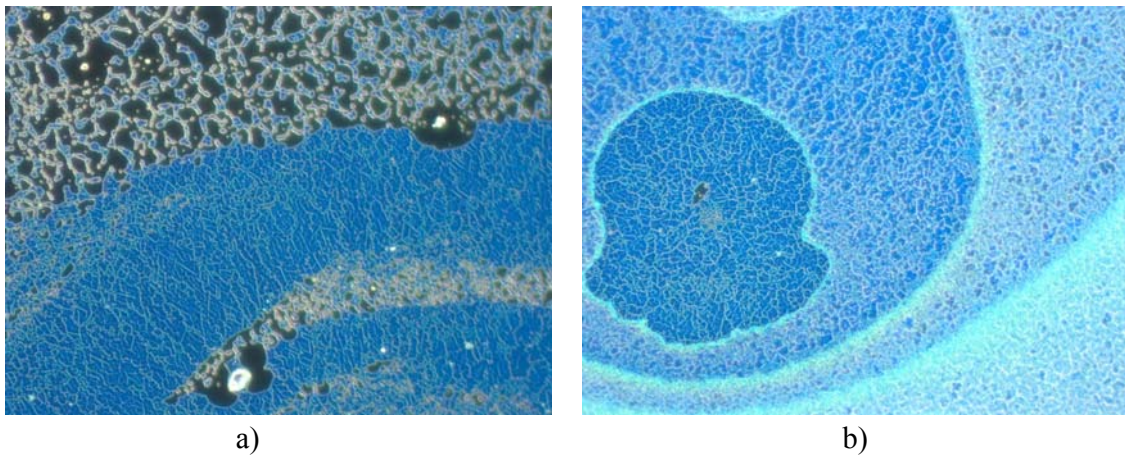


Figure 5-4: Typical image of non-homogeneous NP films on silicon substrate (× 20 times).

a) Unfully covered; b) multi-layer covered.



Figure 5-5: Typical image of homogeneously distributed NP film on silicon substrate ( $\times 20$  times).

### 5.3 Pre-modification effect

The purpose of modification of either NPs or substrate is to improve the stability of the binding between them. The modification effectiveness was examined by solvent (e.g. chloroform, toluene or alcohols) flushing and ultrasonication of the coated substrates immersed in water. The residual amount of NPs was observed optically or determined with LFE sensors from the increase in resonant frequency as a result of the loss of NPs. On the one hand, no significant difference can be found among wafers without modification and with various modifications. It seemed that plenty of hydroxyl groups after piranha solution pretreatment could provide non-covalent binding for NPs to endure the flushing solvents but were incapable to keep them from escaping by ultrasonication. Further modification might provide other kinds of weak non-covalent attachment, but they are still not that strong. On the other hand, the functional groups which NPs bear contributed to the steadiness of the NP film. Compared with non-functionalized NPs, the AA-NPs were less susceptible to disturbance by solvent-flushing. Moreover, the size of NPs also plays a part. It has been observed that NPs with diameter larger than 200 nm failed to withstand the flushing force of solvent (Figure 5-6) while smaller NPs could resist this.

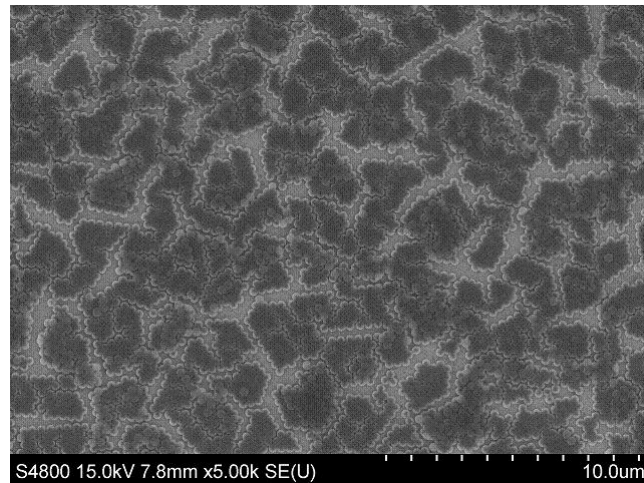


Figure 5-6: Influence of organic solvent (chloroform was used here) droplets on formed NP layer ( $\phi \approx 330$  nm).

In summary, the best results came from the NPs with diameter around 125 nm and undergoing AA-modification. Figure 5-7 exhibits the appearance of two silicon wafers with NPs spin-coated under the optimal conditions (see 5.2.3). The right one is silicon nitride-coated, and the left one is pure silicon wafer. Over thirty spots on the overall area of the wafer have been checked and no disparate topography of NPs was found. Typical morphology of NP coating is illustrated with SEM photos in Figure 5-8.

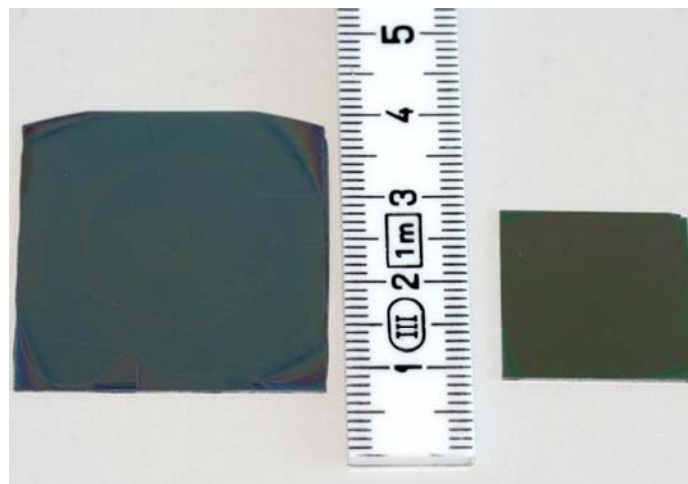


Figure 5-7: Appearance of two NP-coated silicon wafers.

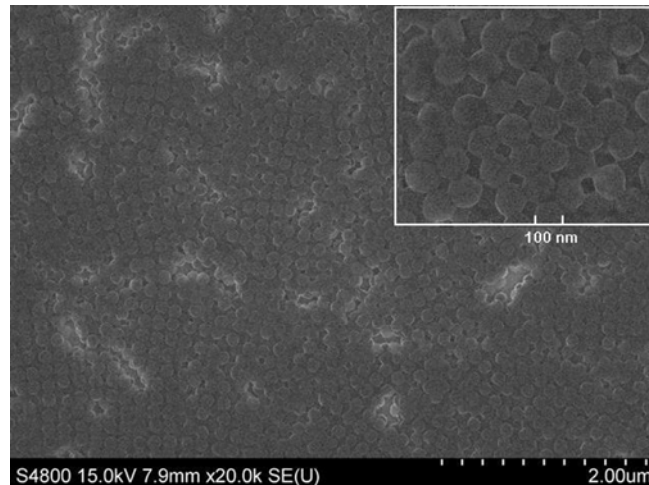


Figure 5-8: SEM pictures of NPs coating on silicon wafer. The inset on the top right corner is under higher magnification.

From the above results one can conclude a rather satisfying homogeneity of the NP layer on a large scale. This conclusion has been corroborated by impedance analysis, in which a series of LFE sensors coated with NPs were measured and the frequency shifts due to NP coating ( $\Delta f_r^{\text{NP}}$ ) were comparable with each other (see Chapter 6.2.1). In addition, different element groups of CMUT sensor experienced the similar operation and analogical  $\Delta f_r^{\text{NP}}$  were obtained as well (see Chapter 6.2.2).

## 5.4 Morphology of complex layers from different approaches for depositing sensing materials

### 5.4.1 Drop coating on NP layer

Although direct drop coating of sensing solution with a pipette can define amount semi-quantitatively, it is virtually impossible to manipulate self-spreading behaviour of droplets on sensor surface (Figure 5-9). The element groups on the CMUT which are expected to be coated are only partly modified, while the neighbour elements receive undesirable coating. Such results will lead to significant decrease in  $Q$ -factor inevitably. And the difference in the number of modified cells and the amount of materials on the cells will result in unpredictable sensitivity and signals. Nevertheless, it can be seen from Figure 5-9 that the second layer evenly modified the NPs underneath.

Circular residual of the solutes is another problem, resulting in non-homogeneous distribution of sensing agents. This phenomenon has been reported in other inkjet studies [51, 104-106] and well-known as “coffee ring” structure [107]. During solvent evaporation, there was considerable outward fluid motion, which could carry most dispersed materials to the edge. Therefore, hand-operated drop-coating only impose minimum control in both covered area and configuration of the formed layer.

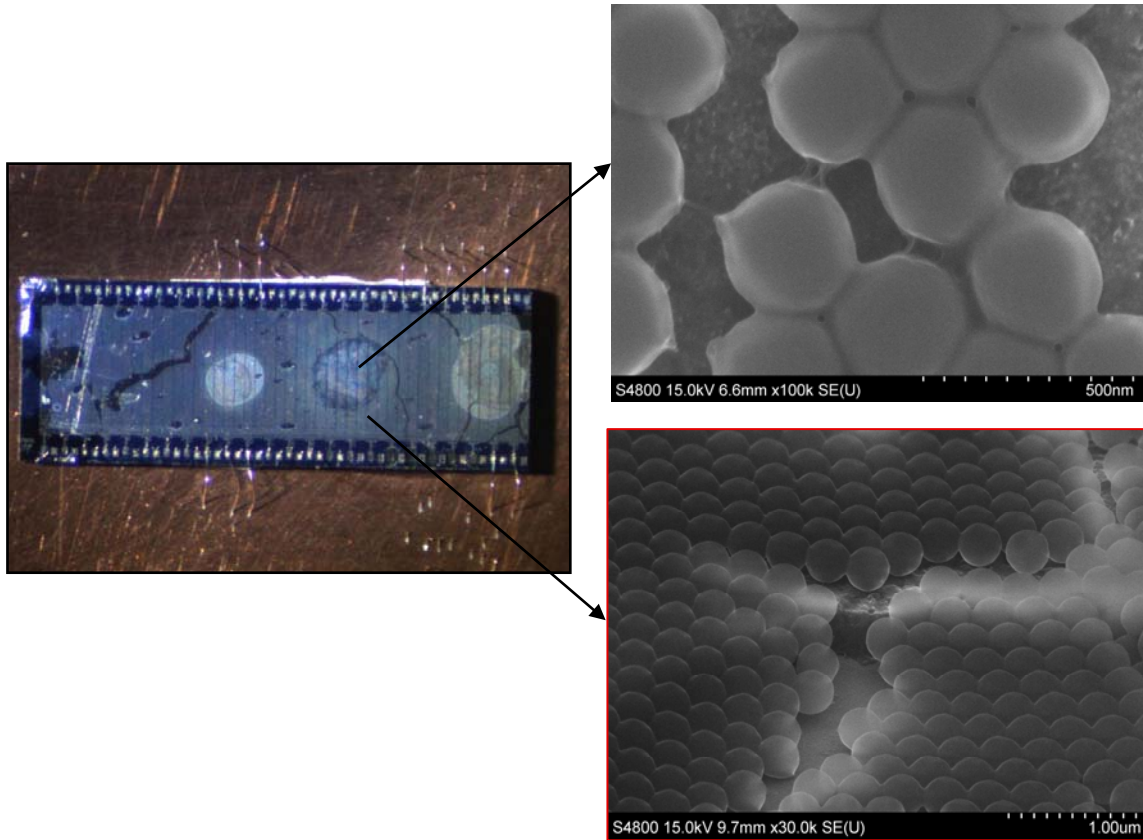


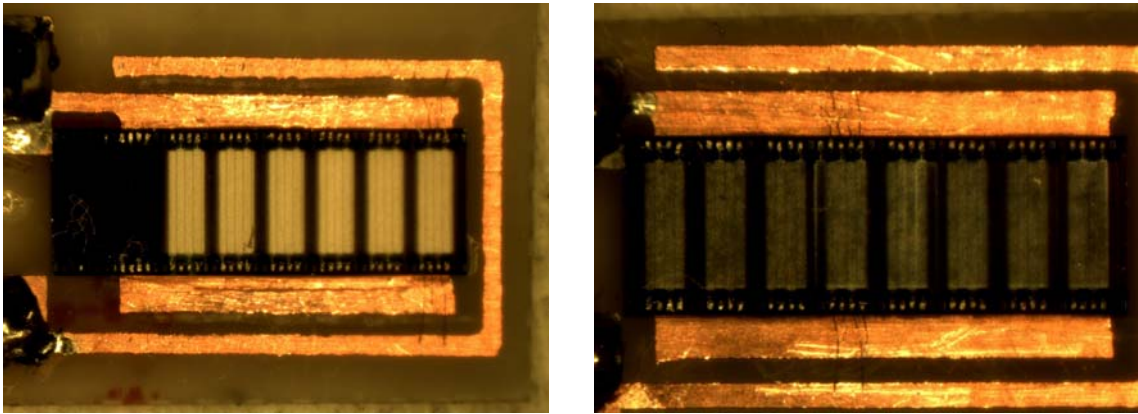
Figure 5-9: NP-coated CMUT wafer with drop-coated sensing materials.

#### 5.4.2 Aerosol jetting on NP layer

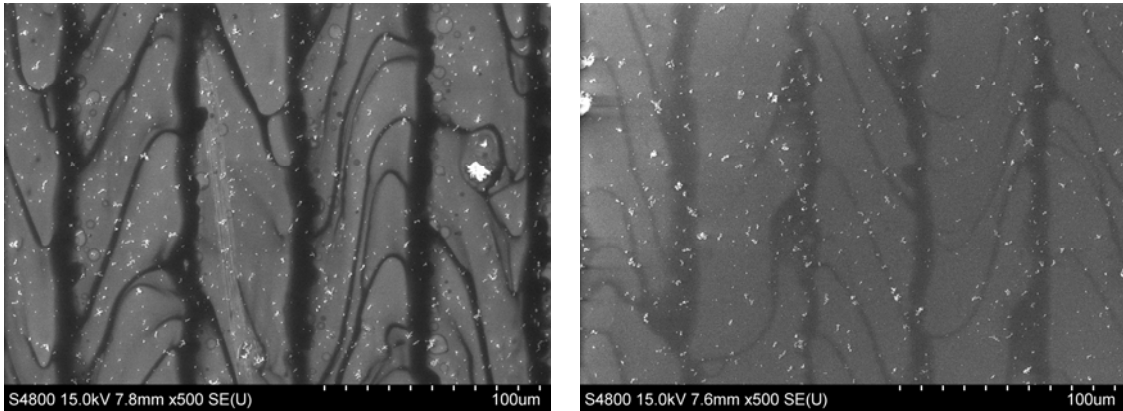
As described in Chapter 4.5.4, aerosol jetter is able to prepare films with precise control and regulation both in amount and area (Figure 5-10). Since most solvent has been gone right after being projected onto substrate, it has no free fluidity to diffuse onto adjacent region.

Figure 5-11 demonstrates the SEM morphology of single CA coating and double coating (NP+CA), which exhibits no significant improvement for CA jetting with NPs on the bottom. However, OV 225 coating benefits a lot from the NP loading, as this viscous liquid tends to form conglomerated droplets on bare substrate (Figure 5-12 a)), while in the double coating system, no drops can be viewed (Figure 5-12 b)). NP layer has no alteration after sensitive material deposition.

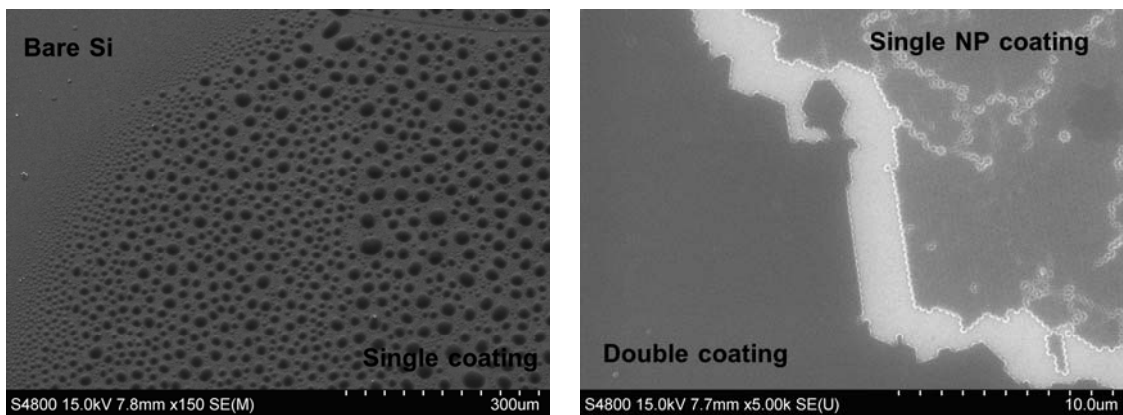
The positive effect by using NPs as bottom layer has also been proved by impedance analysis, where the increase in resistance and decrease in  $Q$ -factor originating from second coating was less in the double coating system than that without NP layers (see Chapter 6.2.2).



a) b)  
 Figure 5-10: CMUT sensors modified by aerosol jetting.  
 a) With CA (solid); b) with OV 225 (liquid).



a) b)  
 Figure 5-11: SEM images of aerosol jetted CA on Si wafers.  
 a) Bare Si wafer; b) NP-covered Si wafer.



a) b)  
 Figure 5-12: SEM images of aerosol jetted OV 225 on Si wafer.  
 a) Bare Si wafer; b) NP-covered Si wafer.

Based on the above observations, one can make a comparison among the strategies applied in the 2-step modification.

For the NP deposition in the first step: LB like deposition is unable to produce uniform NP layer on a large area although NPs can be arranged quite uniformly in small regions; selective self-precipitation of NPs can be achieved through modification of substrates with photolithography but the number of NPs located on the substrates is out of control and the layers are not uniform; finally, spin coating gives rise to the best results by using NPs with diameter around 125 nm and having acrylic acid functional groups. The optimal spin condition is: spinning at 1100 rpm for 5 seconds followed by 3800 rpm till the end, and the concentration of NP suspension is around 50 - 60 mg/mL.

As to the sensitive material deposition in the second step, manual drop coating is unsuitable in realizing uniform layers. Aerosol jetting shows good control in defining the desired coating areas. Moreover, there is nearly no limit concerning the jetted substances and all the five sensing agents in this research have properly modified the sensors by this technique.

By comparing the morphologies of the single OV 225 coating and the double coating (NP+OV 225), it is clear to see that the close packed and regularly distributed NPs play an important part in helping the viscous liquid to be uniformly dispensed on the previous smooth wafer.

---

## Chapter 6

# Chemical Characterization by Impedance Analysis

---

### 6.1 Measurement setting

The impedance spectra of LFE and CMUT sensors were measured either with an HP 4395 A network analyzer (Japan) or with a home-made fast impedance spectrum analyzer [108], interfaced to a PC running resonator-measurement software for display and processing. It took about 12 seconds to finish one frequency scan (801 frequency points, 300 Hz IF BW), impedance analysis and data transfer to the computer. CMUT chips were glued on and wire-bonded to 14×10 mm PCBs made of epoxy resin (see Chapter 4.1), which were enclosed in a metal measurement chamber (Figure 6-1 a)). Another home-manufactured cell was applied to mount LFE sensors (Figure 6-1 b)). Both cells were designed to avoid unwanted disturbances from pressure shocks and possible turbulence. All the measurement settings were initially calibrated to subtract the potential system errors and make the frequency baseline at the magnitude of zero. The experiments were performed under ambient circumstances at room temperature about 25 °C and relative humidity around 33 %.

For CMUT, the DC bias was optimized to guarantee operation of the sensor at the highest  $Q$ -factor. One example was shown in Figure 6-2, which illustrated that the optimal DC bias for this CMUT was 78 V, for relatively high  $Q$ -factor and maximum conductance ( $G_{\max}$ ) value were obtained under this voltage. Further low voltage generally gives higher  $Q$ -factor but at the expense of reduced amplitude of  $G_{\max}$ . Note that the optimal DC bias may differ from one CMUT to another and also rely on the elements involved. Hence selection of optimal DC bias was carried out for each connection.



Figure 6-1: Measurement cells.

a) CMUT; b) LFE sensors.

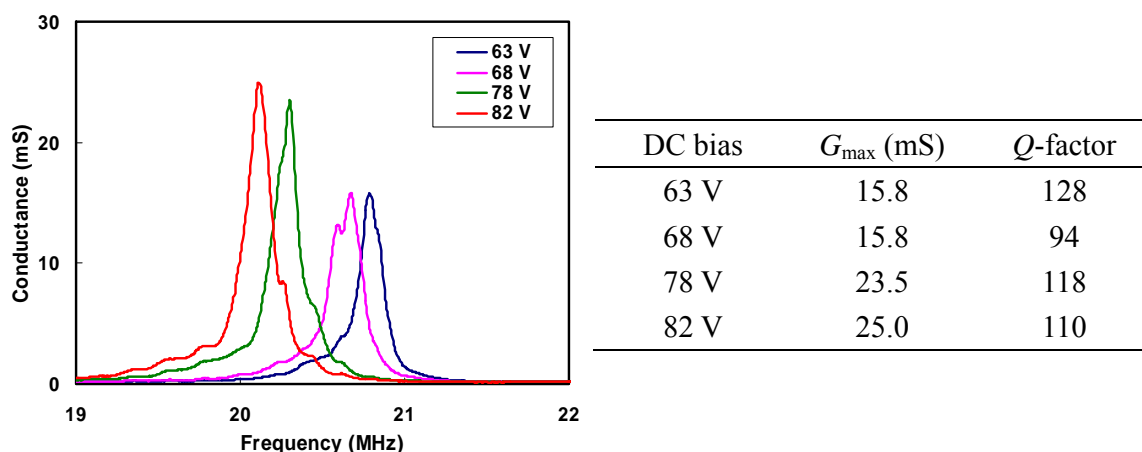


Figure 6-2: Selection of optimal DC bias for CMUT sensor and the corresponding values.

## 6.2 Coating influence on sensor behavior

### 6.2.1 The behavior of LFEs

The impedance data of the LFE sensor were recorded in each step. Figure 6-3 shows the conductance ( $G$ ) spectra of the LFE sensor in four conditions and the related values are listed in Table 6-1. It is apparent that both NP and  $\beta$ -CD coatings lead to negligible influence on the shape of conductance peak but only shift the whole curve to left side. For sensing films deposited either on bare sensor (Figure 6-3 B) or on NP-coated sensor (Figure 6-3 D), nearly no change in resistance ( $R_1$ ) was observed. Therefore, it could be concluded that, due to the rigidity of the cast material and the uniformity of the NP films, the coatings can be used without any attenuation of the acoustic wave and decrease in  $Q$ -factor of the LFE sensor. The added mass on sensors was estimated according to the Sauerbrey equation. For the 5 MHz crystals coated with NPs under the optimal spin speed of 3800 rpm, the mass loading from NP coating was about  $20 \mu\text{g}/\text{cm}^2$  and the thickness was about 200 nm assuming the polymer density of  $1 \text{ g}/\text{cm}^3$ . As the diameter of the NPs was around 120 nm, the coating morphology could be viewed as double NP layers with some vacant spots, which was just in agreement with SEM images (see Figure 5-8).

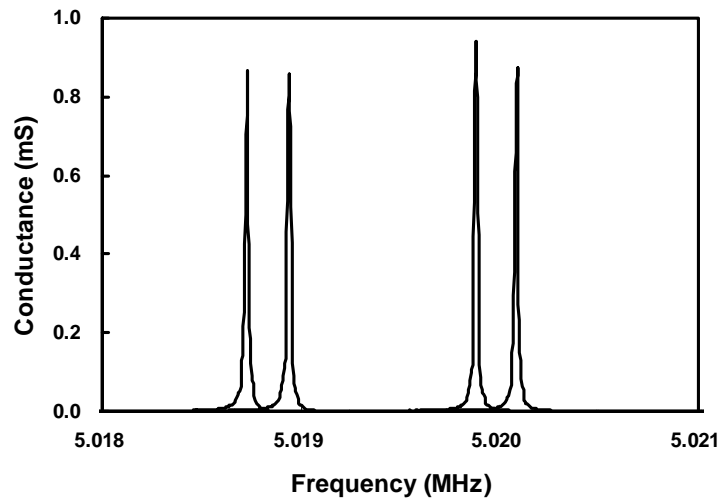


Figure 6-3: Conductance spectra of LFE sensor under four conditions.

A: in bare status; B: with  $\beta$ -CD coating;  
C: with NP coating; D: with NP+ $\beta$ -CD composite films.

Spectrum	$G_{\max}$ (mS)	$R_1$ ( $\Omega$ )	$\Delta f_r$ (Hz)	$h$ (nm)	$Q$ -factor ( $\times 10^3$ )
A	0.865	1156	-	-	268
B	0.940	1064	206	36	297
C	0.859	1151	1147	203	260
D	0.868	1152	1359	37	268

Table 6-1: Conductance spectral data for LFE resonators under four conditions in open air.

A, B, C and D correspond to those in Figure 6-3.

$G_{\max}$ : maximum value of conductance in spectrum;  $R_1$ : resistance;  $R_1 = 1 / G_{\max}$ ;  $\Delta f_r$ : frequency shift due to each coating;  $h$ : height of coating calculated with the Sauerbrey equation;  $Q$ -factor: Quality factor;  $Q$ -factor =  $f_r / \Delta f_w^{1/2}$ ,  $\Delta f_w^{1/2}$ : full width at half height of conductance spectrum.

These results proved that, the self-prepared NPs are materials with high shear modulus, and more importantly, spin-coating is competent to create a quite homogeneous film over entire crystal surface and potentially on larger substrate as well. The NP layer is thin compared to the acoustic wavelength and rigidly attached to the quartz crystal, ensuring synchronous motion with the oscillating surface. Despite of non-uniform NP coating in partial regions, the overall surface is coated by stiff NPs arranged in a similar way. Although stress will be unavoidably introduced to the sensor from film preparation procedure, if the extra layer is homogenous over the whole sensor surface, it will not generate negative effect on the acoustic wave energy of the sensor. The small size of NPs ( $\phi = 125$  nm) compared to the larger scale of one CMUT membrane ( $\phi \approx 20$   $\mu$ m) also reduce the risk in energy dissipation.

As one can see here, the  $Q$ -factor and equivalent resistance have no change for the LFE sensor during the 2-step modification, which proves the homogeneity in stress distribution from the films.

Repeated results were obtained for more than 10 different crystals with RSD of  $\Delta f_r^{\text{NP}}$  less than 1.0 %, which further suggests the reliability of the spin coating technique in preparing NP films. LFE sensors coated with different amount of NPs were prepared by adjusting spin-speed. The resistance increase kept close to zero, independent on the quantity of particles on sensor surface.

Concerning the further modification with sensing materials on NP surface, non-covalent forces like van der Waals force, electrostatic attraction are supposed to bind sensitive agent and NPs through active groups existing in both materials.

### 6.2.2 The behavior of CMUTs

CMUT sensors before and after NP deposition were driven by various DC voltages and their performance was recorded with impedance analyzer. In Figure 6-4, plot a) is impedance vs. frequency and plot b) is the same data illustrated in the form of conductance vs. frequency. After NP coating, the whole curves moved to the lower frequency range. The  $\Delta f_r^{\text{NP}}$  was about 270 kHz. The  $R_1$  increased by  $\sim 4 \Omega$  (10 %) and the decrease of  $Q$ -factor was just by  $\sim 1.4 - 2.6 \%$  relative to the values from the bare CMUT sensor. Different DC voltages had no influence on the value of frequency shift, and as for  $R_1$ , its changing levels measured under different DC had only slightly distinction.

Since CMUT has the inherent array structure, the magnitude of  $\Delta f_r^{\text{NP}}$  can be collected from individual element group and compared with each other to provide useful information about the uniformity of NP film. It was found that the  $\Delta f_r^{\text{NP}}$  on different element groups had very small deviation (RSD = 1.2 %,  $n = 5$ ), indicating that the amounts of NPs on different element groups were quite comparable and the NP coating showed a satisfied uniformity over the whole sensor surface.

The reproducibility of NP deposition by spin coating was examined on four CMUT sensors (all the NP-coated CMUTs we have). It turned out that three of them gave  $\Delta f_r^{\text{NP}}$  of 272, 273, 270 kHz, respectively. The rest CMUT had  $\Delta f_r^{\text{NP}}$  of 330 kHz, mainly owing to application of NPs prepared from another synthetic process.

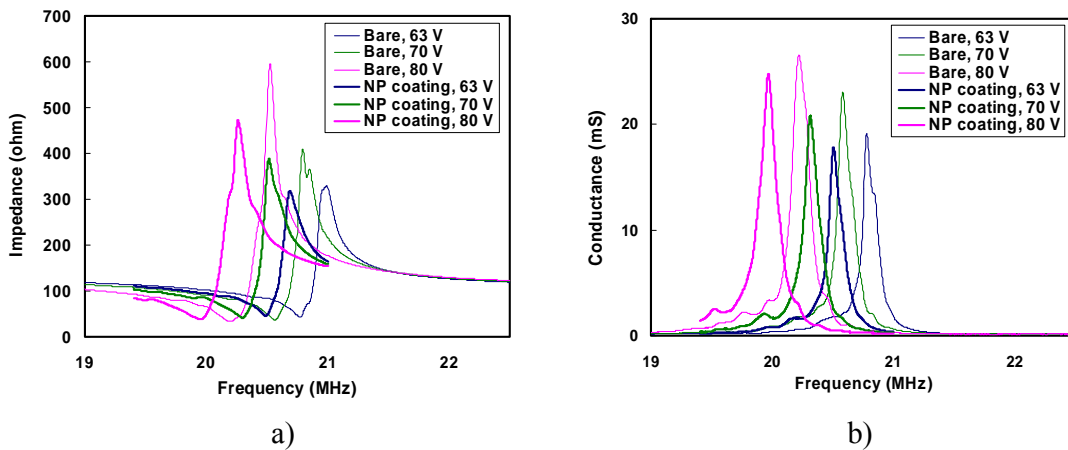


Figure 6-4: Influence of NP coating on CMUT behavior under different DC voltages.

The second layer deposition was investigated on the basis of two types of CMUT sensors: NP-coated ones and bare ones. Figure 6-5 shows the results with OV 225 applied as sensing agent. Firstly, the second layer resulted in much less frequency shift compared with the NP layer. Secondly, the OV 225 film coated with a preceding NP layer on the bottom had fewer disturbances on the sensor behavior, in terms of the decrease of  $Q$ -factor as well as increase of  $R_1$ . The increase of  $R_1$  before and after OV 225 deposition on the double layer system was  $\sim 1.5 \Omega$  (3 %) and the decrease of  $Q$ -factor was by  $\sim 1.3$  % (Figure 6-5 a)), while in the single layer system, these values were around  $3 \Omega$  (6 %) and 5 %, respectively (Figure 6-5 b)). Therefore, the direct coating of the second layer (sensing layer) without the bottom loading of NP film generates higher level of negative influence on performance of CMUTs.

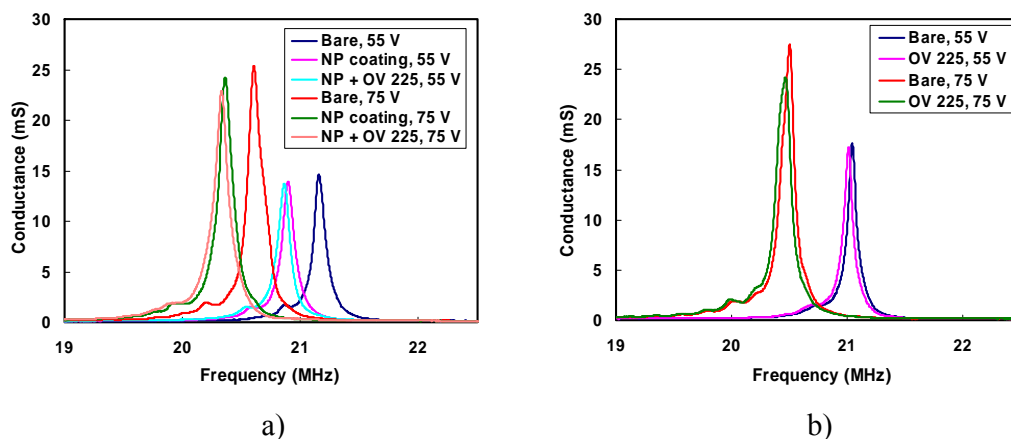


Figure 6-5: Conductance spectra of CMUT sensors with different coatings under two DC voltages.

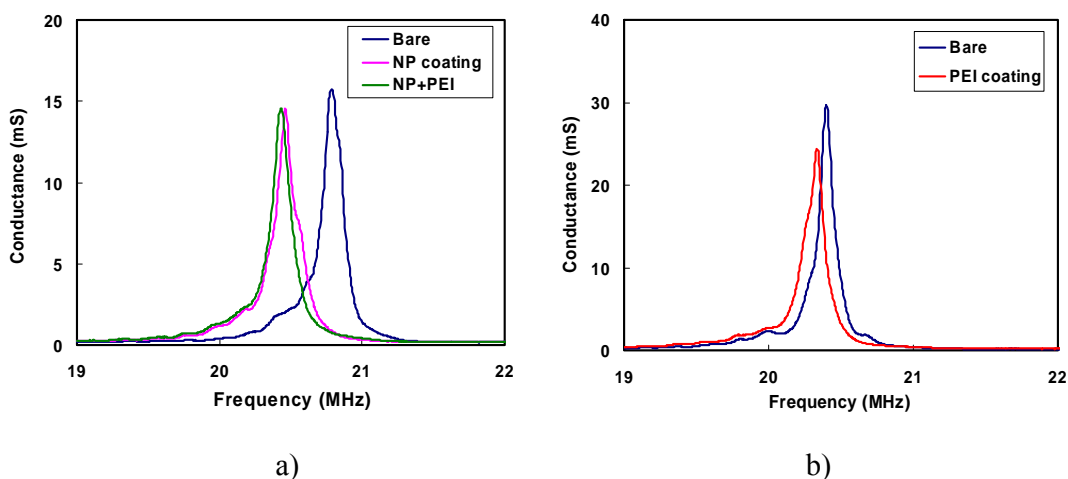


Figure 6-6: Conductance spectra of CMUT sensors with different coatings.

The similar results were obtained from CMUTs with PEI as sensing agent. The spectra in Figure 6-6 a) were obtained from a CMUT sensor experiencing NP and further PEI coating while Figure 6-6 b) exhibits the performance of a CMUT with direct PEI deposition. With regard to PEI coating impact, the change level in  $R_1$  and  $Q$ -factor were 16.8 % (6.8  $\Omega$ ) and 27.9 % for the right one, and no changes at all for the left one. Even considering the overall influence of the external coating on sensor behavior, the  $R_1$  and  $Q$ -factor for the double coated sensor altered by 6.96 % (4.7  $\Omega$ ) and 5.47 %, still smaller than those from direct PEI coating. On the ground of these results, it is fair to deduce that the NP layer plays an important part in enhancing the uniformity of the second coating and reducing the adverse effect imposed from external circumstance. Nevertheless, the operation of aerosol jetting technique should be improved in order to raise the total sensor performance.

### 6.2.3 The behavior of NP-coated CMUTs with ceramide AP membrane

As shown in Figure 6-7, the conductance spectrum of CMUT wafer has slight left-side movement after LB film deposition of ceramide AP. The magnitude of  $R_1$  increased by  $\sim$  0.8 % and the resonance frequency shift is about 7 - 8 kHz. Therefore, it can be concluded that the LB film deposition is able to be used for CMUT modification and the stability of NP films is rather satisfied for no loss of NPs has been found during the whole assembling process.

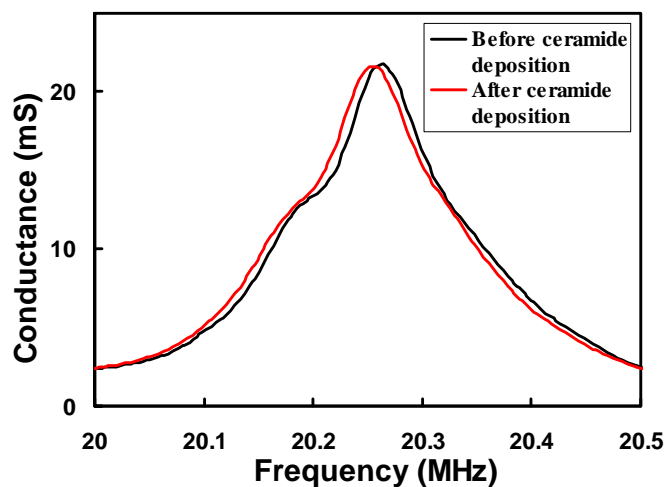


Figure 6-7: Conductance spectra of NP-coated CMUT wafer before and after LB film deposition.

It can be finally concluded that, the NP coatings on both LFE and CMUT sensors illustrate a rather homogeneous property over the entire sensor surface. The NP layer is thin and the self-prepared NPs are materials with high shear modulus. All these features contribute to the sensor performance in terms of restraining dissipation of the acoustic wave energy and keep the  $Q$ -factor from decrease. The sensor-to-sensor difference has been checked with both sensors and repeated results are obtained concerning the amount of NPs deposited onto sensor surface. The RSD of  $\Delta f_r^{\text{NP}}$  for over ten LFE sensors is less than 1.0 % and for three CMUTs it is 0.56 %. The RSD of  $\Delta f_r^{\text{NP}}$  from five different element groups on one CMUT is 1.2 %. All these results suggest the reliability of the spin coating technique in preparing NP films.

It is also found the the bottom NP film is beneficial to the deposition of the second layer. It can lower the level of  $\Delta R_1$  by helping a more homogeneous dispersion of the sensing materials onto the sensor surface.

In addition, deposition of artificial layers is possible onto NP-coated CMUT. Since ceramides cover all the membranes, the measurement conception should be changed. Inspired by the “Microtiter plate” instrument, the whole-surface modified CMUTs can be utilized as a “microplate”, where various samples can be localizedly dispensed to form a sample array. Interactions between the analytes in the samples and the underlying coatings can be monitored and measured by the sensor. In this way, inexpensive and rapid analysis of multiple samples in parallel is possible.

---

## Chapter 7

# VOC Measurement

---

The modified LFE sensors and CMUTs as described in the previous chapters were used to measure several VOCs. Responses were originated by exposing the sensors to varying concentrations of different VOCs in air background. Sorption of analyte brought about mass loading on the sensor and resulted in a decreased resonant frequency. Here focus was placed on the selection and characterization of sensing agents suitable for VOCs from different categories. The detection sensitivity, selectivity, response time, release time and long-time stability were studied as key characters to evaluate the sensor's performance in gas testing. The factors of interest were directly obtained or calculated from the recorded signals.

### 7.1 Measurement setting

Most of the experimental settings in VOC measurement were the same as those applied for chemical characterization of modified sensors depicted in Chapter 6.1. Some exceptions were: IF BW was increased from 300 Hz to 1000 Hz during VOC determination, so as to get a faster span time (about 4 seconds). Measurement cell used for LFE sensors had another cover with gas inlet and outlet (Figure 7-1). The width of the frequency scan was adjusted to just encompass the expected frequency changes in gas testing, in order to maximize frequency resolution. A much wider frequency range was set for CMUT than that for LFE sensor owing to the low  $Q$ -factor of CMUTs. CMUTs were driven under respectively optimized DC bias.

All the measurements have been performed at room conditions. The working scheme of VOC detection is portrayed in Figure 7-2.



Figure 7-1: VOC measurement cell for LFE sensor.

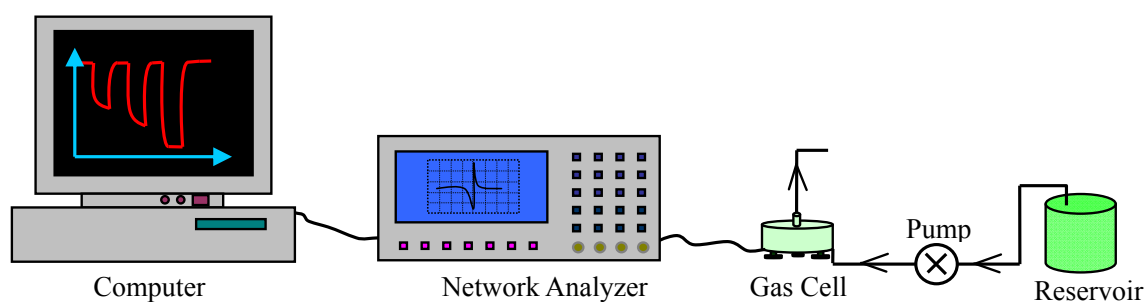


Figure 7-2: Schematic diagram of gas sensor measurement setup.

## 7.2 Gas application system

The vapour stream was generated by flowing synthetic air through a reservoir containing target organic solvents. The temperature of the reservoir was controlled by a thermostat (Julabo F 25, Seelbach, Germany). Then the saturated vapors were diluted with carrier gas (the same synthetic air) in varying ratio to achieve desired concentration. The vapor concentrations in gas phase at respective temperatures were calculated based on the ideal gas laws and the Antoine equation [109]. Dilution ratio was realized by adjusting the flow rates of both organic vapor stream and the carrier gas with a computer-driven mass-flow controller. Valves were used for introduction of analyte gas into the chamber. Typical experiments included alternating exposures of sensor to pure air and vapor/air mixture. Exposure in certain time (mostly 10 min) was followed by purging the chamber with pure synthetic air. The total flow rate through the test cell was kept constant at 80 cm<sup>3</sup>/min, in order to lessen the potential sensor response on the change of flow rate.

In detail, the sensors were mounted into the sealed gas cells. After a period of balance time, basic resonant frequency ( $f_r^1$ ) was recorded, and then a series of standard analyte vapors were purged through the detection chamber. The corresponding frequency ( $f_r^2$ ) was monitored until equilibrium was reached when analyte adsorption and desorption on the sensors came to a balance. The shift of resonant frequency for each analyte was got with  $\Delta f_r = f_r^2 - f_r^1$ . The  $\Delta f_r$  was used for calculation of the amount of sorbed vapors and partition coefficient ( $K$ ) in each coating systems. Calculation of  $K$  is based on Equation (2.5) in Chapter 2.1.2.

Uncoated reference sensors (LFE and CMUT) were mounted into the cells in the beginning and exposed under several vapor samples at their maximum testing concentration. No signals were obtained from the reference sensors on vapor pulses. Hence, no correction was needed for the sorption of vapor to both of the sensors applied.

## 7.3 Mass sensing verification

Acoustic wave-based microsensors obtain their chemical sensitivity and selectivity from a chemically active coating, which interacts with the surrounding environment. As stated in

Chapter 2.1.2, the frequency shift of the sensor during vapor sorption may be a result of gravimetric effect and viscoelastic change of the coating. One way to determine whether the frequency shift corresponds predominately to simple mass effect without or with viscoelastic contribution is to monitor motional resistance ( $R_1$ ) before and during exposure of sensor to vapor, since increase of  $R_1$  signifies accretion of energy loss in sensor performance, mainly arising from coating softening.

Two sensing agents,  $\beta$ -CD and CA, were employed to coat bare or NP-coated LFE sensors. During VOC detection with LFE sensors, nearly no change was observed in  $R_1$  except in exposure to water.

The experimental consequence for CMUT was somewhat different. A general impression during exposure of CMUT to VOCs was that nearly all the vapors conduce to an increase of  $R_1$ , and the increment level relied on the vapor-coating couple and the vapor concentration. Detailed data and analysis are presented in 7.5.2.

## **7.4 Performance of LFE gas sensor**

LFE sensors were only modified by  $\beta$ -CD and CA. The present study was undertaken to examine the different sensing ability of these two materials to a broader set of solvent vapors.

### **7.4.1 Modification effect**

By comparing  $\Delta f_r$  before and after exposure to four representative organic vapors, we found that, the final sensitivity in composite film system was consistent with that in single sensitive layer (Figure 7-3). On NP film, toluene created the highest response, while on single  $\beta$ -CD layer, it was 1-propanol; NP+ $\beta$ -CD film inherited the similar recognition behavior as the single  $\beta$ -CD layer, especially by showing decreased frequency shift to toluene compared with the NP film. The same phenomenon happened in the case of *n*-octane as well, which had the second highest response on NP film and the lowest on  $\beta$ -CD single layer. When it came to the NP+ $\beta$ -CD complex, the response reduced to the lowest. NP+CA film evinced recognition strength also alike that on single CA layer. The above results imply that the sensitive materials are able to modify the NP support underneath properly, and moreover, even alter or determine the sensitivity of the whole gas sensor. Analogous phenomena have been observed with respect to CMUTs (see 7.5.2).

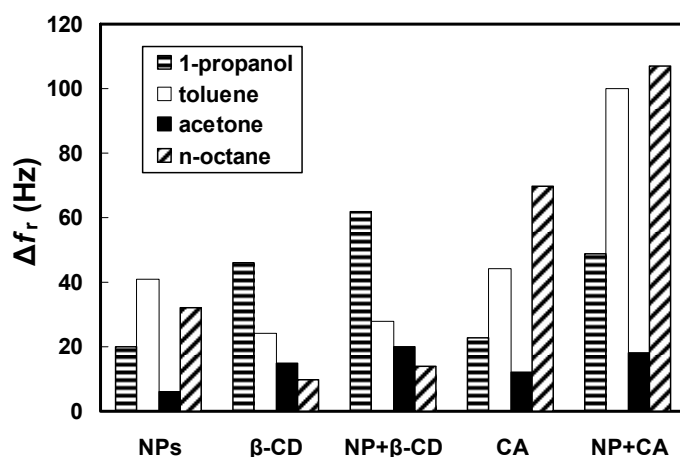


Figure 7-3: The response of LFE sensors with different modification to four VOCs at the concentration of 0.5 %.

#### 7.4.2 Real-time response

Real-time responses of LFE sensors coated with composite films of NP+β-CD or NP+CA to three vapors are shown in Figure 7-4. In comparison with single sensing material, the gas diffusion time was slightly increased with application of PS-*co*-DVB NPs. Inspecting the three VOCs tested, one can observe that the response and recovery time were faster for 1-propanol and acetone than that for toluene with both complex films.

The polarity of toluene is the lowest in the three solvents, so that it is preferably sorbed by the less hydrophilic groups and structures of the host molecules. In the case of NP+β-CD, the recognition towards toluene must be based on the vapor diffusion and interaction with the interior cavities of β-CD, where the hydrophilicity is considerably lower than that in the exterior of the β-CD toroid. Such process takes longer time than the interaction occurring on exterior region, leading to long response and recovery time for toluene.

As to NP+CA, sensor signals in response to toluene show a dual mode including a fast decline of resonant frequency and a slow decrease afterwards. These may be ascribed to combination of several interacting sites on the sensor, which can be the amyl groups and benzene ring in CA, as well as the bottom NPs.

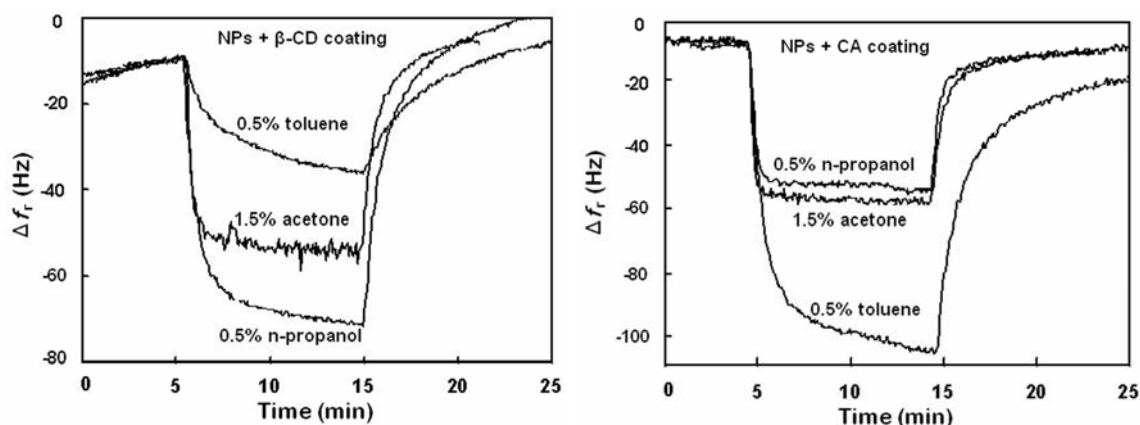


Figure 7-4: Real time response of LFE sensors with different modification.

#### 7.4.3 Sensitivity and selectivity to various VOCs

Vapors in subsets of alkanes, alcohols, ketones and aromatic compounds, plus chloroform and water, have been tested with the present LFE sensors at the concentration of 0.5 %. Saturated vapor pressure ( $P_0$ ) of all tested vapors were calculated from Antoine equation and Antoine parameters [109] at the temperature of 20 °C. The analytes in Table 7-1 were laid in order of decreased  $P_0$ . However,  $\Delta f_r$  corresponding to steady state conditions does not follow the sequence, neither does partition coefficient  $K$ .

The sensing layers provide selective detection of VOCs related to both  $P_0$  values of the analytes and specific interactions. It is very likely that the VOCs are differentiated primarily according to their identities, i.e. the categories they belong to according to their molecular structures. NP+CA coating shows significantly higher response towards chloroform, aromatic compounds (toluene and *p*-xylene) and non-polar alkanes with low  $P_0$  (*n*-octane), in comparison with that towards alcohols. Both coatings have low response capability towards the two VOCs with high  $P_0$  (*n*-hexane and acetone). It is assumed that the CA molecules bind with NPs via the hydroxyl groups on the narrow rim, leaving the wide upper rim to the vapors. The para-tert-amyl substituents there preferentially interact with non-polar organic molecules. In the case of NP+ $\beta$ -CD coating, high response occurs to water and alcohols, which could be attributed to the hydrophilicity imparted by the exterior region of  $\beta$ -CD's toroid structure and the residual hydroxyl groups. High  $K$  for water testing may be the result of its strong polarity and swelling of the sensing films.

In summary, with regard to the two sensing agents used for modifying LFE sensors, it is possible to use CA to gauge aliphatic and aromatic compounds, and  $\beta$ -CD to polar or low-polar alcohols.

Analyte	$M_v$ (g/mol)	$P_0$ (mbar)	NP+ $\beta$ -CD		NP+CA	
			$\Delta f_r$ (Hz)	$K$	$\Delta f_r$ (Hz)	$K$
Acetone	58.1	247.3	49	761	54	707
Chloroform	119.4	206.9	56	1269	95	1814
<i>n</i> -Hexane	86.2	161.8	18	565	34	900
Methanol	32.0	127.5	22	1857	14	996
Ethanol	46.1	59.5	30	1761	27	1336
Toluene	92.1	29.1	28	822	100	2474
Water	18.0	23.4	40	6011	40	5067
1-Propanol	60.1	19.9	62	2790	49	1859
<i>n</i> -Octane	114.2	13.9	12	284	107	2136
<i>p</i> -Xylene	106.2	8.7	47	1198	135	2899

Table 7-1: Frequency response and  $K$  of LFE sensors with NP+CA and NP+ $\beta$ -CD composite films towards various vapors.

The concentration of all the vapors was 0.5 % except acetone of 1.5 %.

$M_v$ : molar mass;  $P_0$ : saturated vapor pressure.

#### 7.4.4 Stability

LFE sensors coated with single and complex films were stored in normal environment and their responses to toluene and 1-propanol were tested again in one week, one month and two months. On the one hand, the sensing capacity of all sensors decreased to different extent in one week (20 - 30 %) and then had smaller change in the following tests (~ 5 %). On the other hand, it has been found that the stability of the modified sensors is very much material-dependent. Within the two agents applied for LFE sensors,  $\beta$ -CD showed much smaller loss of sensitivity than CA did.

#### 7.5 Performance of CMUT gas sensor

In total, CMUT sensors have been coated with five sensing agents (see Chapter 4.5.4). Figure 7-5 shows the responses of differently modified CMUTs as a function of time for stepwise exposure to toluene and 1-propanol at varied concentrations in synthetic air. The duration for one vapor pulse underwent 10 min except otherwise specified. Note the different scaling at the ordinates. The sensor's behavior has been elaborated in the following sub-sections.

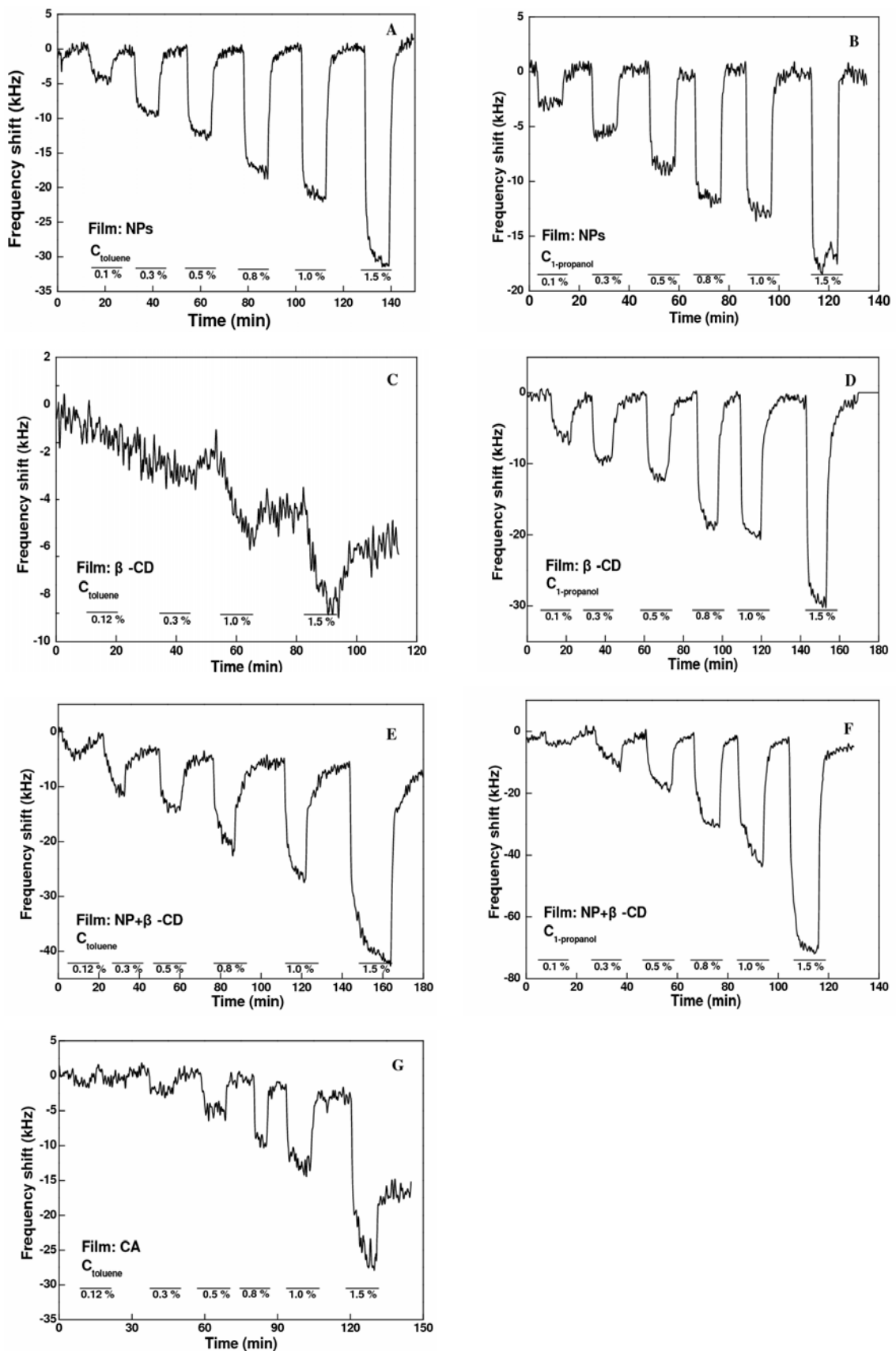


Figure 7-5: Transient response of CMUTs modified with various coatings in exposure to toluene and 1-propanol.

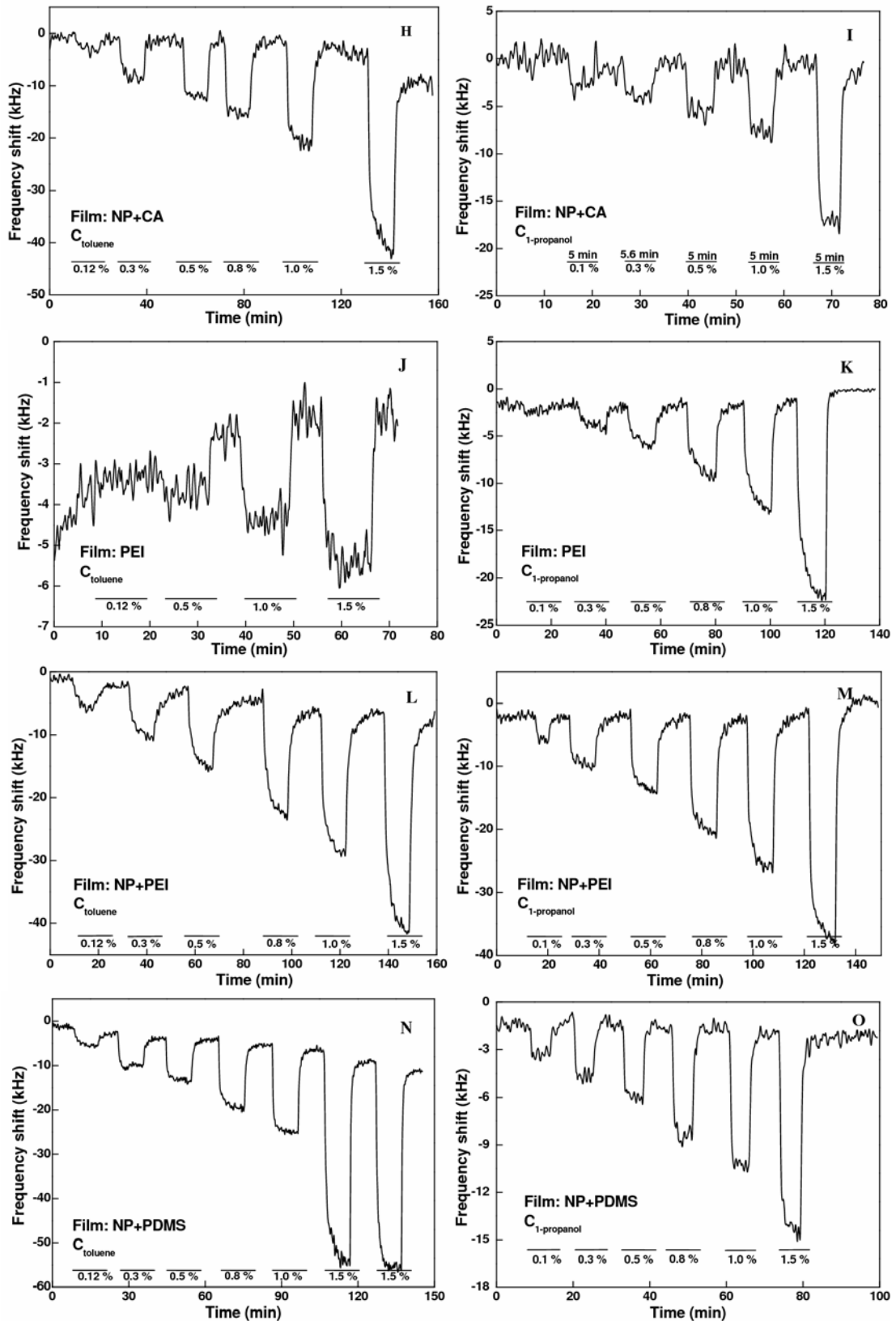


Figure 7-5 cont.: Transient response of CMUTs modified with various coatings in exposure to toluene and 1-propanol.

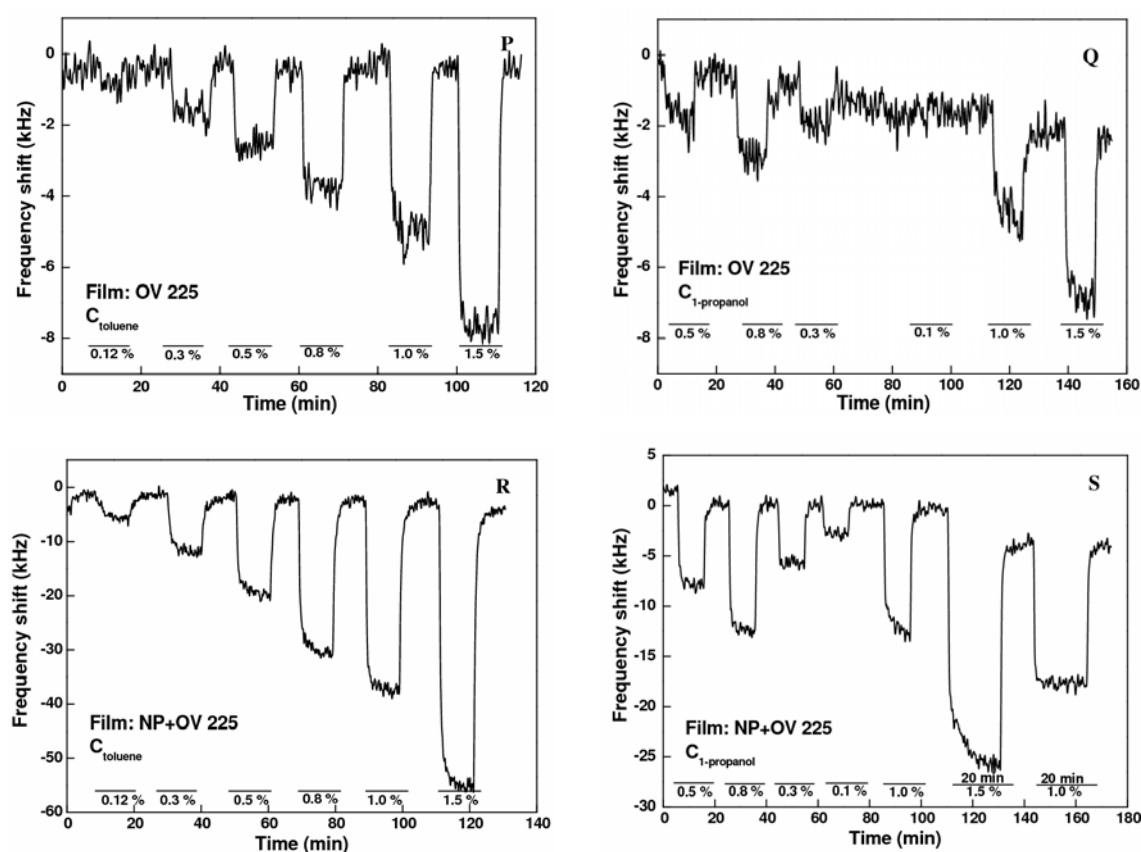


Figure 7-5 cont.: Transient response of CMUTs modified with various coatings in exposure to toluene and 1-propanol.

### 7.5.1 Response and recovery time

For most of sensors, the sorption processes are fully reversible, and the time to reach 85 % response and recovery equilibrium is within 4 min. The majority of the responses could be characterized by a rapid initial frequency dropping, followed by slow decrease and decay times. The initial rapid mass increase, which determines the total frequency change during vapor exposure, suggests the existence of a limited number of open surface sites within the film [110]. Furthermore, relatively slow uptake and release of vapors on or in sensing matrix in the following steps may be attributed to the gradual interplay between them.

The desorption and sorption usually occupy comparable time for one couple of sensor-analyte, which indicates the same interaction mechanism during these two periods.

In some cases, exposure of sensors to vapor pulses caused an irreversible decrease in the base value of  $f_r$  but reversible  $\Delta f_r$  during each vapor exposure (Figure 7-5 L, N, S).

Similar to the conclusion made on LFE sensors, the different sensing behavior on CMUTs with various coatings should be mainly referable to the distinction of coating's structure and feature. Further comments on specific vapor-sorbent interactions have been narrated in the following section.

### 7.5.2 Sorption isotherm analysis

The resonant frequency shifts due to vapor sorption onto CMUTs,  $\Delta f_v$ , were recorded at a series of vapor concentrations. The adsorption isotherm of toluene and 1-propanol on the differently modified CMUTs were shown in Figure 7-6 to 7-10. What is immediately evident for most of the plots is the highly linear correlation between  $\Delta f_v$  and vapor concentration ( $C_v$ ) over the tested range of 0.1 - 1.5 %, signifying that the underlying sorption principles follows Henry's law. However, as the concentration increased to certain extent, a few unexpected phenomena appeared and some of them were thought to be faulty. Nevertheless, in combination with other parameters, the possible causes responsible for the observations could still be extracted.

The following points have been derived by analyzing the sorption isotherm curves.

Linear isotherm through the range of tested vapor concentration existed for most of vapor-sensor systems, denoting Henry's law behavior.

Inflection took place in two forms, yielding curves either concave or convex against the  $C_v$  axis (x axis). Isotherm from NP+ $\beta$ -CD coating was categorized into a concave curve without showing a discernible inflecting point (Figure 7-6 b)). The curves from NP+CA (Figure 7-7) and NP+PDMS (Figure 7-9 a)) showed convex structures to  $C_v$  with a clear inflection point. The existence of isotherm discontinuities appears to be associated with phase changes of materials.

It was found that the magnitude of resistance ( $R_1$ ) altered along with resonant frequency. In most conditions,  $R_1$  increased upon vapor exposure. The  $R_1$  accretion level went higher with increased vapor concentration, which was especially apparent in double coated CMUTs.

Take the double coating NP+PDMS for instance. When the coating was exposed to toluene at the concentration of 0.12 %,  $R_1$  increased by 1.19 % from no toluene status. When the concentration of toluene was 1.5 %,  $R_1$  increased dramatically by a level of 23.4 %. When the analyte was 1-propanol,  $R_1$  increased by 1.68 % at the concentration of 0.1 % and 8.63 % at the concentration of 1.5 %. On the other hand, dramatic rise in  $R_1$  may be accompanied by unexpectedly large  $\Delta f_r$ . In the NP+PDMS coating, when the sensor was exposed to 1.5 % toluene,  $\Delta f_r$  was 48.4 kHz, presenting an inflection in the sorption isotherm (Figure 7-9 a)).

The  $R_1$  alteration reveals possible change in the physical state of the film. Therefore, the jumping of isotherm curves at high vapor concentration may well be attributed to the variation in film modulus, instead of large amount uptake of toluene vapors.

All the isotherm curves exhibited no sign of a saturation response up to the tested concentration of 1.5 %, for both toluene and 1-propanol. However, a gradual saturation tendency could be observed for NP+ $\beta$ -CD films in exposure to 1-propanol, appearing as a logarithmic relation in concentration range from 0.1 % to 1.5 %. This gas affinity isotherm may be accounted for by a dual mode model of sorption, represented by a combination of Henry's law and Langmuir theory [111-114].

Single PDMS layer did not render detectable signals for toluene and 1-propanol, thus it can be viewed as an “inert” material. The isotherm curves for NP+PDMS film were unexpected, when the double coating afforded a lower sensitivity to both of the vapors than NP coating (Figure 7-9). We do not have a definitive explanation for this, but one reason might be that PDMS screened some of the recognition sites initially located in the NP coating and resulted in a less sensitive coating for these two vapors. Similarly, CA film showed “inert” to 1-propanol and which may account for the lower sensitivity in NP+CA film compared with that in NP film (Figure 7-7). For the rest complex coating systems (NP+PEI, NP+OV 225, and NP+ $\beta$ -CD), the values of  $\Delta f_v$  were close to the sum of the bottom NPs and the second layer.

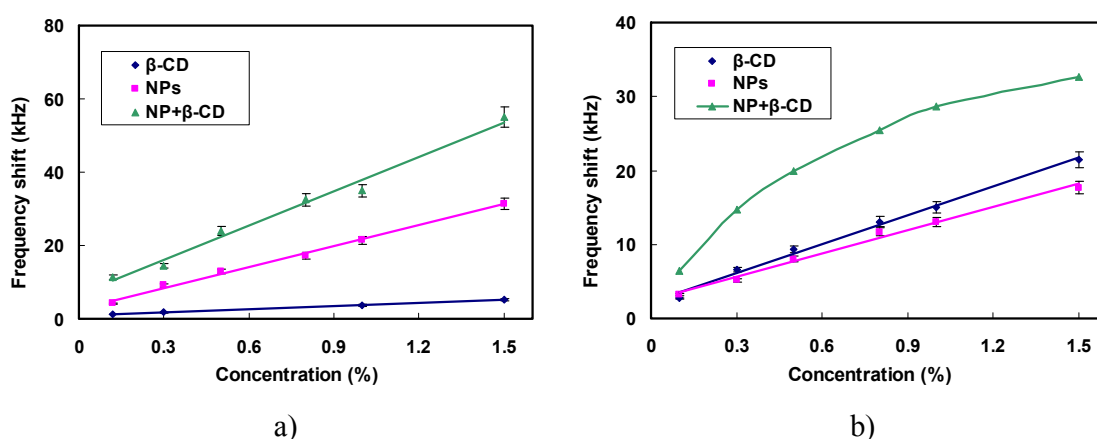


Figure 7-6: Sorption isotherm of  $\beta$ -CD film series. a) Toluene; b) 1-propanol.

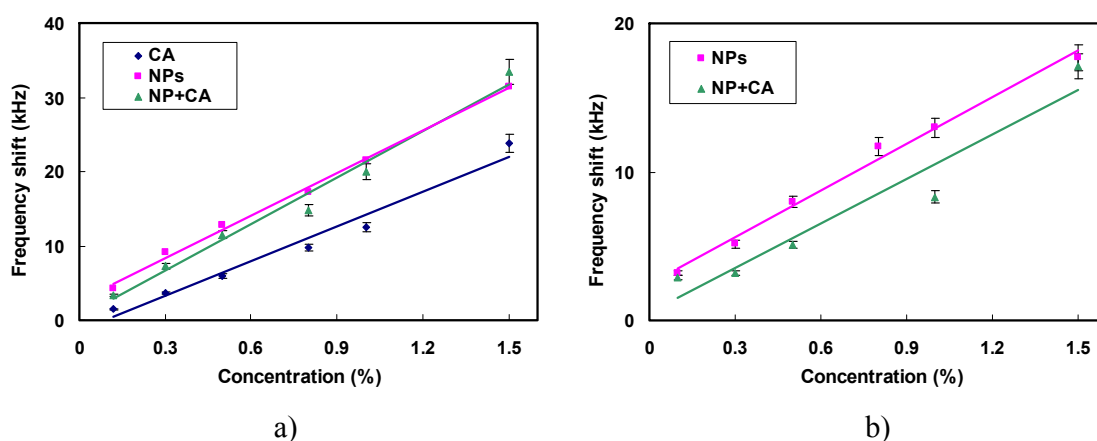


Figure 7-7: Sorption isotherm of CA film series. a) Toluene; b) 1-propanol.

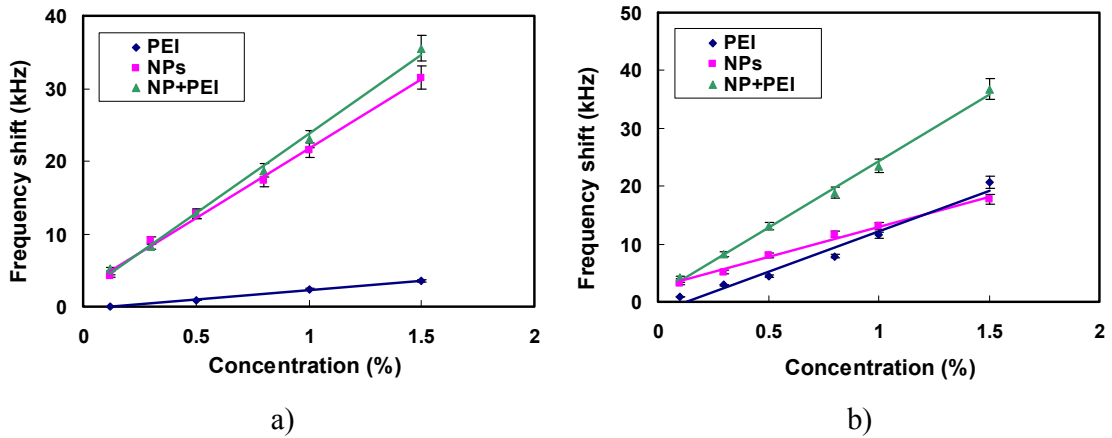


Figure 7-8: Sorption isotherm of PEI film series. a) Toluene; b) 1-propanol.

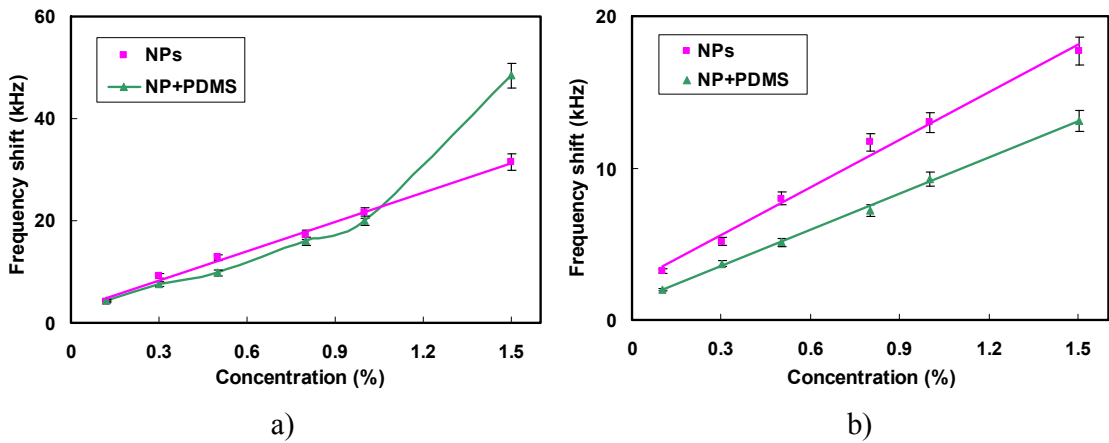


Figure 7-9: Sorption isotherm of PDMS film series. a) Toluene; b) 1-propanol.

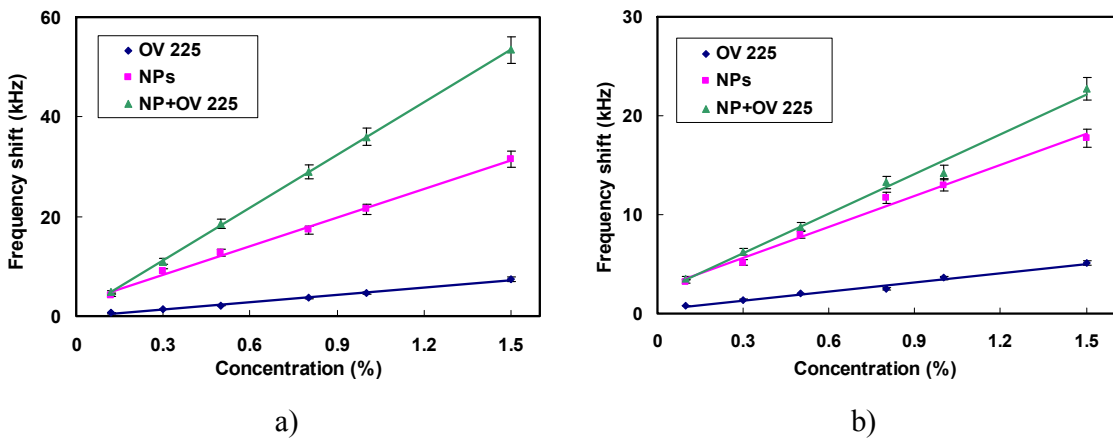


Figure 7-10: Sorption isotherm of OV 225 film series. a) Toluene; b) 1-propanol.

### 7.5.3 Sensitivity

Partition coefficients  $K$  were firstly calculated for vapor-sorbent pair at different vapor concentrations and then the values were averaged for each pair. The  $K$  average were listed

in Table 7-2 and plotted in Figure 7-11. Since calculating  $K$  not only considers the amount of the deposited sensing materials, but takes the molar weight of vapors into account as well, comparison of  $K$  is more meaningful in assessment of sensitivity.

	Toluene		1-Propanol	
	Single	Double	Single	Double
NP	2284.04	--	2181.42	--
$\beta$ -CD	1376.06	1757.73	10959.20	4440.72
CA	3477.92	1863.47	-	1747.21
PDMS	-	1484.05	-	856.36
PEI	737.20	2149.46	5122.51	3342.43
OV 225	3779.81	3213.94	4633.84	2236.14

Table 7-2: Partition coefficient of toluene and 1-propanol with different sensing films.

Single: only one sensing layer. Double: NP plus another layer.

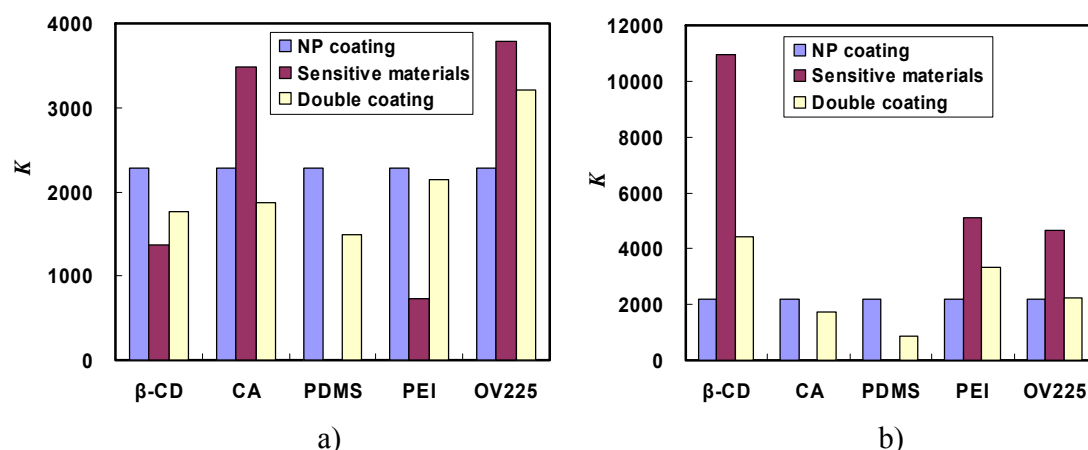


Figure 7-11: Partition coefficient with different sensing films.

a) Toluene; b) 1-propanol.

The NPs alone respond to both tested gases in a noticeable manner. However, the calculated  $K$  has little discrepancy between toluene and 1-propanol, implicating unspecific response capacity of NP film. Inspecting Figure 7-11, one can observe that the overall magnitude of sensitivity of each double layer have unanticipated values, some of which are less than the values from NP film, rather than an increase based on that of the bottom NP layer, similar to the summary made through analyzing the isotherm curves. The coating showing the greatest response to 1-propanol is  $\beta$ -CD, whereas it is relatively insensitive to toluene. OV 225 exhibits the highest sensitivity in contact with toluene, while the other polysiloxane, PDMS, gives the lowest response to toluene. These results designate that some degree of specificity has been obtained with coatings which have preferring interaction to different vapors.

#### 7.5.4 Reproducibility and aging effects

The CMUT sensors modified with sensitive materials were remeasured and their sensing ability was retested. The base frequency of all sensors was found some changes to different degrees. Most of them displayed less change than the intrinsic frequency noise of CMUT, which include CMUTs coated with NPs,  $\beta$ -CD, NP+ $\beta$ -CD, OV 225, NP+OV 225, NP+PDMS, CA and NP+CA. For PDMS, PEI and NP+PEI films, the resonant frequency went up by 0.05 - 0.1 %, indicating the possible loss of the initial film loading. On the other side, the increase of base frequency may also arise from follow-up desorption of the solvent residuals coming from the sensing coating preparation.

Long time stability of the gas sensors was checked for 1-propanol, toluene and acetone. It was found that their vapor uptake ability decayed by 10 - 35 % from the first exposure to the next one after about two weeks. However, the signals then went stable as repeatable responses were obtained in the following measurements. Over this period, all the sensors were stored in desiccator without control in temperature.

Another interesting result was that the lost recognition capability was higher for 1-propanol than that for toluene. It is assumed that the major interaction between 1-propanol and the sensitive materials is based on hydrogen bond through the hydroxyl groups owned by both substances. Such groups may be passivated when exposed to air. Apart from this, the weak sticking of the NPs on CMUT surface could also spoil the long-term stability. This problem could be solved by chemical modification of the sensor surface or the NPs.

#### 7.5.5 Response mechanism analysis

Sensing agents may either physically incorporate or covalently combine analytes. For most of interactions, noncovalent ones take less time than covalent ones, in both response and recovery period. Considering the relatively short time and reversible response (see 7.5.1), noncovalent interactions should dominate in most sensing processes.

In particular, hydrophobic forces between alkyls of toluene molecules and sensitive materials may be the leading interaction and results in loosely bonded complex at sensor surface.

The mass gain was found to increase monotonically with increasing vapor concentration, indicating a bulk adsorption mechanism. Taking into consideration all the obtained experimental facts, a somewhat complex adsorption mechanism can be derived out. This includes, in addition to the conventional host - guest binding, the interaction of guest molecules with alkyl chains, vapor penetration into the film bulk through pores, as well as further condensation of vapors into liquid state. Concrete discussion has been made as follows.

Since the two supramolecular sensing agents are both cavitands, cavity filling is firstly considered for  $\beta$ -CD and CA, which has been well known for forming inclusion complexes

with various materials in both liquid and gaseous phases [21, 22, 115, 116]. The minimum requirement for the inclusion complex formation is the size compatibility between host and guest molecules. The complexes thus formed are stabilized by various inter-molecular forces, such as hydrophobic interaction, hydrogen bonding, and others. Besides, the side chains of the supramolecules could either hinder or facilitate the inclusion of vapors into the host molecules. As for size, the inner cavity diameters of  $\beta$ -CD and CA are about 7 and 10 Å [117], while toluene, 1-propanol and acetone are 5.68, 5.15 and 4.82 Å, respectively [118]. All of the three are smaller than the supramolecules' inner cavity diameter. Therefore, the cavity radius of the supramolecules does not have much impact on the gas adsorption but the functional groups will play a key role.  $\beta$ -CD, for instance, is supposed to be more sensitive to hydrophilic alcohols, because of the formation of hydrogen bonds between the hydroxyl groups existing in both analyte vapors and  $\beta$ -CD molecules. In the case of CA, the presence of alkyl chains is important for the formation of vapor-sorbent complex. Aromatic hydrocarbon compound, toluene, can therefore be sorbed by CA derivatives.

It has been reported that CA self-assembly films tend to form nanoporous architectures [119], with empty spaces between the molecules and between the substitute alkyl chains. Organic vapors can penetrate through these pores inside the film matrix and condense there, accompanied by film swelling [120]. Because the size of the pores is in the nanometer range, condensation of vapor may take place at pressures much lower than the corresponding saturated limit, particularly at 1.5 % for toluene. The proposed adsorption model does not contradict the conventional host-guest mechanism of molecular recognition, but complements it in the high vapor concentration range. Thus the results can be interpreted in terms of capillary condensation of organic vapors in the nanoporous matrix of CA films accompanied by film swelling due to accumulation of liquid adsorbate within the film matrix.

PDMS has methyl groups linked on the siloxane backbones and its response is mainly aimed to non-polar vapors. Since the polarity of toluene is smaller than that of alcohols, the interaction between 1-propanol and PDMS is weaker than that between toluene and PDMS. The side chain components of OV 225 are 50 % methyl groups, 25 % phenyl groups and 25 % cyanopropyl groups. The cyano group has strong polarity, while other groups impart other forces such as hydrophobicity. Therefore, the response to toluene and 1-propanol has varied levels, in single layer and double layer (Table 7-2).

PEI is a water soluble agent, so it is inclined to adsorb polar compounds, e.g. water (not shown) and alcohols. As a consequence, the  $K$  value for 1-propanol is much higher than that for toluene.

The comparison of  $K$  among vapor-matrix couples intimates that the sorption is also dependent on other factors. It can be seen from Table 7-1 that  $P_0$  of 1-propanol is lower than that of toluene, and acetone has the highest  $P_0$  among all the tested gases. Generally speaking, the higher the  $P_0$  of one vapor, the harder it is to be adsorbed if other conditions are kept the same. This could explain the difficulty in acetone detection (most of the films

had no detectable response to acetone). However, if there exist specific interactions between sensitive materials and vapors,  $P_0$  should not be considered as the major factor in determining sensor response. In general, the possible contributing factors include a structural coincidence between host and guest molecules, specific interactions between active groups of sorbents and sorbates, and solubility of vapor or sensing agents with each other. Solubility is mainly associated with their configurational likeness. To better understand the influence of molecular structure on sensing activity in a semi-quantitative manner, Hansen Solubility Parameter (HSP) analysis has been applied to investigate the interaction forces and their strength between sensitive materials and vapors.

Hansen Solubility Parameters have been developed, among other applications, as a way for the rational selection of solvents since 1967 [121, 122]. They are based on the idea that “like dissolves like” [123], where one molecule is defined as being “like” another if they have a similar chemical structure. Such analysis could be expected to estimate or predict a general intermolecular interaction force.

Specifically, each molecule is given three Hansen parameters, representing three kinds of intermolecular forces, with  $(\text{MPa})^{0.5}$  as unit in the SI system of units.

$\delta_d$ : the dispersion HSP;

$\delta_p$ : the dipolar HSP;

$\delta_h$ : the hydrogen-bond HSP.

These three parameters can be treated as co-ordinates for a point in three dimensions also known as the Hansen space. The “distance” ( $R_a$ ) between material 1 and 2 in Hansen space can be calculated using Equation (7.1). The nearer two molecules are in this three dimensional space, the more likely they are to dissolve into each other.

$$(R_a)^2 = 4(\delta_{d2} - \delta_{d1})^2 + (\delta_{p2} - \delta_{p1})^2 + (\delta_{h2} - \delta_{h1})^2 \quad (7.1)$$

Although the HSPs of the detected VOCs can be directly found in this handbook [124], for most of the sensitive materials involved in the research, their HSPs are not available. Therefore calculation of their HSPs has been carried out on the basis of group-contribution approach.

The first step was to split the molecular structures of each compound or the repeating unit in the case of polymer or supramolecule. The group segments were identified and summarized, and their occurrences in the whole structure were counted. With the reported partial solubility parameters of all the constituent groups and the equations in [125], the HSPs were calculated out. In the second step, the solubility parameter “distance”,  $R_a$ , in respective guest-host pairs was obtained with Equation (7.1). The smaller the  $R_a$  is, the higher the solubility between the two substances.

Table 7-3 presents the computed HSPs for the five sensing agents and all the HSPs for both vapor and sensing agents are tabulated in Table 7-4.  $N_i$  is the occurrence of the group in corresponding structure;  $C_i$  refers to the contribution of each group to the solubility from

[125]. The equation to get  $\delta_d$ ,  $\delta_p$ ,  $\delta_h$  is:

$$\delta = \sum N_i C_i + C \quad (7.2)$$

where  $C$  is a given constant, which is 17.3231, 7.3548, 7.9793, respectively for  $\delta_d$ ,  $\delta_p$ ,  $\delta_h$ .

PEI,  $\beta$ -CD and CA all have active hydrogen in either secondary amino group (for PEI) or hydroxyl group (for  $\beta$ -CD and CA). They are supposed to be dissociated on the surface of the sensor, therefore not lending themselves to the solubility parameters.

As supramolecules,  $\beta$ -CD and CA contain repeating unit involved in one molecule, and the number of the basic unit is 7 for  $\beta$ -CD and 8 for CA. However, multiplication was not involved in calculating HSPs since solubility is majorly related to the groups constituting the compound, instead of its steric structure.

$\beta$ -CD has three hydroxyl groups and in our case, the one applied is partially methyl-substituted (m- $\beta$ -CD). Because of this, the partition of the residual hydroxyl and methoxyl groups should be estimated first. The molecular weight ( $M_w$ ) of the applied product is 1310 g/mol, and  $M_w$  of  $\beta$ -CD with one-hydrogen replacement and two-hydrogen replacement are 1232 and 1330 g/mol. Thus it can be predicted that about 80 % of  $\beta$ -CD molecules are under two-hydrogen replacement and 20 % under one-hydrogen replacement. Therefore, the  $N_i$  for -OCH<sub>3</sub> and -OH groups in  $\beta$ -CD were set as 1.6 and 0.4 due to such partial methylation.

$\beta$ -CD		$\delta_d$		$\delta_p$		$\delta_h$	
1st-order groups	$N_i$	$C_i$	$N_i C_i$	$C_i$	$N_i C_i$	$C_i$	$N_i C_i$
-OCH <sub>3</sub>	1.6	-0.5828	-0.93248	0.1764	0.28224	0.1460	0.2336
-OH	0.4	-0.3462	-0.13848	1.1404	0.45616	7.1908	2.87632
-CH <sub>2</sub> -	1	-0.0269	-0.0269	-0.3045	-0.3045	-0.4119	-0.4119
-CHO (ethers)	1	0.8833	0.8833	1.6853	1.6853	0.4470	0.447
-CH< (cyclic)	5	0.6450	3.225	0.6491	3.2455	-0.2018	-1.009
-CHO (cyclic)	1	0.2753	0.2753	0.1994	0.1994	-0.1610	-0.161
$C$			17.3231		7.3548		7.9793
$\sum N_i C_i + C$			20.60884		12.9189		9.9543

CA		$\delta_d$		$\delta_p$		$\delta_h$	
1st-order groups	$N_i$	$C_i$	$N_i C_i$	$C_i$	$N_i C_i$	$C_i$	$N_i C_i$
-AC	3	0.8446	2.5338	0.6187	1.8561	0.0084	0.0252
-ACH	2	0.1105	0.221	-0.5303	-1.0606	-0.4305	-0.861
-ACCH <sub>2</sub>	1	0.6933	0.6933	0.6517	1.3034	-0.1375	-0.275
>C<	1	1.2686	1.2686	2.0838	2.0838	0.0866	0.0866
-CH <sub>3</sub>	3	-0.9714	-2.9142	-1.6448	-4.9344	-0.7813	-2.3439
-CH <sub>2</sub>	1	-0.0269	-0.0269	-0.3045	-0.3045	-0.4119	-0.4119
<i>C</i>			17.3231		7.3548		7.9793
$\Sigma N_i C_i + C$			19.0987		6.2986		4.1993

PEI		$\delta_d$		$\delta_p$		$\delta_h$	
1st-order groups	$N_i$	$C_i$	$N_i C_i$	$C_i$	$N_i C_i$	$C_i$	$N_i C_i$
CH <sub>2</sub>	4	-0.0269	-0.1076	-0.3045	-1.218	-0.4119	-1.6476
-NH	2	1.4681	2.9362	2.8345	5.669	1.2505	2.501
<i>C</i>			17.3231		7.3548		7.9793
$\Sigma N_i C_i + C$			20.1517		11.8058		8.8327

OV 225		$\delta_d$		$\delta_p$		$\delta_h$	
1st-order groups	$N_i$	$C_i$	$N_i C_i$	$C_i$	$N_i C_i$	$C_i$	$N_i C_i$
CH <sub>3</sub>	2	-0.9714	-1.9428	-1.6448	-3.2896	-0.7813	-1.5626
CH <sub>2</sub>	3	-0.0269	-0.0807	-0.3045	-0.9135	-0.4119	-1.2357
CN	1	-0.3392	-0.3392	6.5341	6.5341	-0.8892	-0.8892
AC	1	0.8446	0.8446	0.6187	0.6187	0.0084	0.0084
<i>C</i>			17.3231		7.3548		7.9793
$\Sigma N_i C_i + C$			15.805		10.3045		4.3002

PDMS		$\delta_d$		$\delta_p$		$\delta_h$	
1st-order groups	$N_i$	$C_i$	$N_i C_i$	$C_i$	$N_i C_i$	$C_i$	$N_i C_i$
CH <sub>3</sub>	4	-0.9714	-3.8856	-1.6448	-6.5792	-0.7813	-3.1252
<i>C</i>			17.3231		7.3548		7.9793
$\Sigma N_i C_i + C$			13.4375		0.7756		4.8541

Table 7-3: First-order group approximation for HSPs of various sensing substances.

Vapor	$\delta_d$	$\delta_p$	$\delta_h$
Toluene	18	1.4	2
1-propanol	16	6.8	17.4
Acetone	15.5	10.4	7

Sensing agent	$\delta_d$	$\delta_p$	$\delta_h$
$\beta$ -CD	20.6088	12.9189	9.9543
CA	19.0987	6.2986	4.1993
PEI	20.1517	11.8058	8.8327
OV 225	15.805	10.3045	4.3002
PDMS	13.4375	0.7756	4.8541
PS	18.5	4.5	2.9

Table 7-4: HSP list for vapors and sensing agents.

Based on the above data, the distance  $R_a$  between each pair of vapor analyte – coating agent was further calculated out (Table 7-5).

Substance	$R_a$		
	Toluene	1-propanol	Acetone
$\beta$ -CD	14.9392	13.3358	10.9303
CA	5.8019	14.5917	8.7446
PEI	13.1714	12.9384	9.5858
OV 225	10.1908	13.5661	2.7695
PDMS	9.5813	14.8310	10.6888
PS	3.3793	15.5094	9.3606

Table 7-5:  $R_a$  between each vapor-coating couple.

By comparing the values of  $R_a$  in Table 7-5, one can make a rough estimation in sorption capacity of the sensing agents between toluene and 1-propanol. Most of them are in agreement with the experimental results (Table 7-2), except OV 225 and NPs. It is easy to explain the inconsistency of NPs' response in contact with the vapors because the practically used NPs are a cross-linked copolymer with surface modification of acrylic acid, whose chemical structure must be very different from the PS in the handbook.

Concerning OV 225, both experimental and calculation errors might be the cause for the discord.

Note that no experimental data for acetone, for CMUTs always had very low sensitivity to acetone molecules.

### 7.5.6 Equilibrium analysis on vapor sorption

It is known that, due to mass loading by purging vapors into gas measurement cell, the sensor inside yields electrical signals by decreasing its resonant frequency. Typically this appears as a rapid decline of frequency, and then the speed slows down to a balance status. But we did find some sensors showed continuous and slow descent behavior after the initial fast response, which is seemingly endless. The CMUT coated with NP+ $\beta$ -CD complex film was one example, when it was exposed to toluene vapors (Figure 7-12).

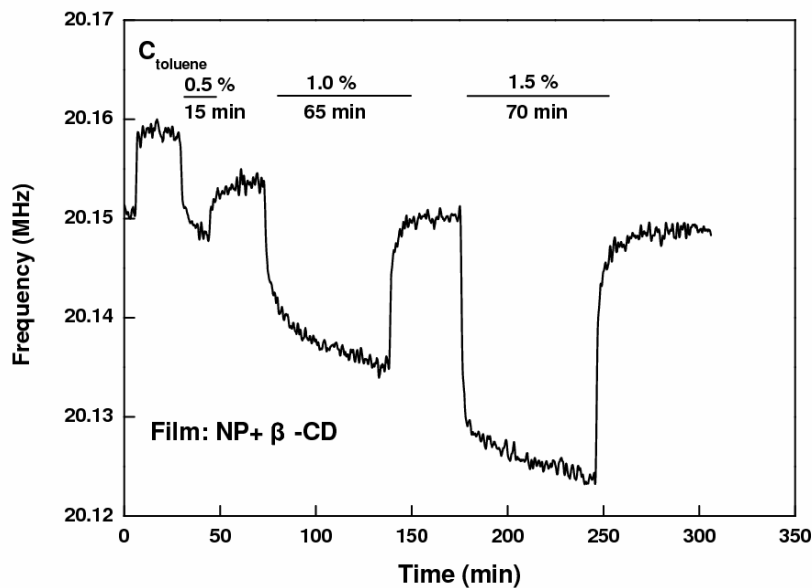


Figure 7-12: Exposure of NP+ $\beta$ -CD modified CMUT sensor to toluene at different concentration.

In order to figure out the real cause behind such behavior, a long time gas measurement was done on this sensor with the concentration of toluene at 1.0 %. The obtained signals are plotted in Figure 7-13. The sensor is seen to give an increase of resonant frequency to an extra air flow (from air = 0 to air = 80 cm<sup>3</sup>/min at 0.31 h), and then a balance came very soon. After rapid frequency dropping as a result of toluene sorption (exposure to toluene vapor at 1.57 h), a sustained and slow downward shift of frequency lasted for about 19 hours and no balance tendency occurred. After repurging the sensor with pure air (80 cm<sup>3</sup>/min at 20.58 h) for some time, the recording went on without any air flow (at 26.40 h). A continuous dropping of frequency was observed even no air flowing through the sensor. At 34.20 h, the gas cell was disconnected to the gas system, an increase of frequency lasted till the end of the whole experiment. The overall impression of these phenomena is that it is very likely that the long time dropping of frequency is not because of toluene sorption but the consequence of sealing the sensor into the gas cell.

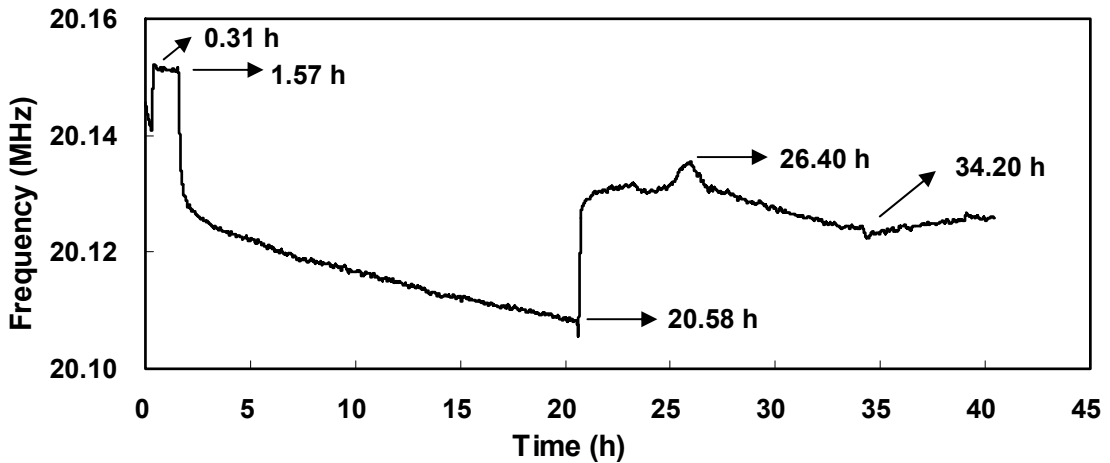


Figure 7-13: Long time exposure of NP+ $\beta$ -CD modified CMUT sensor to toluene at the concentration of 1.0 %.

Despite of this, the continuous frequency dropping did not happen to all of the sensing coatings. Even for the same film, it is not necessarily so under exposure to other vapors (Figure 7-14).

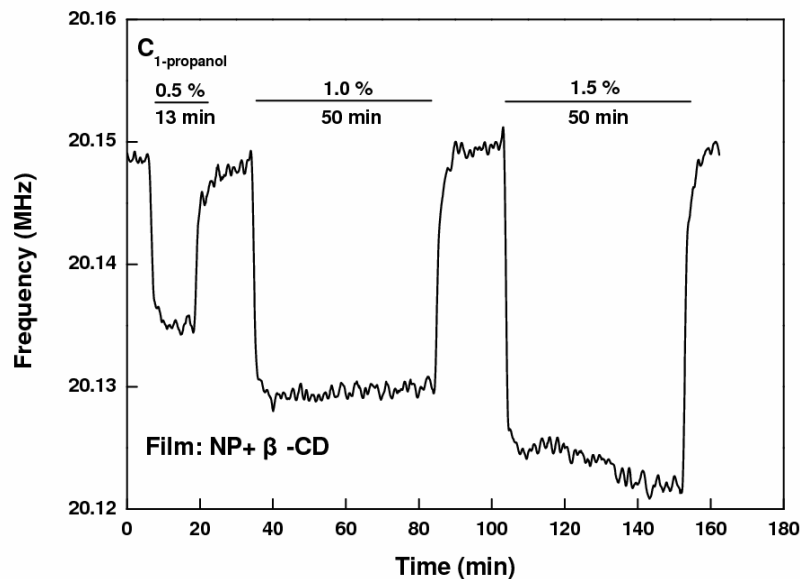


Figure 7-14: Exposure of NP+ $\beta$ -CD modified CMUT sensor to 1-propanol at different concentration.

### 7.5.7 Study of pre-condition

Conditioning is a phenomenon referring to the dilation of a polymer in contact with a highly swelling gas [126]. It often results in larger levels of sorption and permeation of the gas in the polymeric matrix [112].

Interpretation of the conditioning behavior is on the basis of the hypothesis that, as the

polymer is swollen, the mobility of the chains is enlarged, causing disruptions of subtle chain-packing in the polymer. The breakups offer more sorption sites owing to decreased energy demands for sorption, appearing as elevated capacity in the overall polymer response under exposure to vapors.

In order to determine if the sensing agents involved in this research also exhibit conditioning response, the double-coated CMUT sensors with the sensing layer of supramolecule ( $\beta$ -CD), glassy polymer (NPs) or rubbery polymers (OV 225 and PDMS) were tested by repeated toluene and 1-propanol pressurization at a fixed volumetric flow rate with vapors at a given concentration. The vapor concentration was kept at 0.5 % in all the transient cycles, unless specified otherwise. Change in base frequency was considered as an indicator of conditioning effect.

The performance of different kinds of coating materials was described as follows.

1. For the two rubbery polymer coatings, a slight decrease of frequency baseline occurred when the sorbate is toluene and no change when it is 1-propanol (Figure 7-15 and 7-16).

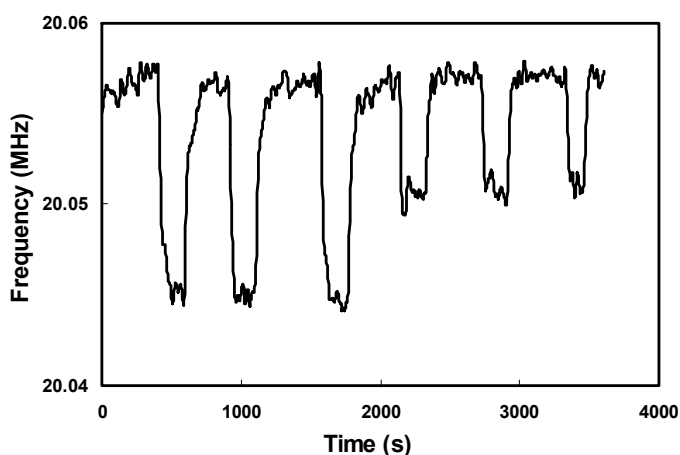


Figure 7-15: Transient response of CMUT sensor coated with NP+OV225 complex films at room temperature to toluene (the first three cycles) and 1-propanol (the following three cycles) at the concentration of 0.5 %.

In particular, for the NP+OV225 coating, during toluene purging, the base frequency before the preliminary one was reduced by  $\sim 600$  Hz compared with those before the subsequent cycles. Then this CMUT sensor was stored in desiccator for 48 hours and then retested again with an opposite sampling sequence, i.e. 1-propanol flowing through the sensor first. The behavior for 1-propanol was the same that it led to no significant frequency baseline reduction. The influence due to toluene preliminary purging became insignificant as well when the vapor flew through sensor after 1-propanol measurement (Results were not shown).

For the NP+PDMS modified CMUT sensor, the conditioning effect was especially apparent as the frequency baseline dropped by 5 kHz as a result of the first contacting with toluene (Figure 7-16).

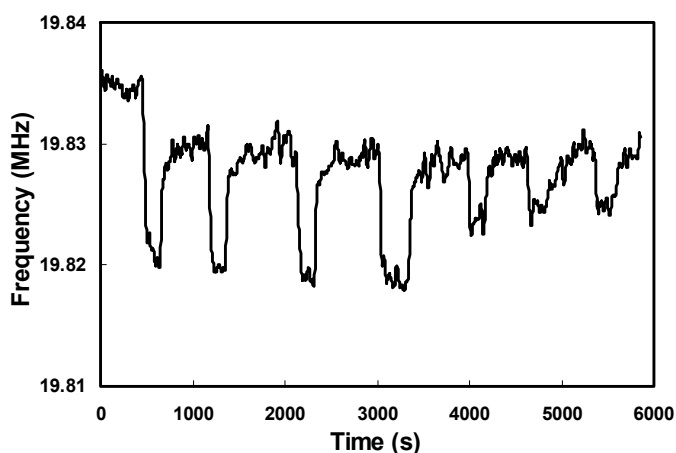


Figure 7-16: Transient response of CMUT sensor coated with NP+PDMS complex films at room temperature to toluene (the first four cycles) and 1-propanol (the following three cycles) at the concentration of 0.5 %.

2. NP+ $\beta$ -CD indicated discrepant response upon toluene and 1-propanol: the former vapor resulted in a large decrease of frequency baseline and 1-propanol did not (Figure 7-17).

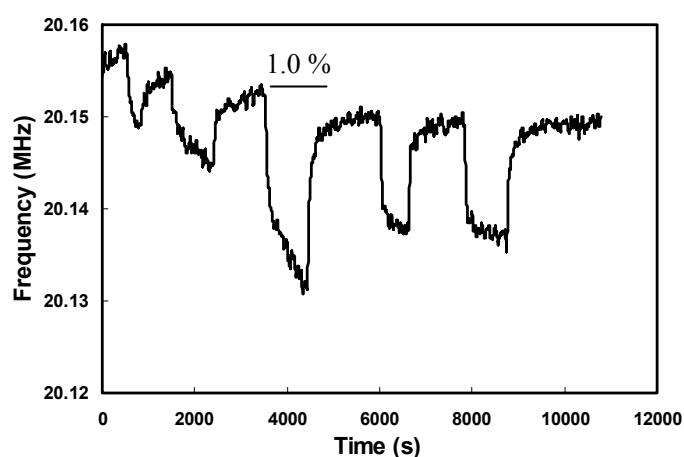


Figure 7-17: Transient response of CMUT sensor coated with NP+ $\beta$ -CD complex film at room temperature to toluene (the first three cycles) and 1-propanol (the following three cycles).

3. NP coating showed slightly positive change in base frequency, which was independent on the vapor type and did not rely on the sampling sequence either (Figure 7-18 and 7-19).

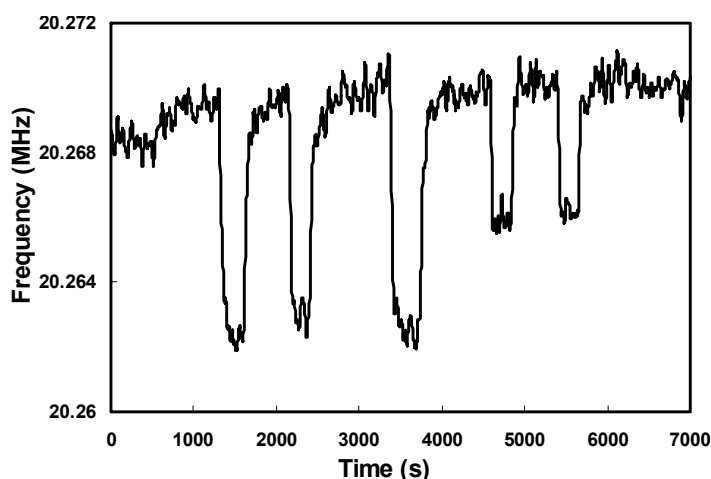


Figure 7-18: Transient response of CMUT sensor coated with NP film at room temperature to toluene (the first three cycles) and 1-propanol (the following two cycles) at the concentration of 0.5 %.

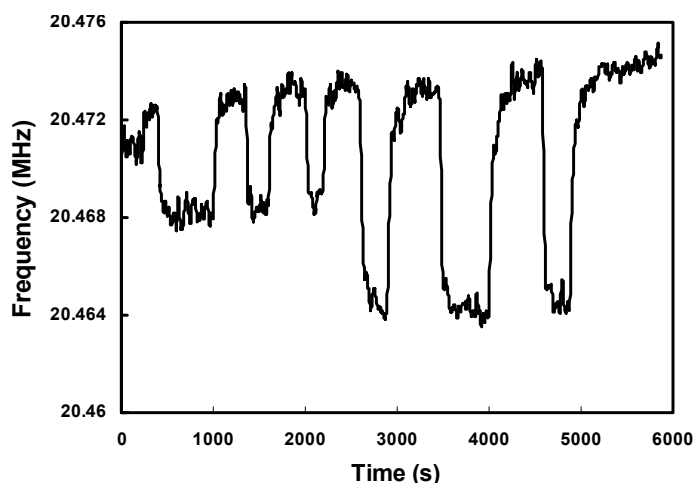


Figure 7-19: Transient response of CMUT sensor coated with NP film at room temperature to 1-propanol (the first three cycles) and toluene (the following three cycles) at the concentration of 0.5 %.

From the above results, we could conclude:

1. For rubbery polymers involved in this research, conditioning phenomenon exists, where preliminary exposure to highly swelling gases causes subsequently higher sorption, dilation, and permeation properties, allowing for some excess volume relaxing around packing disruptions but leaving the disruptions as sorption sites with lowered sorption energy requirements. In the two vapors tested here, toluene can be viewed as a highly swelling gas for OV225 and PDMS.
2. The NP+ $\beta$ -CD coating also implied the existence of conditioning response upon toluene vapor. Another supramolecule CA illustrated a similar conditioning behavior (Figure 7-5 G).
3. For the highly cross-linked polymeric NPs (poly styrene-*co*-DVB here), no conditioning

phenomenon was observed. Although as stated in the beginning, it has been reported that many glassy polymers show conditioning behaviors, the high cross-linking property of the NPs synthesized for modifying CMUTs are not prone to be swelled and relaxing upon toluene and 1-propanol.

4. It is worth to note that the two rubbery polymer coatings indicated no further change in the base frequency after the preliminary transient cycle. This suggests that repeated exposures to vapor do not cause subsequent relaxations, so the polymers show no further increase in sorption capacity and essentially no further increase in overall volume upon the following repressurization after desorption, when compared to samples which had not been exposed to vapor. This absence of conditioning could be explained by that the relaxation of coating was limited and already complete (or nearly complete) in the initial contact with vapor molecules. After that, the polymers were less susceptible to disruption of chain packing.

5. In summary, concerning conditioning response, the complex films' behavior was mostly in line with the second layers', since the bottom NP coating did not exhibit conditioning phenomenon. In order to decrease the conditioning influence on the accuracy of vapor determination, preliminary experimental data were not recommended to be involved in the calculation of sensor's sensitivity and other parameters.

### **7.5.8 Tentative kinetics study on vapor sorption**

The fundamental study of VOC sorption and diffusion in sensing agents, has been actively pursued for many years [127-130]. It can not only provide useful information on sensor behavior, coating morphology, interaction between analyte and sensor, but also help to realize predictive estimation of sensing response versus time and put forward pertinent comments or suggestions on some experimental situations to improve the sensor performance.

Several measurement conditions thought to have influence on kinetic parameters of gas sensing process were fixed (controlled room temperature, fixed gas cell, total gas flow rate at 80 ml/min), in order to spectacularly study the factors of interest.

A typical result is illustrated in Figure 7-20 for one CMUT sensor modified with NP+PEI complex films in exposure to 1-propanol at different concentrations (the same plot shown in Figure 7-5 M). By magnifying the initial 300-second exposure period of the sensor, one can observe an induction phase following a 'knee' in the curve and then a frequency decline which is nearly linear along with time (Figure 7-21 a)). The desorption behavior is similar in all respects except for the direction of frequency change (Figure 7-21 b)). It should be noted that the partially amplified curves shown in Figure 7-21 were plotted with normalized time axis, i.e. the starting time ( $t = 0$ ) is at the point when toluene vapor was introduced into the gas cell.

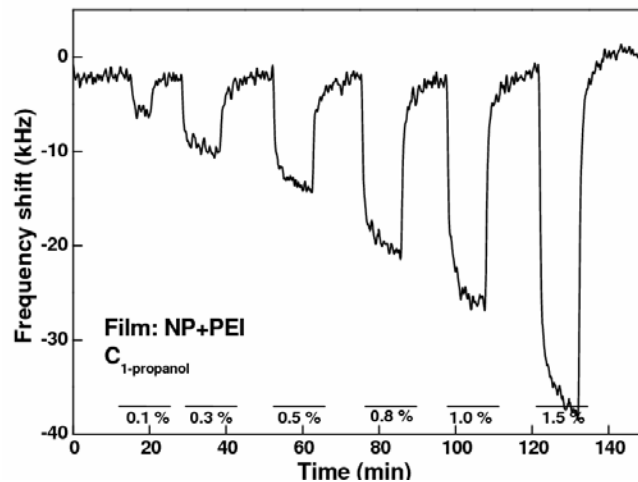


Figure 7-20: Transient response of NP+PEI coated CMUT sensor in response to 1-propanol.

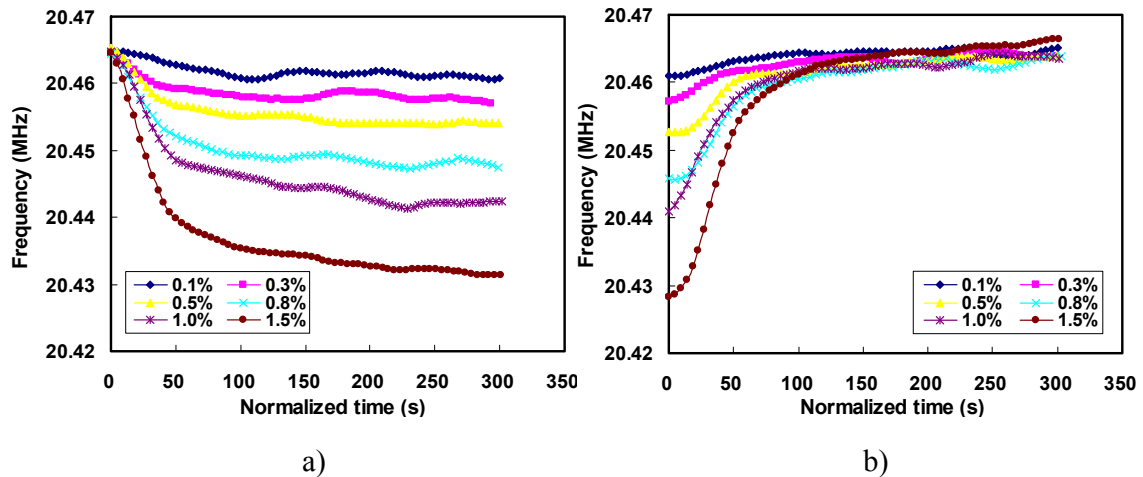


Figure 7-21: Partially amplified transient response of 1-propanol vapor on NP+PEI modified CMUT sensor showing induction time and linear time dependence.

a) Sorption; b) desorption.

Brace *et al* showed the dependence of the initial induction and ‘knee’ period on gas flow rate, and found an inversely proportional relation [131]. This fact implies a geometric influence of testing system, for instance, the dead volume of gas cell. Thus a constant flow rate is necessary for the analysis of kinetics. Provided the same flow rate and the same sorbate-sorbent couple, vapor concentration (partial pressure) will act as the key factor on the time length before slow adsorption period comes. As shown in Figure 7-21, higher concentration of 1-propanol shortens the time period of the linear frequency decline. However, it is not necessarily faster for establishing sorption equilibrium under higher vapor concentration.

Since the operation temperature was not changed during the whole vapor measurement, the activation energy was assumed constant. However, shift of temperature up to a few degrees can not be avoided as the gas cell was placed in the normal circumstance without using a

thermostat. This could be the reason for some drifting phenomena of the frequency baseline.

### 7.5.9 Anomalous response analysis

Spaeth *et al.* reported that spectroscopic ellipsometry study of PDMS film showed that exposure of the films to toluene vapor caused an increase in refractive index [132], which is related to the condensation of vapor inside the capillaries at pressures lower than their saturated pressure ( $P_0$ ) at a certain temperature [120, 133]. Hence, it can be equally deduced that the films participating in our study, such as PDMS, OV 225, have been affected in the same way during vapor sorption.

Compared with 1-propanol, capillary condensation is more likely to occur in the case of toluene, mainly owing to the higher volatility of toluene vapor (larger  $P_0$ ).

Kelvin equation can be used to determine the pressure required for vapor condensation, in the form of Equation (7.3).

$$\frac{P}{P_0} = \exp\left(-\frac{2V\gamma}{rRT} \cos \theta\right) \quad (7.3)$$

where  $P$  and  $P_0$  are the saturated vapor pressure inside the capillaries with a radius  $r$  and in normal conditions, respectively.  $V$  is the molar volume and  $\gamma$  is the surface tension of the vapor.  $\theta$  is the wetting angle in the capillary.  $R$  is the universal gas constant, and  $T$  is temperature.

According to this equation, the pressure needed for particular adsorbate to condense in capillary structure is related to the parameters  $V$ ,  $\gamma$  and  $P_0$  for the adsorbates, taking the assumption that other factors kept identical. A rough estimation for toluene and 1-propanol was made and it turned out that ratio between  $P$  and  $P_0$  for toluene was about 1.6 - 3 times higher than that for 1-propanol. This may be the reason why in NP+PDMS coating, condensation happened at the vapor concentration larger than 1.0 % for toluene (corresponding  $P/P_0 = 0.35$ ) while for 1-propanol, no condensation was observed (no apparent curve inflection occurred). Besides, in NP+CA coating, the concentration limit necessary for toluene condensation was found to be 0.8 % (corresponding  $P/P_0 = 0.28$ ) while it was 1.0 % (corresponding  $P/P_0 = 0.51$ ) for 1-propanol.

In conclusion, varied solubility parameters and volatility of the tested vapors account for the difference in partition coefficient. Moreover, the physical and chemical features of sensing matrix, including morphology, roughness, porosity and solubility also strongly influence the generic vapor sorption. Thirdly, variational response strength is correlative to the presence of specific interactions between sensing materials and vapors as well.

## 7.6 Conclusion

The performance of the fabricated sensors has been evaluated by means of exposure to several VOCs. Modified LFE sensors have been used to detect ten vapors from different categories of organic compounds and two representative vapors (toluene and 1-propanol) have been extensively employed for studying CMUTs.

Most coatings responded to step changes in vapor concentration of the gas molecules rapidly and reversibly. The uptake and release time were found to be less than four minutes when 85 % of sorption or desorption equilibrium was reached for most of vapor-coating couples. Among different pairs of vapor and sensor, there exists variation in respects of sensitivity, stability etc. LFE sensors were coated by two sensitive materials,  $\beta$ -CD and CA,. Comparing their responses to the ten analytes, one can find that  $\beta$ -CD is more sensitive to alcohols (methanol, ethanol and 1-propanol), acetone and water, while CA shows higher sorption capacity to chloroform, alkanes (*n*-hexane and *n*-octane), aromatics (toluene and *p*-xylene). As for CMUT, the sensitive coatings,  $\beta$ -CD, PEI and OV 225, give rise to larger partition coefficient  $K$  in exposure to 1-propanol and the rest two materials, CA and PDMS, indicate higher sensitivity in response to toluene.

The measurement results demonstrate that the sensitive materials involved in the research can be used to detect analytes of pharmaceutical interests as well as for flexible automobile fuels.

Concerning the magnitude of  $\Delta f_v$ , it was interesting to find that in comparison with NP films, not all the double layers (NP+sensing agents) necessarily provided the highest sensitivity (value of  $\Delta f_v$ ) upon vapor exposure, some of which showed the response capacity less than that from single NP layer (NP+CA and NP+PDMS). While for other complex coating systems, the values of  $\Delta f_v$  were close to the sum of the bottom NPs and the second layer (NP+PEI, NP+OV 225, and NP+ $\beta$ -CD).

The underlying mechanism for the interaction between vapors and sorbents has been concretely expounded. By analyzing the HSPs of these compounds, selectivity can be estimated semi-quantitatively and the theoretic prediction is in agreement with the experimental results for most of the interactions. It is safe to conclude that the chemical structures of the substances play the primary role in sensing process and the physical properties such as  $T_g$  of the sorbents,  $P_0$  of the vapors, all contribute to the final sensing signals.

The variation of  $R_1$  value is referable to the physical status of the sensing materials in contact with vapors. For CMUTs, the alteration in  $R_1$  has relations with sorbent and vapor types and vapor concentration. Significant change of  $R_1$  was not observed during gas detection with LFE sensors, which is very likely due to the fact that the same coatings on LFE sensors are thinner than those on CMUTs.

In summary, the proposed mechanism of sorption includes specific interaction between vapor and sensor, swelling of sensing film and condensation of sorbate within the film.

For all the odorants it might be generalized that the sensors with single layer have characteristics quite close to their corresponding blends (NPs plus sensing materials).

Although double-coated films do not always provide an elevated sensitivity, they still have potential in keeping sensors' stability, as well as reproducibility in sensing response. It can be expected that the improvements introduced at the fabrication stage – increasing control of the fabrication process – would result in lower variation of sensor responses as compared to the sensors modified by direct aerosol jetting.

The bottom NP layers provide sensitivity to all the vapors as well. On the one hand, this suggests NPs can also be adopted as a kind of sensing agent. However, utilizing NPs as bottom layer materials needs extra calibration or subtraction of their sensitivity. On the other hand, searching for other “inert” substances which have no or little sorption ability to coat sensors firstly in the 2-step modification technique is an alternative way to circumvent this problem.

Long time and repeating exposures of CMUTs to VOCs have been performed in order to get more information related to the sensing process and the accompanied changes of the sensing layers. It was found that the phenomenon that some sensitive materials illustrated endless frequency shift in exposure to certain gas (e.g. NP+ $\beta$ -CD to toluene) did not originate from vapor sorption but pressure effect from the measurement cell. Repeated purging of sensors with VOCs showed reproducible sensing response, although permanent combination between vapor and sensor might occur in their first contact. Vapor concentration had influence on uptake and release time but in concern with interaction rate, little relation was observed.

## Chapter 8

# Conclusion

---

Numerous combinations of materials and processes can be used to get membranes. Although each has advantages and disadvantages, the issues of uniformity, repeatability and controllability are common for all, especially in sensor industrial fabrication.

It is our intention to build up a prototype system by using CMUT sensor array and thus realize controlled sensor modification, characterization, evaluation and selection of new sensing agents, and predictable VOC determination.

In this research, a double-coating process has been developed to modify chemical sensors with complex films made up of nanoparticles (NPs) and sensitive materials. In the first step, NPs formed a layer on the whole surface of sensor and in the second step, localized deposition of various sensitive agents were realized on the NP surface. The films have been characterized with SEM and impedance analysis. Gas detection with the prepared sensors has been carried out and the performance-related parameters such as sensitivity, selectivity, reversibility, response and recovery time, long-time stability, etc. have been studied and presented in detail.

Firstly, NPs have been synthesized by copolymerization of styrene and divinylbenzene and further functionalized to improve their cohesion on sensor surface as well as to better immobilize other sensing agents.

Several strategies for NP deposition have been attempted for the purpose of getting homogeneous NP coating to avoid significant decrease in  $Q$ -factor of sensor performance. Spin coating has finally been chosen since it is able to create relatively uniform NP layer and the approach itself has shown satisfied reproducibility in respect of the coating's morphology. Besides, repeated results have been obtained concerning the amount of NPs deposited onto sensor surface. The RSD of  $\Delta f_r^{NP}$  for LFE sensor is less than 1.0 % ( $n > 10$ ), and for CMUT it is 0.56 % ( $n = 3$ ), which further suggests the reliability of the spin coating technique in preparing NP films. The NP-deposited sensors can be washed with most common organic solvents and nearly no particles stripped off the substrates.

Different commercially available compounds have been directly patterned onto selected regions of CMUT sensors by aerosol jetting technique. In this sense, the prepared double films possess robust property of the co-polymeric NPs and diverse chemical features imparted by the upper layers.

In the SEM and impedance measurement, the influence of the prepared coatings on sensor behaviour has been investigated to evaluate and optimize coating strategies. It has been found that the obtained NP film has a well-organized bi-layer structure, high thermal

stability and uniformity. By introducing such as an antecedently cast NPs rather than direct deposition of sensing materials, “coffee ring” structure of the second coating has been found to be alleviated, because of the close packed NP films with regular conformation. Thereby, it allows for a similar mass loading onto each element (membrane). As revealed in SEM photos, viscous matrix such as OV 225 has formed a far more continuous film on NP surface, in comparison with that on bare sensor surface. Moreover, the influence of external coating on  $Q$ -factor has also been reduced.

No significant attenuation of the acoustic wave energy of the sensors has been observed, which is mainly attributed to the rigidity of the cast materials and the fair uniformity of the complex films.

With respect of film thickness, NPs always take up the larger part compared with the materials on top. Hence, the bottom uniformly-arranged NP layer defines the acoustic properties of the whole device.

General sensor responding behavior in exposure to VOCs is: due to the mass loading by purging vapors through the testing cell, the sensor displayed a rapid decline of frequency, which is followed by a slow decrease and then a balance or near-balance status.

Reversible sorption and desorption of these vapours has been confirmed with repeated experiments. Most of the sensors are able to reach 85 % response equilibrium with 4 min. It has been assumed that responses of sensors to vapor pulses result from the changes in mass and viscoelasticity of sensing agents on the surface owing to vapor sorption. Certain degree of selectivity has been achieved based on the physical and chemical properties of both host and guest molecules.

The interacting mechanism between different analyte-sensor couples has been analyzed and useful information has been extracted from isotherm curves. By calculating and comparison of the Hansen solubility parameters (HSPs) between hosts and guests, it is possible to explain the different response capacity of sensitive materials in exposure to toluene and 1-propanol. It is summarized that the overall sensing signals are the result of specific interaction between vapor and sensor, swelling of sensing film and condensation of sorbate within the film.

In our study, not only the contribution of nano-structure to the elevation of the recognition sites, but also the fact that the bottom layer shares the majority of mass loading on resonators compared with the second coating, makes the technique very promising in industrial sensor manufacture, since the latter advantage is assumed to alleviate or even obviate laborious and complicated calibration work, which is necessary for mass production of sensors. The use of such composite structure consisting of NP+sensitive material is supposed to make significant improvement in sensor performance.

In addition, CMUTs have also been modified by a bioactive material, ceramide AP, with assistance of a LB film trough. The film thickness is in accordance between experimental results and theoretic calculation.

In the end, it can be concluded that the double-coating process is highly efficient and reproducible for fabricating multi-layers with desirable uniformity and stability. Both deposition steps are direct and thus can be easily controlled and adjusted, which has compatibility with various coating matrixes, making nearly no limits to incorporate amountless other sensing candidates. The abundant sources of sensitive materials will open out a wide application scale and greatly increase the diversity and versatility of the sensor system, as well as the sensitivity and selectivity of the films. Moreover, since spin coating and aerosol jetting technology have been well-established for many years, the whole deposition procedure can be transferred from laboratory to industry out of question. Since some of the detected organic compounds have founded their positions as automotive fuel and biomarker in disease diagnosis, the application of the modified sensors for flexible fuel vehicle detection, as well as in pharmaceutical and medical fields, is positively expectable.

In retrospect of the 2-step deposition technique, it is possible to derive another detection tool from the modified CMUT sensor array. Firstly, the whole CMUT wafer can be coated by NPs, ceramides or other media, either through spin-coating or with help of a LB film trough. A homogeneous layer is obtainable, as have been demonstrated in this research, which is the premise to guarantee the reliability of the following application. Then various samples can be dispensed onto different element groups of the modified CMUTs. Sorption, interaction or penetration of the analytes in the samples may occur in the interface of the coatings. These processes can be tracked and perceived by the sensor, and represented in the form of electrical signals.

Analogous to the “Microtiter plate”, the above described conception can serve as a cheap, rapid and simultaneous analysis of multiple samples. Since the detector is based on the frequency change of acoustic wave rather than photometry of normal Microtiter plate, such instrument has potential to provide more precise measurement.

The future work will be focused on establishment of construction of sensor array system on the ground of CMUT. Pattern recognition techniques will be applied to transducing signals obtained from the multiple-sensors for identification of vapour mixtures.

---

## References

---

- [1] T. Hofmann, F. Beckmann, S. Michaelis, J. Zacheja, J. Binder and S. Tagliante, Comparison of a conventional with an advanced micromachined flexible-fuel sensor, *Sens. Actuators, A*, 61, 1997: 319-322.
- [2] J. Binder, New generation of automotive sensors to fulfill the requirements of fuel economy and emission control, *Sens. Actuators, A*, 31, 1992: 60-67.
- [3] W. J. Fleming, New automotive sensors – a review, *IEEE Sensors J.*, 8, 2008: 1900-1921.
- [4] A. R. V. Benvenho, R. W. C. Li and J. Gruber, Polymeric electronic gas sensor for determining alcohol content in automotive fuels, *Sens. Actuators, B*, 136, 2009: 173-176.
- [5] F. Beckmann, J. Marschner, T. Hofmann and R. Laur, Analysis of complex impedances in CMOS technology for chemical sensor applications, *Sens. Actuators, A*, 62, 1997: 734-738.
- [6] L. Wallace, T. Buckley, E. Pellizzari and S. Gordon, Breath measurements as volatile organic compound biomarkers, *Environ. Health Perspect.*, 104, 1996: 861-869.
- [7] M. Fleischer, E. Simon, E. Rumpel, H. Ulmer, M. Harbeck, M. Wandel, C. Fietzek, U. Weimar and H. Meixner, Detection of volatile compounds correlated to human diseases through breath analysis with chemical sensors, *Sens. Actuators, B*, 83, 2002: 245-249.
- [8] A. D. Amico, R. Bono, G. Pennazza, M. Santonico, G. Mantini, M. Bernabei, M. Zarlenga, C. Roscioni, E. Martinelli, R. Paolesse and C. D. Natale, Identification of melanoma with a gas sensor array, *Skin Res. Technol.*, 14, 2008: 226-236.
- [9] X. Liu, J. Hu, B. Cheng, H. Qin, M. Jiang, Acetone gas sensing properties of  $\text{SmFe}_{1-x}\text{Mg}_x\text{O}_3$  perovskite oxides, *Sens. Actuators, B*, 134, 2008: 483-487.
- [10] G. Neri, A. Bonavita, G. Micali and N. Donato, Design and development of a breath acetone MOS sensor for ketogenic diets control, *IEEE Sensors J.*, 10, 2010: 131-136.
- [11] D. L. A. Fernandes, T. A. Rolo, J. A. B. P. Oliveira and M. T. S. R. Gomes, A new analytical system, based on an acoustic wave sensor, for halitosis evaluation, *Sens. Actuators, B*, 136, 2009: 73-79.
- [12] M. Phillips, Method for the collection and assay of volatile organic compounds in breath, *Anal. Biochem.*, 247, 1997: 272-278.
- [13] J. W. Gardner, A. Pike, N. F. de Rooij, M. Koudelka-Hep, P. A. Clerc, A. Hierlemann and W. Göpel, Integrated array sensor for detecting organic solvents, *Sens. Actuators, B*, 26, 1995: 135-139.
- [14] P. Ciosek and W. Wroblewski, Sensor arrays for liquid sensing - electronic tongue systems, *Analyst*, 132, 2007: 963-978.
- [15] D. James, S. M. Scott, Z. Ali and W. T. O'Hare, Chemical sensors for electronic nose systems, *Microchim. Acta*, 149, 2005: 1-17.

- 
- [16] A. Hierlemann and H. Baltes, CMOS-based chemical microsensors, *Analyst*, 128, 2003: 15-28.
- [17] R. Arshady, Desk reference of functional polymers: syntheses and applications, Washington DC: American Chemical Society, 1997: 601-620.
- [18] J. W. Grate, S. J. Martin and R. M. White, Acoustic wave microsensors, *Anal. Chem.*, 65, 1993: 940-948.
- [19] G. Sauerbrey, Verwendung von Schwingquarzen zur Wägung dünner Schichten und zur Mikrowägung, *Z. Phys.*, 155, 1969: 206-222.
- [20] S. W. Wenzel and R. M. White, Flexural plate-wave gravimetric chemical sensor, *Sens. Actuators, A*, 22, 1989: 700-703.
- [21] H. O. Finklea, M. A. Phillippi E. Lompert and J. W. Grate, Highly sorbent films derived from Ni(SCN)<sub>2</sub>(4-picoline)<sub>4</sub> for the detection of chlorinated and aromatic hydrocarbons with quartz crystal microbalance sensors, *Anal. Chem.*, 70, 1998: 1268-1276.
- [22] K. D. Schierbaum, A. Gerlach, W. Göpel, W. M. Müller, F. Vögtle, A. Dominik and H. J. Roth, Surface and bulk interactions of organic molecules with calixarene layers, *Fresenius J. Anal. Chem.*, 349, 1994: 372-379.
- [23] J. W. Grate, M. Klusty, R. A. McGill, M. H. Abraham, G. Whiting and J. Andonian-Haftvan, The predominant role of swelling-induced modulus changes of the sorbent phase in determining the responses of polymer-coated surface acoustic wave vapor sensors, *J. Anal. Chem.*, 64, 1992: 610-624.
- [24] S. J. Martin, G. C. Frye and S. D. Senturia, Dynamics and response of polymer-coated surface acoustic wave devices: effect of viscoelastic properties and film resonance, *Anal. Chem.*, 66, 1994: 2201-2219.
- [25] R. Lucklum and Peter Hauptmann, The quartz crystal microbalance: mass sensitivity, viscoelasticity and acoustic amplification, *Sens. Actuators, B*, 70, 2000: 30-36.
- [26] R. Lucklum, C. Behling and P. Hauptmann, Gravimetric and non-gravimetric chemical quartz crystal resonators, *Sens. Actuators, B*, 65, 2000: 277-283.
- [27] X. Su and Y. Li, A QCM immunosensor for Salmonella detection with simultaneous measurements of resonant frequency and motional resistance, *Biosens. Bioelectron.*, 21, 2005: 840-848.
- [28] J. W. Grate, Acoustic wave microsensor arrays for vapor sensing, *Chem. Rev.*, 100, 2000: 2627-2648.
- [29] J. W. Grate, S. J. Patrash and M. H. Abraham, Method for estimating polymer-coated acoustic wave vapor sensor responses, *Anal. Chem.*, 67, 1995: 2162-2169.
- [30] J. J. McCallum, Piezoelectric devices for mass and chemical measurements: an update, *Analyst*, 114, 1989: 1173-1189.
- [31] J. W. Grate and E. T. Zellers, The fractional free volume of the sorbed vapor in modeling the viscoelastic contribution to polymer-coated surface acoustic wave vapor sensor responses, *Anal. Chem.*, 72, 2000: 2861-2868.
-

- 
- [32] R. Pinalli, M. Suman and E. Dalcanale, Cavitands at work: from molecular recognition to supramolecular sensors, *Eur. J. Org. Chem.*, 2004: 451-462.
- [33] F. L. Dickert, S. Landgraf and R. Sikorski, Host-guest chemistry and chemical sensors: FT-IR-analysis and spectra simulation of  $\text{CDCl}_3$  inclusion, *J. Mol. Model.*, 6, 2000: 491- 497.
- [34] A. Ikeda and S. Shinkai, Novel cavity design esing calix[n]arene skeletons: toward molecular recognition and metal binding, *Chem. Rev.*, 97, 1997: 1713-1734.
- [35] J. W. Grate, S. J. Patrash, S. N. Kaganove and B. M. Wise, Hydrogen bond acidic polymers for surface acoustic wave vapor sensors and arrays, *Anal. Chem.*, 71, 1999: 1033-1040.
- [36] S. P. J. Higson and P. M. Vadgama, Biosensors: a viable monitoring technology? *Med. Biol. Eng. Comput.*, 32, 1994: 601-609.
- [37] G. Bunte, J. Hürttlen, H. Pontius, K. Hartlieb and H. Krause, Gas phase detection of explosives such as 2,4,6-trinitrotoluene by molecularly imprinted polymers, *Anal. Chim. Acta*, 591, 2007: 49-56.
- [38] F. L. Dickert, O. Hayden and K. P. Halikias, Synthetic receptors as sensor coatings for molecules and living cells, *Analyst*, 126, 2001: 766-771.
- [39] G. Wulff, W. Vesper, R. Grobe-Einsler and A. Sarhan, Enzyme-analogue built polymers, 4. On the synthesis of polymers containing chiral cavities and their use for the resolution of racemates, *Makromol. Chem.*, 178, 1977: 2799-2816.
- [40] R. Arshady and K. Mosbach, Synthesis of substrate-selective polymers by host-guest polymerization, *Makromol. Chem.*, 182, 1981: 687-692.
- [41] J. L. Urraca, M. C. Moreno-Bondi, G. Orellana, B. Sellergren, and A. J. Hall, Molecularly imprinted polymers as antibody mimics in automated on-line fluorescent competitive assays, *Anal. Chem.*, 79, 2007: 4915-4923.
- [42] O. Y. F. Henry, D. C. Cullen and S. A. Piletsky, Optical interrogation of molecularly imprinted polymers and development of MIP sensors: a review, *Anal. Bioanal. Chem.*, 382, 2005: 947-956.
- [43] X. Su, H. T. Ng, C. Dai, S. J. O'Shea and S. F. Y. Li, Disposable, low cost, silver-coated, piezoelectric quartz crystal biosensor and electrode protection, *Analyst*, 125, 2000: 2268-2273.
- [44] H. Fan, Y. Lu, A. Stump, S. T. Reed, T. Baer, R. Schunk, V. Perez-Luna, G. P. López and C. J. Brinker, Rapid prototyping of patterned functional nanostructures, *Nature*, 405, 2000: 56-60.
- [45] K. B. Blodgett, Monomolecular of fatty acids on glass, *J. Am. Chem. Soc.*, 56, 1934: 495.
- [46] K. B. Blodgett, Films built by depositing successive monomolecular layers on a solid surface, *J. Am. Chem. Soc.*, 57, 1935: 1007-1022.
- [47] M. Ohring, Material science of thin films: deposition and structure, San Diego, CA: Academic Press, 1999.
-

- 
- [48] H. O. Pierson, Handbook of chemical vapor deposition (CVD): principles, technology and applications, Westwood, NJ: Noyes Publ., 1992.
- [49] U. Lange, N. V. Roznyatouskaya and V. M. Mirsky, Conducting polymers in chemical sensors and arrays, *Anal. Chim. Acta*, 614, 2008: 1-26.
- [50] C. Alexander, H. S. Andersson, L. I. Andersson, R. J. Ansell, N. Kirsch, I. A. Nicholls, J. O'Mahony and M. J. Whitcombe, Molecular imprinting science and technology: a survey of the literature for the years up to and including 2003, *J. Mol. Recognit.*, 19, 2006: 106-180.
- [51] D. Soltman and V. Subramanian, Inkjet-printed line morphologies and temperature control of the coffee ring effect, *Langmuir*, 24, 2008: 2224-2231.
- [52] W. H. King, Piezoelectric sorption detector, *Anal. Chem.*, 36, 1964: 1735-1739.
- [53] J. Hlavay and G. G. Guilbault, Applications of the piezoelectric crystal detector in analytical chemistry, *Anal. Chem.*, 49, 1977: 1890-1898.
- [54] M. D. Ward and D. A. Buttry, In situ interfacial mass detection with piezoelectric transducers, *Science*, 249, 1990:1000-1007.
- [55] Ö. Oralkan, A. S. Ergun, J. A. Johnson, M. Karaman, U. Demirci, K. Kaviani, T. H. Lee and B. T. Khuri-Yakub, Capacitive micromachined ultrasonic transducers: next-generation arrays for acoustic imaging? *IEEE Trans. Ultrason. Ferroelectr. Freq. Control*, UFFC 49, 2002, 1596-1610.
- [56] J. D. Fraser and K. Philips, Capacitive micromachined ultrasound transducers, U. S. Patent 6, 443, 901, B1, 2002.
- [57] A. Caronti, G. Caliano, R. Carotenuto, A. Savoia, M. Pappalardo, E. Cianci and V. Foglietti, Capacitive micromachined ultrasound transducers (CMUT) arrays for medical imaging, *Microelectron. J.*, 37, 2006, 770-777.
- [58] X. Zhuang, A. Nikoozadeh, M. A. Beasley, G. G. Yaralioglu, B. T. Khuri-Yakub and B. L. Pruitt, Biocompatible coatings for CMUTs in a harsh, aqueous environment, *J. Micromech. Microeng.*, 17, 2007, 994-1001.
- [59] M. I. Haller and B. T. Khuri-Yakub, A surface micromachined ultrasonic air transducer, *IEEE Trans. Ultrason. Ferroelectr. Freq. Control*, UFFC 43, 1996: 1-6.
- [60] Schindel DW and Hutchins DA, The design and characterization of Micromachined air-coupled capacitance transducers, *IEEE Trans. Ultrason. Ferroelectr. Freq. Control*, UFFC 42, 1995: 42-50.
- [61] M. Buigas, F. M. Espinosa, G. Schmitz, I. Ameijeiras, P. Masegosa and M. Domínguez, Electro-acoustical characterization procedure for cMUTs, *Ultrasonics*, 43, 2005: 383-390.
- [62] H. J. Lee, K. K. Park, P. Cristman, Ö. Oralkan, M. Kupnik and B. T. Khuri-Yakub, A low-noise oscillator based on a multi-membrane CMUT for high sensitivity resonant chemical sensors, *Micro Electro Mechanical Systems, IEEE 22nd International Conference*, 2009: 761-764.
-

- 
- [63] X. Jin, I. Ladabaum and B. T. Khuri-Yakub, The microfabrication of capacitive ultrasonic transducers, *J. Microelectromech. Syst.*, 7, 1998: 295-302.
- [64] Eccardt PC, Niederer K and Fischer B, Micromachined transducers for ultrasound applications, *IEEE International Ultrasonics Symposium*, 1997: 1609-1618.
- [65] J. K. Chen, Capacitive micromachined ultrasonic transducer arrays for minimally invasive medical ultrasound, *J. Micromech. Microeng.*, 20, 2010: 1-13.
- [66] H. J. Lee, K. K. Park, Ö. Oralkan, M. Kupnik and B. T. Khuri-Yakub, CMUT as a chemical sensor for DMMP detection, *Frequency Control Symposium, IEEE International*, 2008: 434-439.
- [67] M. Thränhardt, P. C. Eccardt, H. Mooshofer and P. Hauptmann, A resonant CMUT-based fluid sensor: Modeling and simulation, *Sens. Actuators, A*, 156, 2009: 191-195.
- [68] Y. Li, R. Lucklum, P. Hauptmann, 2-step surface modification technology for acoustic chemical sensor arrays based on CMUTs, *IEEE Ultrasonics Symposium*, 2008, 1030-1033.
- [69] B. Boutevin, C. Boyer, I. Csetneki, G. David *et al*, Oligomers, polymer composites, molecular imprinting, Berlin, Heidelberg: Springer, 206, 2007.
- [70] M. Komiyama, T. Takeuchi, T. Mukawa and H. Asanuma, Molecular imprinting: from fundamentals to applications, Weinheim: Wiley-VCH, 2002.
- [71] Y. Li, Q. Fu, Q. Zhang and L. He, Preparation and evaluation of uniform-size (-)-ephedrineimprinted polymeric microspheres by multi-step swelling and suspension polymerization, *Anal. Sci.*, 22, 2006: 1355-1360.
- [72] G. Wulff, W. Vesper, R. Grobe-Einsler and A. Sarhan, Enzyme-analogue built polymers, 4. On the synthesis of polymers containing chiral cavities and their use for the resolution of racemates, *Makromol. Chem.*, 178, 1977: 2799-2816.
- [73] R. Arshady and K. Mosbach, Synthesis of substrate-selective polymers by host-guest polymerization, *Makromol. Chem.*, 182, 1981: 687-692.
- [74] F. L. Dickert, P. Forth, P. Lieberzeit and M. Tortschanoff, Molecular imprinting in chemical sensing – Detection of aromatic and halogenated hydrocarbons as well as polar solvent vapors, *Fresenius J. Anal. Chem.*, 360, 1998: 749-762.
- [75] F. L. Dickert and O. Hayden, Molecular imprinting in chemical sensing, *Trends Anal. Chem.*, 18, 1999: 192-193.
- [76] F. L. Dickert and O. Hayden, Imprinting with sensor development – On the way to synthetic antibodies, *Fresenius J. Anal. Chem.*, 364, 1999: 506-511.
- [77] R. H. Schmidt, K. Mosbach and K. Haupt, A simple method for spin-coating molecularly imprinted polymer films of controlled thickness and porosity, *Adv. Mater.*, 16, 2004: 719-722.
- [78] R. H. Schmidt and K. Haupt, Molecularly imprinted polymer films with binding properties enhanced by the reaction-induced phase separation of a sacrificial polymeric porogen, *Chem. Mater.*, 17, 2005: 1007-1016.
-

- 
- [79] U. Hempel, R. Lucklum, J. F. Vetelino and P. Hauptmann, Advanced application of the impedance spectrum of a lateral field excited sensor, *Sens. Actuators, A*, 142, 2008: 97-103.
- [80] T. Vossmeier, B. Guse, I. Besnard, R. E. Bauer, K. Müllen and A. Yasuda, Gold nanoparticle/polyphenylene dendrimer composite films: preparation and vapor-sensing properties, *Adv. Mater.*, 14, 2002: 238-242.
- [81] T. Okajima, H. Sakurai, N. Oyama, K. Tokuda and T. Ohsaka, Electrical equivalent circuit parameters for montmorillonite clay film-coated quartz crystal oscillators in contact with air, moisture and electrolyte solutions, *Electrochim. Acta*, 38, 1993: 747-756.
- [82] S. H. Si, Y. S. Fung and D. R. Zhu, Improvement of piezoelectric crystal sensor for the detection of organic vapors using nanocrystalline TiO<sub>2</sub> films, *Sens. Actuators, B*, 108, 2005: 165-171.
- [83] P. A. Lieberzeit, A. Afzal, A. Rehman and F. L. Dickert, Nanoparticles for detecting pollutants and degradation processes with mass-sensitive sensors, *Sens. Actuators, B*, 127, 2007: 132-136.
- [84] R. Shinar, G. J. Liu and M. D. Porter, Graphite microparticles as coatings for quartz crystal microbalance-based gas sensors, *Anal. Chem.*, 72, 2000: 5981-5987.
- [85] U. Hempel: Lateral field excited quartz crystal resonators – From theoretical approach to sensor application, Ph.D. Thesis, Otto-von-Guericke University Magdeburg, 2008.
- [86] U. Hempel, R. Lucklum, P. Hauptmann, E. P. EerNisse, D. Puccio and R. F. Diaz: Quartz crystal resonator sensors under lateral field excitation – a theoretical and experimental analysis, *Meas. Sci. Technol.*, 2008, 19, 055201, 1-11.
- [87] K. J. Seu, A. P. Pandey, F. Haque, E. A. Proctor, A. E. Ribbe and J. S. Hovis, Effect of surface treatment on diffusion and domain formation in supported lipid bilayers, *Biophys. J.*, 92, 2007: 2445-2450.
- [88] J. Cho and F. Caruso, Investigation of the interactions between ligand-stabilized gold nanoparticles and polyelectrolyte multilayer films, *Chem. Mater.*, 17, 2005: 4547-4553.
- [89] S. L. Clark, M. F. Montague and P. T. Hammond, Ionic Effects of sodium chloride on the templated deposition of polyelectrolytes using layer-by-layer ionic assembly, *Macromolecules*, 30, 1997: 7237-7244.
- [90] A. Krozer, S. Nordin and B. Kasemo, Layer by layer deposition of 5–50-nm colloidal silica particles studied by quartz microbalance, *J. Colloid Interface Sci.*, 176, 1995: 479-484.
- [91] S. Srivastava and N. A. Kotov, Composite Layer-by-layer (LBL) assembly with inorganic nanoparticles and nanowires, *Acc. Chem. Res.*, 41, 2008: 1831-1841.
- [92] H. Yu, T. Cao, L. Zhou, E. Gu, D. Yu and D. Jiang, Layer-by-layer assembly and humidity sensitive behavior of poly(ethyleneimine)/multiwall carbon nanotube composite films, *Sens. Actuators, B*, 119, 2006: 512-515.
-

- [93] K. Reybiera, S. Zairib, N. Jaffrezic-Renault and B. Fahysa, The use of polyethyleneimine for fabrication of potentiometric cholinesterase biosensors, *Talanta*, 56, 2002: 1015-1020.
- [94] J. C. Lötters, W. Olthuis, P. H. Veltink and P. Bergveld, The mechanical properties of the rubber elastic polymer polydimethylsiloxane for sensor applications, *J. Micromech. Microeng.*, 7, 1997: 145-147.
- [95] W. P. Carey, K. R. Beebe and B. R. Kowalski, Multicomponent analysis using an array of piezoelectric crystal sensors, *Anal. Chem.*, 59, 1987: 1529-1534.
- [96] S. V. Patel, T. E. Mlsna, B. Fruhberger, E. Klaassen, S. Cemalovic and D. R. Baselt, Chemicapacitive microsensors for volatile organic compound detection, *Sens. Actuators, B*, 96, 2003: 541-553.
- [97] R. M. Crooks and A. J. Ricco, New organic materials suitable for use in chemical sensor arrays, *Acc. Chem. Res.*, 31, 1998: 219-227.
- [98] F. L. Dickert, U. P. A. Bäumlner and H. Stathopoulos, Mass-sensitive solvent vapor detection with calix[4]resorcinarenes: tuning sensitivity and predicting sensor effects, *Anal. Chem.*, 69, 1997: 1000-1005.
- [99] F. L. Dickert and O. Schuster, Supramolecular detection of solvent vapours with calixarenes: mass-sensitive sensors, molecular mechanics and BET studies, *Mikrochim. Acta*, 119, 1995: 55-62.
- [100] S. Wartewig and R. H. H. Neubert, Properties of ceramides and their impact on the stratum corneum structure: A review, Part 1: Ceramides, *Skin Pharmacol. Physiol.*, 20, 2007: 220-229.
- [101] A. Ruettinger, M. A. Kiselev, Th. Hauss, S. Dante, A. M. Balagurov and R. H. H. Neubert, Fatty acid interdigitation in stratum corneum model membranes: a neutron diffraction study, *Eur. Biophys. J.*, 37, 2008: 759-771.
- [102] K. Raith, J. Darius and R. H. H. Neubert, Ceramide analysis utilizing gas chromatography-mass spectrometry, *J. Chromatogr. A*, 876, 2000: 229-233.
- [103] M. A. Kiselev, N. Y. Ryabova, A. M. Balagurov, S. Dante, T. Hauss, J. Zbytovska, S. Wartewig and R. H. H. Neubert, New insights into the structure and hydration of a stratum corneum lipid model membrane by neutron diffraction, *Eur. Biophys. J.*, 34, 2007: 1030-1040.
- [104] B.-J. d. Gans, U. S. Schubert, Inkjet printing of well-defined polymer dots and arrays, *Langmuir*, 20, 2004: 7789-7793.
- [105] A. Bietsch, J. Zhang, M. Hegner, H. P. Lang and C. Gerber, Rapid functionalization of cantilever array sensors by inkjet printing, *Nanotechnology*, 15, 2004: 873-880.
- [106] T. Kawase, T. Shimoda, C. Newsome, H. Sirringhaus and R. H. Friend, Inkjet printing of polymer thin film transistors, *Thin Solid Films*, 438-439, 2003: 279-287.
- [107] R. D. Deegan, O. Bakajin, T. F. Dupont, G. Huber, S.R. Nagel and T. A. Witten, Capillary flow as the cause of ring stains from dried liquid drops, *Nature*, 389, 1997: 827-829.

- 
- [108] J. Schroeder, S. Doerner, T. Schneider and P. Hauptmann, Analogue and digital sensor interfaces for impedance spectroscopy, *Meas. Sci. Technol.*, 15, 2004: 1271-1278.
- [109] J. A. Dean and N. A. Lange, Lange's handbook of chemistry, 15th Edition, Section 5, Physical Properties, Columbus, OH: McGraw-Hill, 1998: 5.30.
- [110] P. N. Bartlett and S. K. Ling-Chung, Conducting polymer gas sensors part II: response of polypyrrole to methanol vapour, *Sens. Actuators*, 19, 1989: 141-150.
- [111] S. Kanehashi and K. Nagai, Analysis of dual-mode model parameters for gas sorption in glassy polymers, *J. Membr. Sci.*, 253, 2005: 117-138.
- [112] D. S. Pope, W. J. Koros and H. B. Hopfenberg, Sorption and dilation of poly(1-(trimethylsilyl)-1-propyne) by carbon dioxide and methane, *Macromolecules*, 27, 1994: 5839-5844.
- [113] B. Xing and J. J. Pignatello, Dual-mode sorption of low-polarity compounds in glassy poly(vinyl chloride) and soil organic matter, *Environ. Sci. Technol.*, 31, 1997: 792-799.
- [114] W. J. Koros, Model for sorption of mixed gases in glassy polymers, *J. Polym. Sci., Part B: Polym. Phys.*, 18, 1980: 981-992.
- [115] A. Mele, R. Mendichi and A. Selva, Non-covalent associations of cyclomaltooligosaccharides (cyclodextrins) with trans- $\beta$ -carotene in water: evidence for the formation of large aggregates by light scattering and NMR spectroscopy, *Carbohydr. Res.*, 310, 1998: 261-267.
- [116] I. Y. Shilov and M. G. Kurnikova, Energetics and dynamics of a cyclic oligosaccharide molecule in a confined protein pore environment. A molecular dynamics study, *J. Phys. Chem. B*, 107, 2003: 7189-7201.
- [117] K. Ariga and T. Kunitake, Supramolecular chemistry – fundamentals and applications: advanced textbook, Berlin, Heidelberg: Springer, 2006: 22, 25.
- [118] Y. Marcus, The properties of solvents, Chichester: Wiley, 1998: 90, 91.
- [119] J. Vicens, J. Harrowfield and L. Baklouti, Calixarenes in the nanoworld, Dordrecht, The Netherlands: Springer, 2007: 335.
- [120] V. Nabok, A. K. Hassan and A. K. Ray, Condensation of organic vapours within nanoporous calixarene thin films, *J. Mater. Chem.*, 10, 2000: 189-194.
- [121] C. M. Hansen, The three dimensional solubility parameter and solvent diffusion coefficient, Copenhagen: Danish technical press, 1967.
- [122] C. M. Hansen, The Universality of the solubility parameter, *Ind. Eng. Chem. Prod. Res. Dev.*, 8, 1969: 2-11.
- [123] K. L. Williamson, Macroscale and microscale organic experiments, 2nd Edition, Lexington, MA: D. C Heath, 1994: 40.
- [124] C. M. Hansen, Hansen solubility parameters - a user's handbook, New York: CRC Press LLC, 2000.
- [125] E. Stefanis, C. Panayiotou, Prediction of hansen solubility parameters with a new group-contribution method. *Int. J. Thermophys.*, 29, 2008: 568-585.
-

- [126] S. M. Jordan and W. J. Koros, Characterization of CO<sub>2</sub>-induced conditioning of substituted polycarbonates using various “exchange” penetrants, *J. Membr. Sci.*, 51, 1990: 233-247.
- [127] F. Rouquerol, J. Rouquerol and K. Sing, Adsorption by powders and porous solids, San Diego, CA: Academic Press, 1999.
- [128] J. W. Gardner, A non-linear diffusion-reaction model of electrical conduction in semiconductor gas sensors, *Sens. Actuators, B*, 1, 1990: 166-170.
- [129] F. Müller-Plathe, Permeation of polymers - a computational approach, *Acta Polymer.*, 45, 1994: 259-293.
- [130] J. J. Pignatello and B. Xing, Mechanisms of slow sorption of organic chemicals to natural particles, *Environ. Sci. Technol.*, 30, 1995: 1-11.
- [131] J. G. Brace, T. S. Sanfelippo and S. G. Joshi, A study of polymer/water interactions using surface acoustic waves, *Sens. Actuators*, 14, 1988: 47-68.
- [132] K. Spaeth, G. Kraus and G. Gauglitz, In-situ characterization of thin polymer films for applications in chemical sensing of volatile organic compounds by spectroscopic ellipsometry, *Fresenius J. Anal. Chem.*, 357, 1997: 292-296.
- [133] F. Rouquerol, J. Rouquerol and K. Sing, Adsorption by powders and porous solids: principles, methodology and applications, San Diego, CA: Academic Press, 1999: 208.

# **Schriftliche Erklärung**

Ich erkläre hiermit, daß ich die vorliegende Arbeit ohne unzulässige Hilfe Dritter und ohne Benutzung anderer als der angegebenen Hilfsmittel angefertigt habe; die aus fremden Quellen direkt oder indirekt übernommenen Gedanken sind als solche kenntlich gemacht.

Insbesondere habe ich nicht die Hilfe einer kommerziellen Promotionsberatung in Anspruch genommen. Dritte haben von mir weder unmittelbar noch mittelbar geldwerte Leistungen für Arbeiten erhalten, die im Zusammenhang mit dem Inhalt der vorgelegten Dissertation stehen.

Die Arbeit wurde bisher weder im Inland noch im Ausland in gleicher oder ähnlicher Form als Dissertation eingereicht und ist als Ganzes auch noch nicht veröffentlicht.

Magdeburg, 17. 11. 2010

Yingchun Li

# Curriculum Vitae

## Personal information

**Name:** Li, Yingchun  
**Date of Birth:** Dec. 05, 1982  
**Place of Birth:** Urumqi, Xinjiang, China  
**Nationality:** Chinese  
**Marital Status:** Single

## Education

09/1987 – 07/1993 Primary school, Xinjiang, China  
09/1993 – 07/1996 Junior middle school, Xinjiang, China  
09/1996 – 07/1999 Senior middle school, Xinjiang, China

## Studies

09/1999 – 07/2003 Bachelor degree for Science, Pharmacy  
Shihezi University, Xinjiang, China  
09/2003 – 06/2006 Master degree for Medicine, Pharmaceutical Analysis  
Xi'an Jiaotong University, Shanxi, China

## Experience

09/2006-Present Ph.D. student and research assistant  
Institute for Micro and Sensor System (IMOS)  
Otto-von-Guericke University Magdeburg, Germany

Magdeburg, November 2010